Strain transfer between disconnected, propagating rifts

Afar I Manighetti, P. Tapponnier, V. Courtillot, Y. Gallet, E. Jacques, P.-y Gillot

JOURNAL OF GEOPHYSICAL RESEARCH, VOL. 106, NO. B7, PAGES 13,613–13,665, JULY 10, 2001

Strain transfer between disconnected, propagating rifts in Afar

I. Manighetti, P. Tapponnier, V. Courtillot, and Y. Gallet

Institut de Physique du Globe de Paris, Paris, France

E. Jacques

Institut de Physique du Globe de Strasbourg, Strasbourg, France

P.-Y. Gillot

Université Paris-Sud, Orsay, France

Abstract. We showed before that both the Aden and Red Sea plate boundaries are currently rifting and propagating along two distinct paths into Afar through the opening of a series of disconnected, propagating rifts. Here we use new geochronological, tectonic, and paleomagnetic data that we acquired mostly in the southeastern part of Afar to examine the geometry, kinematics, and time-space evolution of faulting related to strain transfer processes. It appears that transfer of strain is accommodated by a bookshelf faulting mechanism wherever rifts or plate boundaries happen to overlap without being connected. This mechanism implies the rotation about a vertical axis of small rigid blocks along rift-parallel faults that are shown to slip with a left-lateral component, which is as important as their normal component of slip (rates of ~2-3 mm/yr). By contrast, where rifts do not overlap, either a classic transform fault (Maskali) or an oblique transfer zone (Mak'arrasou) kinematically connects them. The length of the Aden-Red Sea overlap has increased in the last ~0.9 Myr, as the Aden plate boundary propagated northward into Afar. As a consequence, the first-order blocks that we identify within the overlap did not all rotate during the same time-span nor by the same amounts. Similarly, the major faults that bound them did not necessarily initiate and grow as their neighboring faults did. Despite these variations in strain distribution and kinematics, the overlap kept accommodating a constant amount of strain (7 to 15% of the extension amount imposed by plate driving forces), which remained distributed on a limited number (seven or eight) of major faults, each one having slipped at constant rates (~3 and 2 mm/yr for vertical and lateral rates, respectively). The fault propagation rates and the block rotation rates that we either measure or deduce are so fast (30-130 mm/yr and 15-38°/Myr, respectively) that they imply that strain transfer processes are transient, as has been shown to be the case for the processes of tearing, rift propagation, and strain jumps in Afar.

1. Introduction

The Red Sea and Aden ridges have been propagating toward one another for the last 30 Myr, as a result of the separation of Arabia away from Africa [e.g., *Courtillot et al.*, 1987; *Manighetti et al.*, 1997] (Plate 1, inset). However, foregoing what might seem to be an easy linkage through the Bab El Mandeb Strait, the two plate boundaries did not directly connect and both have penetrated into Afar where they now are actively opening and propagating through the development of a series of disconnected, propagating rift segments (Plate 1, inset) [e.g., *Barberi et al.*, 1972, 1975; *Schaefer*, 1975; *Barberi and Varet*, 1977; *Varet and Gasse*, 1978; *Courtillot*, 1980, 1982; *Courtillot et al.*, 1980; *Tapponnier et al.*, 1990; *Manighetti et al.*, 1998]. As a consequence, transfer of extension between them, as well as between their rift segments, is presently taking place on dry land in the Afar depression. That situation makes Afar a unique testing ground where one is able to directly observe and measure processes that usually operate below ocean waters, that is, the mechanisms that allow strain transfer, either at large scale between two dis-

Paper number 2000JB900454.
0148-0227/01/2000JB900454$09.00

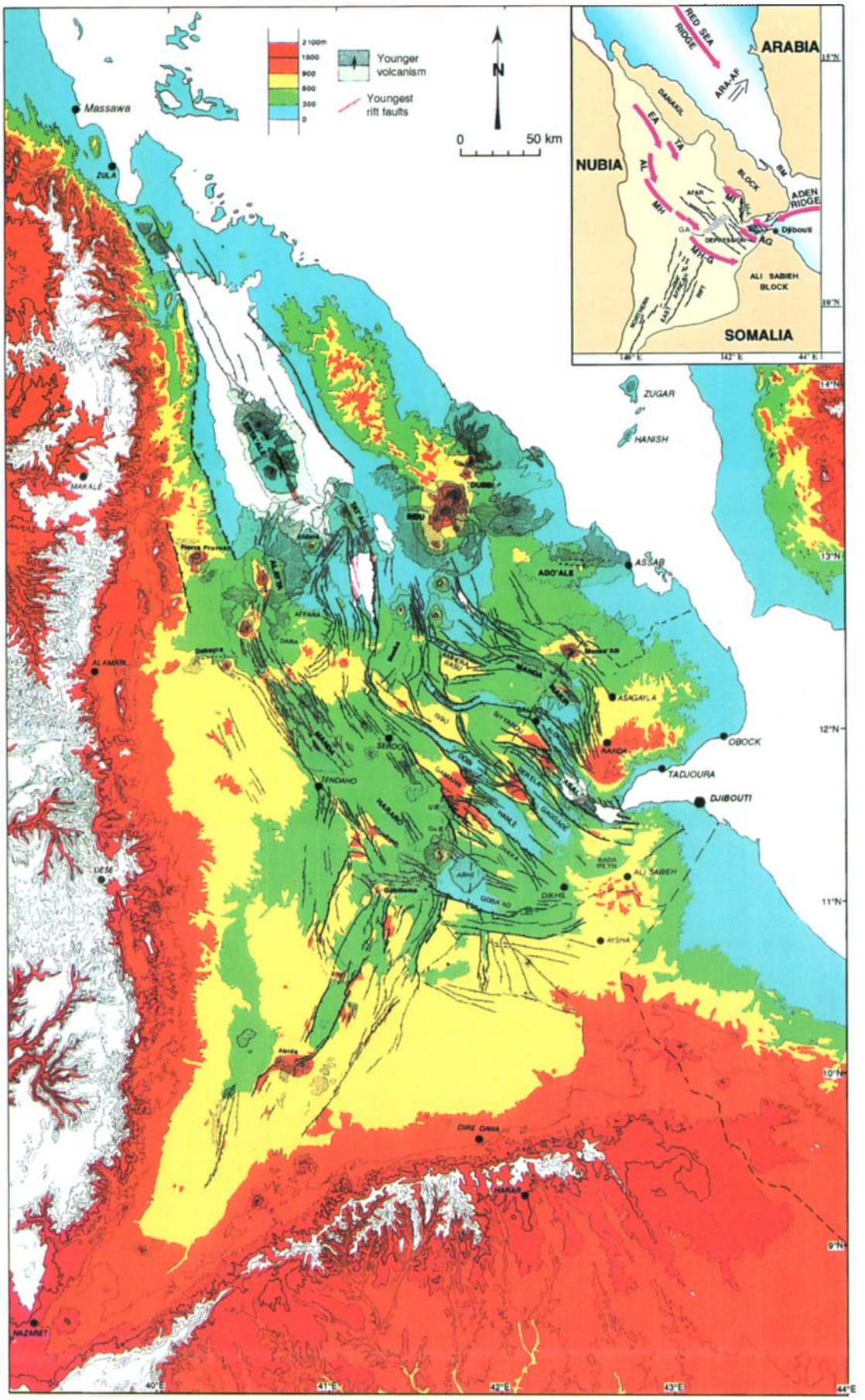
2100m
1500
900
600
300
0
Younger volcanism
Youngest rift faults
N
0
50 km
RED SEA RIDGE
ARABIA
ARA-AF
DANAKIL
EA
TA
NUBIA
AL
BM
BLOCK
AFAR
MI
ADEN RIDGE
MH
GA
DEPRESSION
AG
Djibouti
MH-G
ALI SABIEH BLOCK
RIFT
SOMALIA
15°N
19°N
14°E
42°E
44°E
ZUGAR
HANISH
Massawa
ZULA
MAKALE
DUBBI
ASSAB
ADO'ALE
AFFARA
DAMA
ALAMATA
ASAGAYLA
OBOCK
TADJOURA
DJIBOUTI
SERDO
TENDAHO
HARAMO
DESE
ALI SABIEH
DIKHIL
AYSHA
DIRE DAWA
HARAR
NAZARET
14°N
13°N
12°N
11°N
10°N
9°N
40°E
41°E
42°E
43°E
44°E

tinct, propagating plate boundaries or at smaller scale between two successive, propagating rift segments.

In Afar the two plate boundaries fail to form a clean cut lithospheric break, causing faulting to spread over hundreds of thousands of square kilometers [*Consiglio Nazionale delle Richerche (CNR) and Centre National de la Recherche Scientifique (CNRS)*, 1975, Plate 1]. However, two zones of localized rifting have been recognized through that dense network of crosscutting faults, and interpreted as the subaerial continuations of the Aden and Red Sea ridges [e.g., *CNR and CNRS*, 1975; *Barberi and Varet*, 1977; *Varet and Gasse*, 1978; *Tapponnier et al.*, 1990, *Manighetti et al.*, 1998] (Plate 1). The onland continuation of the Aden ridge ("Aden rifting zone") is a narrow, NNW trending zone of active volcanism and tectonics that includes the northwestern tip of the Tadjoura rift, the Asal-Ghoubbet rift, the Mak'arrasou fault system, and the Manda Inakir rift (Plate 1). It extends along the western side of the Danakil block, at the northeastern edge of the Afar depression. The whole zone has been propagating northward into Afar over the last 2 Myr [e.g., *Manighetti et al.*, 1998]. The subaerial continuation of the Red Sea ridge ("Red Sea rifting zone") also is a narrow, NW trending zone of intense active faulting, fissuring and volcanism, hugging at the southwestern edge of the depression (Plate 1). That zone comprises the Erta'Ale, Tat'Ali, Alayta and Manda Hararo rifts and ends near lake Abhe through the Manda Hararo-Goba'ad rift [*CNR and CNRS*, 1975]. The whole Red Sea rifting zone is taken to have propagated southward into Afar in the last 20 Myr [e.g., *Courtillot et al.*, 1987; *Manighetti et al.*, 1998; *Audin*, 1999]. Thus the two rifting zones face each other and overlap over more than 120 km in length (i.e., perpendicular to the Arabia-Africa relative motion vector, which is $\sim$ N40°E, 16 ± 1 mm/yr [e.g., *Chase*, 1978; *Chu and Gordon*, 1998]) and $\sim$100 km in width (Plate 1). The Quaternary basalts that cover central Afar ("stratoid basalts", Plate 1, inset) are cut by a dense network of parallel, NW-SE striking normal faults, with high scarps (over 1 km in some places). Faulting that would directly connect the two facing rifting zones is not observed. In particular, the familiar orthogonal ridge-transform geometry that one might expect between two plate boundaries is nowhere apparent. One main goal of the paper is to investigate which deformation mechanisms may allow rift-parallel normal faults to accommodate strain transfer between the two exposed, propagating plate boundaries.

At a smaller scale the two plate boundaries occur as a series of disconnected NW striking rifts along which most current strain and volcanic activity are localized. These rifts are currently propagating, northwestward along the Aden rifting zone and southeastward along the Red Sea rifting zone [*Manighetti et al.*, 1997, 1998] (Plate 1, inset). What are the mechanisms operating to transfer extension between these propagating rifts? Are these mechanisms comparable to those operating at the larger scale, between the two emerged ridges? Can we clarify the way transfer zones function and evolve related to rift propagation? In other words, could transient zones transfer propagating deformation, in contrast with the more common steady state transform faults?

Models advocated until now to account for the tectonics of Afar do not allow one to fully answer these fundamental questions because they are based on "end-member" models, such as rigid steady state plate tectonics [e.g., *Barberi and Varet*, 1975, 1977] or continuum deformation of thin viscous sheets [e.g., *Souriot and Brun*, 1992]. In reality, deformation mechanisms are expected to vary with observation scale. At the largest scale ($\sim$1000 km), Arabia, Nubia, and Somalia are three rigid plates in relative motion, and plate tectonic concepts provide a good first-order fit to observations (Plate 1, inset). At a smaller scale ($\sim$100 km) deformation in Afar seems to have involved the rotation of at least two microplates (Danakil and Ali Sabieh blocks, Plate 1; [*Sichler*, 1980; *Courtillot*, 1980; *Souriot and Brun*, 1992; Manighetti, 1993; *Chu and Gordon*, 1998; *Audin*, 1999]), and rigid plate kinematics may still partly provide a consistent second-order picture of deformation in that area. Finally, looking at the Afar depression more closely (tens of kilometers), it appears that the whole area is dissected by a dense network of crosscutting active faults (Plate 1), making deformation so distributed that rigid plate kinematics no longer apply in the interior of Afar.

In order to understand deformation mechanisms at the latter scale, we tried to establish a hierarchy among

Plate 1. Topographic and structural map of the Afar depression [from *Manighetti*, 1993]. Topographic curves are redrawn from ONC K5, 1:1,000,000, 1977 and Ethiopian 1:250,000 topographic maps; Active faults and volcanic areas are identified and mapped from satellite Landsat and SPOT images; U.B., Uddummi Bad; Ge.B., Gêra Bad. Inset sketches position of Afar depression between Arabia, Nubia and Somalia plates; ARA-AF motion vector is from *Manighetti et al.* [1997]; unstretched areas are in pale orange; Stratoid series are in pale green; ridges and rifts are in violet: EA, Erta'Ale; TA, Tat'Ali; AL, Alayta; MH, Manda Hararo; MH-G, Manda Hararo-Goba'ad; T, Tadjoura; AG, Asal-Ghoubbet; MI, Manda Inakir. Arrows indicate direction of propagation; Mak., Mak'arrasou; GA, Gamarri-Alol tear zone (note that grey lines are not faults); BM, Bab El Mandeb Strait. Only main faults in central Afar and northern East African rift are represented.

the faults and fault systems from a geometrical, kinematic, and dynamic point of view. Our approach consisted of considering any fault or fault system as an individual object expected to have its own behavior. Each fault or fault system was therefore analyzed in detail in order to specify its particular behavior. Between 1989 and 1993 we acquired a bulk of new geochronological, tectonic, and paleomagnetic data in the Republic of Djibouti, the analyses of which are presented in sections 2 to 4.

The complete, stereoscopic, panchromatic, satellite SPOT image cover of the Republic of Djibouti at a scale of 1:100,000, combined with satellite Landsat images and air photographs at various scales (1:50,000 to 1:15,000), allowed us to investigate the geometry of cumulative Quaternary faulting at different scales down to a few meters. That finite, cumulative geometry indicates the nature of movements on faults. Faults offsetting mid-late Pleistocene and Holocene ($<10^4$ – 10^5 years) basalts and sediments or exhibiting youthful morphology were the main focus of detailed analysis. Structural and morphological evidence was gathered in the field to constrain offsets on faults. Accurate digital mapping and topographic leveling of offset morphological surfaces or basaltic flows, combined with their radiometric dating (section 2), allowed measurements of fault slip rates. Such morphometric measurements were made on most accessible faults and on temporal markers of various ages, so that we could also uncover changes in those rates in the interior of Afar, over a period covering the last 2 Myr (section 3).

Since much of Afar is floored by Plio-Quaternary volcanism (most <2 Myr [e.g., *Courtillot et al.*, 1984; *Lahitte*, 2000]), paleomagnetism is particularly well suited to detect and measure rotational motions at a scale larger than that allowed by structural analysis. As a matter of fact, the very existence of large and fast rotations near the tip of the oceanic Aden ridge was discovered by paleomagnetism [*Courtillot et al.*, 1984], prior to detailed structural analysis of the type discussed in this paper or in previous ones [e.g., *Tapponnier et al.*, 1990]. *Courtillot et al.* [1984] showed that since $\sim 1.8 \pm 0.4$ Ma, the Stratoid basaltic series between lakes Asal and Abhe (Plate 1) has been rotated clockwise with respect to stable Africa by $\sim 14.5^\circ \pm 7.5^\circ$ when taken as a whole. In order to better constrain the distribution, amounts, and rates of such rotations and to understand their relationships with Quaternary faulting, we carried out additional paleomagnetic sampling of volcanic units in the still unexplored northern and eastern parts of the Republic of Djibouti. More than 1000 cores were collected through basalts of different ages, the analysis of which is presented in section 4.

The combined analysis of these three data sets allows us to show in section 5 that strain transfer between overlapping rifts or plate boundaries is, at all scales, accommodated by a bookshelf faulting mechanism that induces clockwise block rotations about a vertical axis along rift-parallel, normal-left lateral faults.

2. Geochronology

2.1. Basaltic Series

The Afar depression is almost entirely filled with Quaternary, mainly basaltic lavas. In particular, the 1-2 km thick Stratoid basaltic series covers more than 70% of the Afar floor. This series was originally dated between 0.4 and 4.4 Ma, using the conventional K-Ar technique [*Barberi et al.*, 1975; *Varet and Gasse*, 1978]. Using both updated K-Ar and ^{40}Ar-^{39}Ar data, *Courtillot et al.* [1984] reduced this range to 1.3-2.2 Ma (mean 1.8 ± 0.4 Ma) for Stratoid basalts sampled in the southeastern Djiboutian part of the central Afar depression. Numerous, new K-Ar determinations were recently performed by *Kidane* [1999] and *Lahitte* [2000] using the Cassignol-Gillot technique [e.g., *Cassignol and Gillot*, 1982] on a bulk of Stratoid basalt samples taken in the whole depression and south of it in the northern East African Rift termination. The obtained ages suggest that the 1-2 km thick, trap-like Stratoid series erupted rapidly between ~3.5 and 1 Ma. Moreover, the series seems to become younger from SW to NE, being ~3.5 Ma in the northern termination of the East African Rift, ~2-1.5 Ma in central Afar, and ~1 Ma in the northeastern part of Afar, close to the Manda Inakir rift [*Lahitte*, 2000]. As we performed the present study in the southeastern Djiboutian part of the central Afar depression, in what follows, we will consider the mean age of 1.8 ± 0.4 Ma for the surface of the Stratoid series [*Courtillot et al.*, 1984].

The Danakil and Ali Sabieh blocks are overlain with older basaltic and rhyolitic series, the younger and dominant one being the Dahla basaltic series [*Varet and Gasse*, 1978]. This series was originally dated between 4.3 and 8.3 Ma, using the conventional K-Ar technique, with most ages clustering between 6 and 8 Ma [*Varet and Gasse*, 1978]. *Audin* [1999] recently obtained four new K-Ar ages for this series, using the Cassignol-Gillot technique. The samples were taken along the western edge of the Ali Sabieh block. The ages range between 4.8 and 7.7 Ma, with three of them having a similar age of 7.2 ± 0.6 Ma.

In the frame of the present work we sampled and dated, also using the Cassignol-Gillot technique [*Cassignol and Gillot*, 1982] two other basaltic series that crop out in the southeastern part of Afar (Table 1). The petrologic characteristics of the basalts, as well as details on the analysis procedure, are given by *Manighetti et al.* [1998].

We performed seven age determinations on the "northern recent basalt series" that has erupted from the Manda Inakir rift and the Mousâ Alli volcano [e.g., *Manighetti et al.*, 1998]. The obtained ages suggest that the northern recent basalts were emplaced from ~1 Ma on, most of them between ~0.6 and 1 Ma, after Stratoid basalt emplacement.

We also sampled the "gulf basalt series", which crop out on either side of the Asal-Ghoubbet rift and of the Gulf of Tadjoura, and were emplaced during the first

Table 1. K/Ar Analysis Results for Gulf Basalts Cropping Out Between Asal-Ghoubbet and Tadjoura Rifts and on Asal-Ghoubbet Rift Southern Shoulder, and for Northern Recent Basalts Erupted From Manda Inakir Rift Segment and Moussa Ali Volcano[a]

Sample	K, %	^{40}Ar, %	^{40}Ar, 10^{11} at./g	Age + 2σ, ka
Gulf Basalts: Between Asal-Ghoubbet and Tadjoura				
BG13	0.360	0.62	1.361	362 ± 58
G59-I1	0.327	1.16	1.237	362 ± 30
G59-I2	0.138	1.09	0.515	357 ± 32
G55-P1	0.346	0.79	1.207	334 ± 43
G55-F1	0.318	0.60	1.048	315 ± 53
Gulf Basalts: Asal-Ghoubbet Rift, Southern Margin				
G55-N	0.340	1.57	1.714	482 ± 32
G55-S1	0.412	7.28	3.700	858 ± 35
Northern Recent Basalts				
I22	0.777	1.49	7.251	893 ± 60
G55-X	0.985	4.80	7.690	747 ± 17
G55-AE2	2.398	1.80	14.820	592 ± 33
G55-V	1.391	21.50	15.800	1087 ± 13
G55-W1	0.532	3.41	1.927	347 ± 10
G55-W2	0.894	0.37	1.577	187 ± 19
G55-AA	1.490	12.60	13.580	872 ± 15

[a]See *Manighetti et al.* [1998] for precise location, and Figure 11 for synthesis. All analyses were performed at the CFR, Gif Sur Yvette, Laboratory. Each result is mean value of at least two replicated independent analyses for both potassium and argon. Errors are 2σ.

stages of rifting in the western Aden Gulf [*Richard*, 1979]. Five samples were taken between the Asal-Ghoubbet and the Tadjoura rifts, and two others were taken on the southern shoulder of the Asal-Ghoubbet rift. The gulf basalts sampled between the Asal-Ghoubbet and the Tadjoura rifts seem to belong to an homogeneous series, the last flows of which were emplaced at 350 ± 40 ka. Those south of the Asal-Ghoubbet rift appear older, with a maximum age of 858 ± 35 ka. The gulf basalts east of Tadjoura town had previously been dated between 1 and 2 Ma [*Gasse*, 1991; *Gasse and Fournier*, 1983; *Office de la Recherche Scientifique et Technique d'Outre-Mer, ORSTOM*, 1985]. Those exposed on the southern coast of the Gulf of Tadjoura were previously determined to be older, with an age between ~1 and 3 Ma [*Richard*, 1979; *ORSTOM*, 1985].

2.2. Sediments

Although rare, sediments exist in Afar, mainly in the form of Quaternary lacustrine deposits and alluvial fans. *Gasse* [1991] showed that the deposition periods of these two types of sediments are correlated with regional climate changes. Micropaleontological analyses and ^{14}C dating revealed that four more humid (lacustrine) stages separated by arid periods occurred since 30 ka. During the wetter stages, lacustrine limestones were deposited within fault-bounded basins (e.g., Goba'ad, Hanle, Gaggade-Der'Ela, and Asal depressions, Plate 1), while large alluvial fans, fed by rivers, were deposited at the base of the major fault escarpments. In contrast, incision became predominent during the dry periods, the alluvial fans were dissected, and the basins were drained.

Four alluvial fan generations could therefore be deposited in succession, with ages of 30-20 ka, 10-8 ka, 7.5-4.5 ka, and 2-1.5 ka, respectively, each displaying a distinctive incision pattern. *Gasse* [1983] identified an additionnal fan generation, the deposition of which is dated between ~18 and 12-10 ka. Coupled with morphological criteria, these ages are used in our kinematic analyses of the youngest, late Quaternary faults.

3. Strain Distribution

Plates 1 and 2 are topographic and structural maps of the whole Afar depression and of southeastern Afar (Republic of Djibouti), respectively, based on Landsat and SPOT satellite images, aerial photos, topographic (ONC maps, 1:1 000,000; Institut Géographique National (IGN) topographic maps, 1:100,000) and geological maps [*CNR and CNRS*, 1975]. In the southern half of Afar, site of the present study, most strain is localized along the two narrow Aden and Red Sea rifting zones that face each other on either side of the depression [*Barberi and Varet*, 1977; *Tapponnier et al.*, 1990]. The ~ 120 × 100 km^2 area between them (Asal-Manda Inakir/Manda Hararo-Goba'ad overlap zone, hereinafter referred to as AMI/MHG overlap) is cut by a network of distributed, parallel, NW-SE striking normal faults. Outside of the two rifting zones (i.e., outside of the central depression), the regions that bound southeastern Afar (i.e., the Danakil block to the north and the Ali Sabieh block to the SE) are little deformed and show little evidence of Quaternary tectonic activity. South and southwest of the depression, faulting belonging to the northern termination of the East African Rift is either offset by, or merges with, the southern Manda Hararo-Goba'ad rift faults. The East African Rift is therefore kinematically coupled with the southern Manda Hararo fault systems and does not extend north of Manda Hararo into central Afar.

In the Aden rifting zone, rifts are disconnected, separated by zones of distributed faulting [e.g., *CNR and CNRS*, 1975; Tapponnier and Varet, 1974; *Manighetti et al.*, 1998]. The Tadjoura and Asal-Ghoubbet rifts overlap in the Arabia-Somalia motion vector direction, whereas the Asal-Ghoubbet and Manda Inakir rifts do not (Plates 1 and 2). The ~ 30 × 30 km^2 overlap zone between the Asal-Ghoubbet and the Tadjoura rifts (Tadjoura/Asal-Ghoubbet overlap zone, hereinafter referred to as TAG overlap) is dissected by a dense network of distributed, NNW striking, parallel, normal faults. The Asal-Ghoubbet and Manda Inakir rifts are separated by a ~70-km long, 25-km wide zone of closely

spaced, NNW striking normal faults (Mak'arrasou fault zone).

In sections 3.1 to 3.3, we attempt to determine the strain field in the southern half of Afar by analyzing the geometry, kinematics, and organization of Quaternary faulting in the different regions defined above, between rifts and rifting zones.

3.1. Tadjoura/Asal-Ghoubbet (TAG) Overlap Zone

The Tadjoura rift is the westernmost and youngest underwater segment of the Aden ridge, from which the ridge starts encroaching into Afar [*Manighetti et al.*, 1997] (Plates 1 and 2). The Asal-Ghoubbet rift follows ~80 km farther SW, being the first emerged segment of the ridge, although its southeastern half still lies under the shallow Ghoubbet waters [e.g., *Manighetti et al.*, 1998; *Audin et al.*, 2001]. The Asal-Ghoubbet and Tadjoura rifts face each other and overlap in the direction of the Arabia/Somalia motion vector without being connected by any perpendicular or nearly perpendicular faults that could act as transform faults. The overlap zone, where strain transfer between the two rifts must occur, is $\sim 35 \pm 5$ km wide between the two inner rift shoulders and ~26 km long between the two rift tips (Plate 2). The northwestern and southeastern parts of the zone are emerged, showing "old" volcanic units (Mabla rhyolites, Dahla and Stratoid basalts), whereas the Ghoubbet coasts are overlain with the young gulf basalt series (~350 ka old to the north, Table 1 and Figure 1). These northern gulf basalts are sliced by a dense network of closely spaced, NW to NNW striking normal faults (Figure 1). Most of these faults dip NE and exhibit vertical throws a few tens of meters high (~150 m maximum). Most faulted basaltic blocks are tilted by a few degrees toward the SW. Some faults, such as those indicated with white arrows in Figure 2a, offset Pleistocene and Holocene alluvial fans or terraces, or reef limestones [*ORSTOM*, 1985], evidence of their ongoing tectonic activity since ~350 ka.

Figure 2b focuses on the central part of the overlap (with an interpretation in Figure 2c). The whole area appears cut by two normal fault sets: a dominant one forming a dense network of closely spaced, 130°-160° striking, NE dipping, several kilometers long, straight scarps, slicing and tilting the basalts to the SW. These scarps have small vertical throws and are often underlined by fresh-looking spatter cones, which are either elongated along the fault strikes or left-laterally offset by the faults; a secondary set of sparse, shorter, 70°-120° striking faults and open fissures. These faults exhibit the highest scarps, suggesting they are mostly normal. At sites "1" (Figure 2c) the NNW faults offset the more easterly striking ones and bend them clockwise at some places. At sites "2" reverse chronological relationships are observed. This implies that the two fault sets are coeval. Moreover, at many places (such as those noted "3"), the 70°-120° faults join one or both terminations of the NNW faults, so that the latter exhibit horsetail terminations. Such terminations indicate a left-lateral component of slip on the NNW faults, compatible with all other observations above. The two fault sets combine to slice the basalts in rhomb-shaped blocks, a few kilometers long and a few hundred meters wide. These blocks display a parallel, domino arrangement (see "4" in Figure 2c), which suggests they might have rotated clockwise in the horizontal plane.

Going farther east, the faults continue under the Gulf of Tadjoura waters [*Manighetti et al.*, 1997; *Audin*, 1999] (Plate 2). The aftershock distribution in the latest stages of the 1978 Asal seismic sequence [*Lépine et al.*, 1980] (Figure 3) shows that the easternmost, main aftershock swarm, which is also the latest, strikes ~140°, parallel to the faults described farther west, and continues southward onland, where it coincides with the Daba Liba fault scarp. This suggests that the swarm outlines an active, underwater, 140°-striking fault, as confirmed by dive observations [*Cyaden Scientific Team*, 1986] and recent analysis of accurate sonar imagery and bathymetric data [*Audin*, 1999]. *Jacques* [1995] showed that the Daba Liba fault was indeed broken during the latest sequence and left-laterally slipped by ~20 cm. The fault plane solutions calculated for one main shock of the last swarm and for another one farther west [*Lépine et al.*, 1980; *Lépine and Hirn*, 1992] are compatible with left-lateral slip on steep NNW-SSE striking faults (Figure 3). These activated faults are estimated to have left-laterally slipped by 35 cm at the most [*Jacques*, 1995].

Strain transfer between the Asal-Ghoubbet and the Tadjoura overlapping rifts therefore appears to be ac-

Plate 2. Topographic and structural map of southeastern Afar (Republic of Djibouti) [from *Manighetti*, 1993]. Topographic curves are redrawn from Institut Géographique National 1:100,000 topographic maps; Active faults are identified and mapped from satellite SPOT images and aerial photos onland and bathymetric maps under water (from *Manighetti et al.* [1997]). Evidence of recent and Holocene faulting comes from field observations and aerial picture analysis. Dotted line to the west is Ethiopia-Djibouti border; F for fault; D.F., Der'Ela fault; D.G.F., Der'Ela-Gaggade fault; S. Gaggade F., Southern Gaggade fault; E.D.F., Eounda Dôbi fault; U.B., Uddummi Bad; Ge. B., Gêra Bad. Small black arrow indicates Figure 5a; other arrows indicate Figures 7a and 8. Cross sections A-B, C-D, E-F of Figure 9 are indicated; note that E is located slightly farther south than indicated, out of the figure. ARA-SOM plate motion vector is from *Manighetti et al.* [1997].

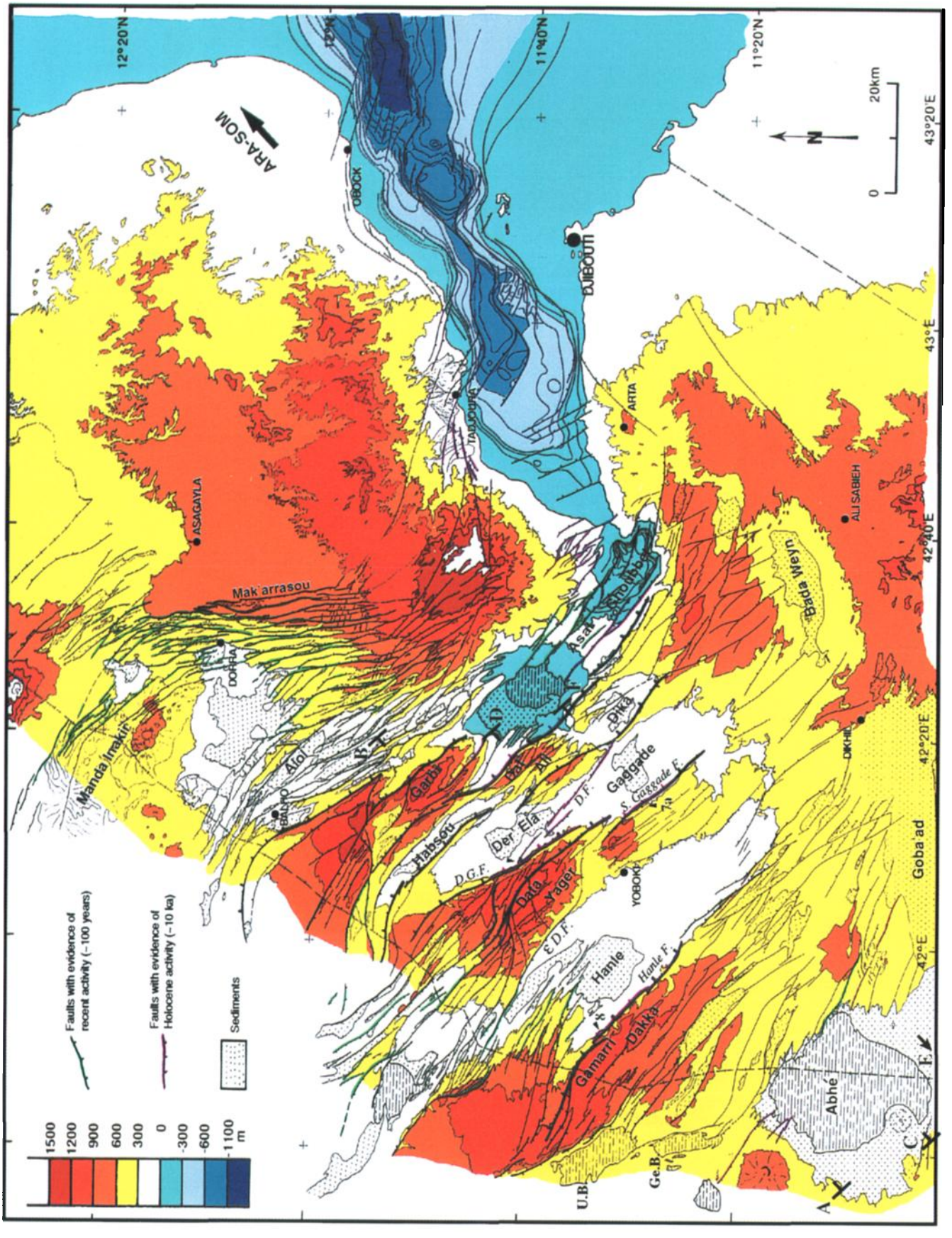
12°20'N
11°40'N
11°20'N
43°20'E
43°E
42°40'E
42°20'E
42°E
20km
0
N
ARA-SOM
OBOCK
DJIBOUTI
TADJOURA
ARTA
ALI SABIEH
DIKHIL
ASAGAYLA
Mak'arrasou
Manda Inakir
DOBA
Afol
BALHO
Asal
Scholibba
Bdda Weyn
Garbi
Bal Ali
D.F.
Gaggade
S. Gaggade F.
Dika
Habsou
Der Ela
D.G.F.
Dala
Yagep
YOBOKI
E.D.F.
Hanle
Hanle F.
Gamarri
Dakka
Goba'ad
Abhé
U.B
Ge.B
A
A'
B
B'
C
C'
Faults with evidence of recent activity (~100 years)
Faults with evidence of Holocene activity (~10 ka)
Sediments
1500
1200
900
600
300
0
-300
-600
-1100
m

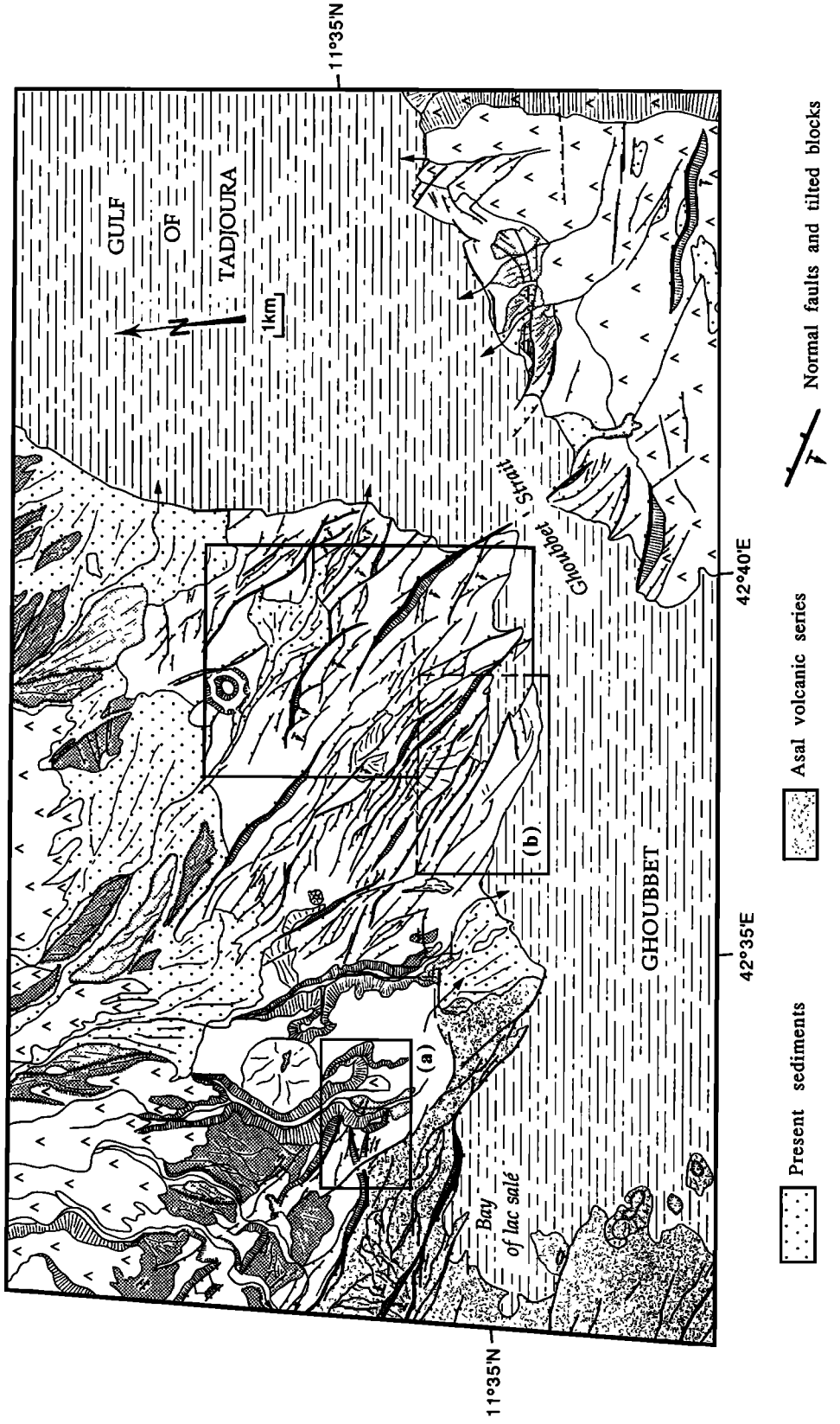

Figure 1. Geological and tectonic map of southern half of Asal-Ghoubbet/Tadjoura overlap, based on interpretation of satellite SPOT images (scale 1:100,000). Boxes a and b indicate Figures 2a, 2b, and 2c.

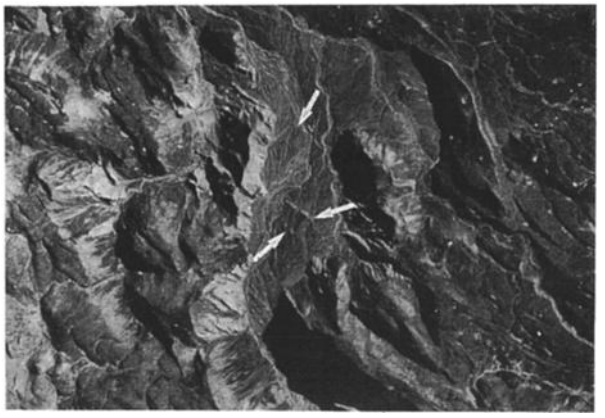

Figure 2a. Aerial picture (box a in Figure 1) showing three recent normal fault scarps (white arrows) cutting Holocene, alluvial terraces (standing just a few meters above present river bed). This attests to ongoing tectonic activity of faults within Asal-Ghoubbet/Tadjoura overlap.

commodated through a dense, rather equidimensional network of parallel, active, normal-left-lateral faults, oblique both to the bounding rifts and to the Arabia-Somalia motion vector, by ~20° and 70°, respectively. That fault network slices the overlap zone in elongated, parallel blocks, the domino geometry of which suggests they might have rotated clockwise in the horizontal plane.

3.2. The Mak'arrasou Fault Zone

Located ~70 km apart, the Asal-Ghoubbet and the Manda Inakir rifts do not overlap in the Arabia-Somalia motion vector direction (Plate 2). They are separated by a ~10-25 km wide, northerly striking zone of closely spaced, NNW normal faults (Mak'arrasou fault zone, [*CNR and CNRS*, 1975; *Manighetti et al.*, 1998]) (Plates 1 and 2) that has been interpreted as a continental transform fault connecting the two rifts [*Tapponnier and Varet*, 1974]. The Mak'arrasou fault zone slices the Stratoid basalts, up to the Manda Inakir rift where it cuts less than 600 ka lava flows erupted from the Inakir and Mousa Eali volcanoes (Table 1).

The Mak'arrasou zone is composed of two fault sets (Plate 2 and Figure 4). The prominent set, which structures the overall topography of the area, is made of closely spaced, straight, 10 to 40 km long, normal faults, the strike of which rotates from ~150° to 180° as one progresses from SW to NE. These faults are arranged en échelon in a left-lateral sense, on a mean NNE direction (Plate 2). They exhibit steep scarps (dips >70°-80°), all major ones facing east but for the easternmost ones (Plate 2), with vertical throws decreasing from south (100-200 m) to north (a few tens of meters). Most of these faults have tilted westward the basaltic blocks that they slice (Figure 4) by amounts which increase as one goes from east to west (up to ~20°). The second fault set is made of shorter (a few kilometers long) and smaller normal faults (vertical throws less than a few tens of meters), striking ~135°. At some sites ("1", Figure 4), the approximately N-S faults offset the secondary ones. At other sites ("2"), reverse relationships are observed. In most cases, the secondary 135° faults branch to the northern termination of the northerly striking faults, forming horsetail terminations on the latter, or connect two successive N-S scarps (Figure 4). This implies that the two fault sets are coeval and that the northerly striking faults have a left-lateral component of slip in addition to their more obvious normal one [see also *Tapponnier and Varet*, 1974; *Abbate et al.*, 1995]. The Mak'arrasou fault zone ends in the north with a spectacular, ~10 km wide horsetail termination (Plate 2) that attests to the existence of a left-lateral component of movement on the whole northerly striking fault zone. The quasi-systematic offset of the westernmost faults by their eastern neighboring faults suggests a northeastward fault migration [e.g., *Manighetti et al.*, 1998]. The overall northward decrease in the vertical throw and the eastward decrease of fault-related tilt amounts support that view. The observation, both on aerial photographs and in the field, of fresh, light colored scarplets at the base of most faults in the northern part of the Mak'arrasou zone suggests that recent (<~200 years) seismic activity took place on the latter [*Tapponnier et al.*, 1990], which also supports the idea of strain localization to the north.

The rooster tail geometry of the whole Mak'arrasou fault zone, which arises from the gradual clockwise rotation of fault strike from SW to NE (from ~135° near Asal to 170°; Plate 2), results from the northward propagation of faulting from Asal-Ghoubbet to Manda Inakir in response to the general northward propagation of the Aden ridge into Afar [*Manighetti et al.*, 1998].

3.3. Asal-Manda Inakir/Manda Hararo-Goba'ad Overlap Zone

The Asal-Manda Inakir/Manda Hararo-Goba'ad overlap region strongly contrasts with its two bounding Aden and Red Sea rifting zones. About 10 times wider (~100 km), it is fully overlain with the thick series of Quaternary Stratoid basalts and characterized by a lack of younger volcanism. The Stratoid surface is dissected by ~10 major 130°-150° striking, normal fault systems with high, steep, cumulative escarpments (100-1000 m; >70°, respectively), and numerous smaller, parallel, normal faults in between (Plates 1 and 2). The major faults bound NW trending basaltic blocks, ~20-30 km wide and 50-80 km long, so that the whole area appears as a succession of horsts and grabens. The overall geometry of these fault systems, horsts and grabens, leads to a division of the overlap zone into three parts.

The southeastern part of the overlap, east of a line that would join lake Gêra (GeB in Plates 1 and 2) to southern Alol, is dominantly sliced by NE dipping, 130°-150° striking normal faults scarps, the major ones being several hundred meters to 1000 m high. Five

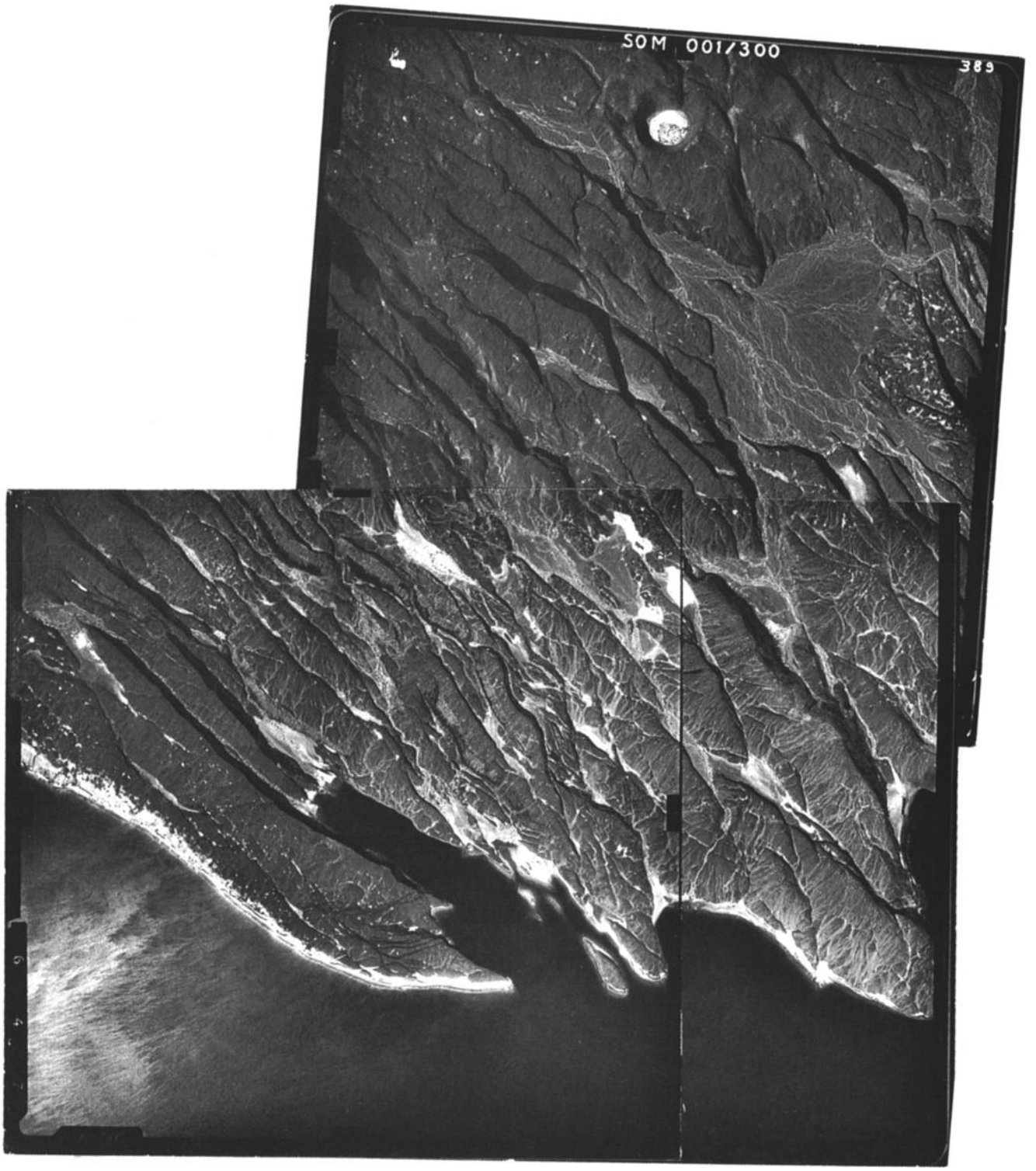

Figure 2b. Mosaïc of aerial photos (scale 1:30,000), corresponding to box b in Figure 1.

major fault systems can be distinguished, each separating a large southwestward tilted block to the SW (tilt <10°; blocks dubbed Gamarri-Dakka, Data Yager-Hanle, Der'Ela-Gaggade, Dat'Ali and Garbi, from SW to NE; Plates 1 and 2), from a sediment-filled half graben to the NE (Hanle, Der'Ela-Gaggade, Habsou-Dika, Asal and southern Alol, from SW to NE). Most major fault scarps are continuous over a few tens of kilometers, with an average length of 50 km. Others are made of disconnected, more easterly striking segments, each ~10 to 30 km long, that form a left-lateral échelon along the mean strike of the fault zones. Most of the major fault systems exhibit sigmoidal traces, striking ~130°-150° in their central part, then curv-

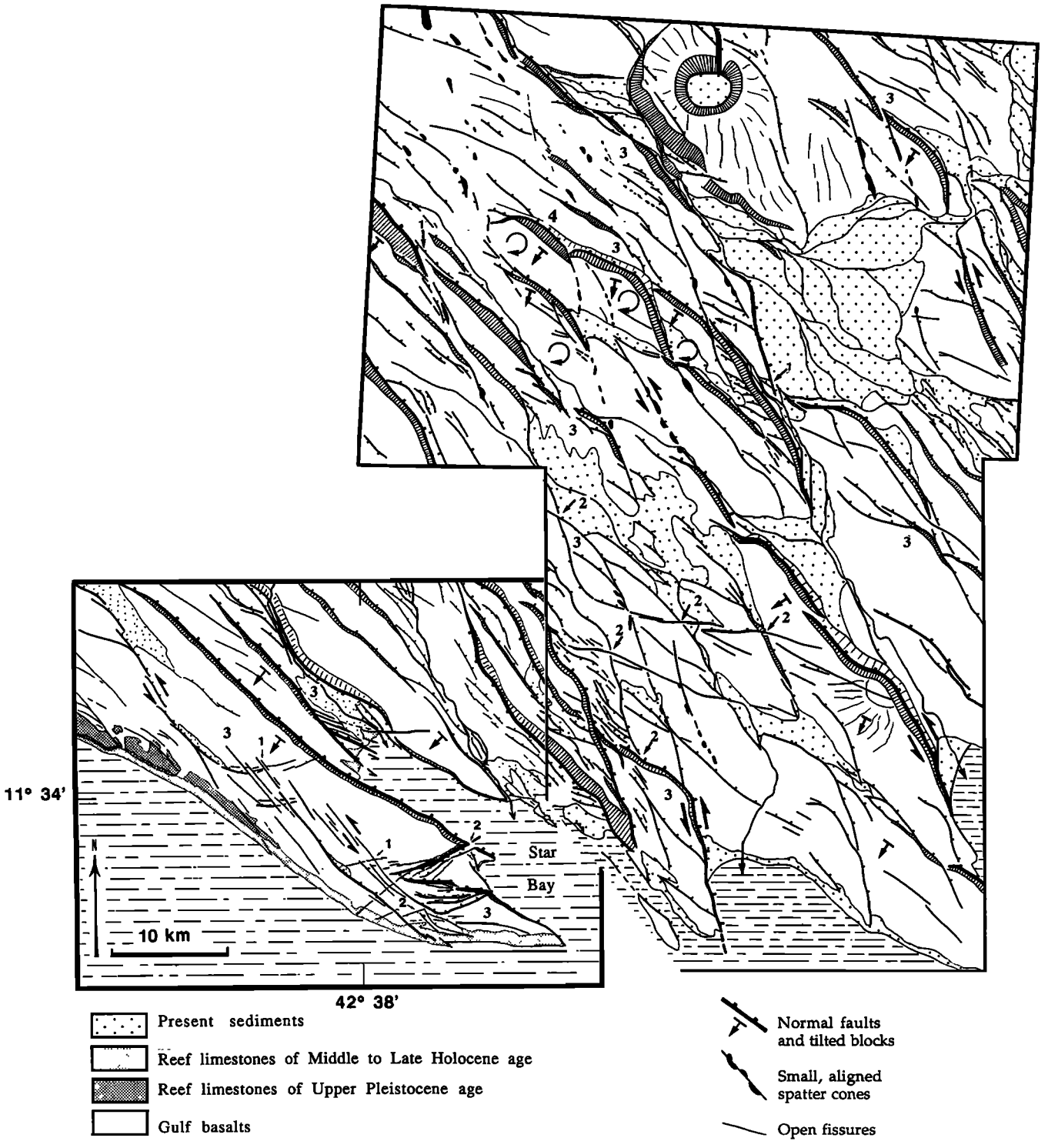

Figure 2c. Structural interpretation of Figure 2b. See text.

ing counterclockwise at both terminations which strike more easterly (Plates 1 and 2). Such terminations are interpreted to be horsetails [*Tapponnier et al.*, 1990], implying that movements on the major, NW striking faults must have a left-lateral component in addition to their normal one. Analysis of air photographs reveals similar and additional fault geometries at smaller scales, such as horsetail terminations, right-stepping segmentation, extensional jogs and pull-aparts between faults, all implying a left-lateral component of shear on the NW striking faults [e.g., *Manighetti*, 1993; *Abbate et al.*, 1995]. The southeastern part of the overlap zone is thus characterized by overall oblique faulting with composite movements, both normal and left-lateral, on most NW faults. A different, secondary fault set can be recognized within a NE trending, ~30 km wide strip

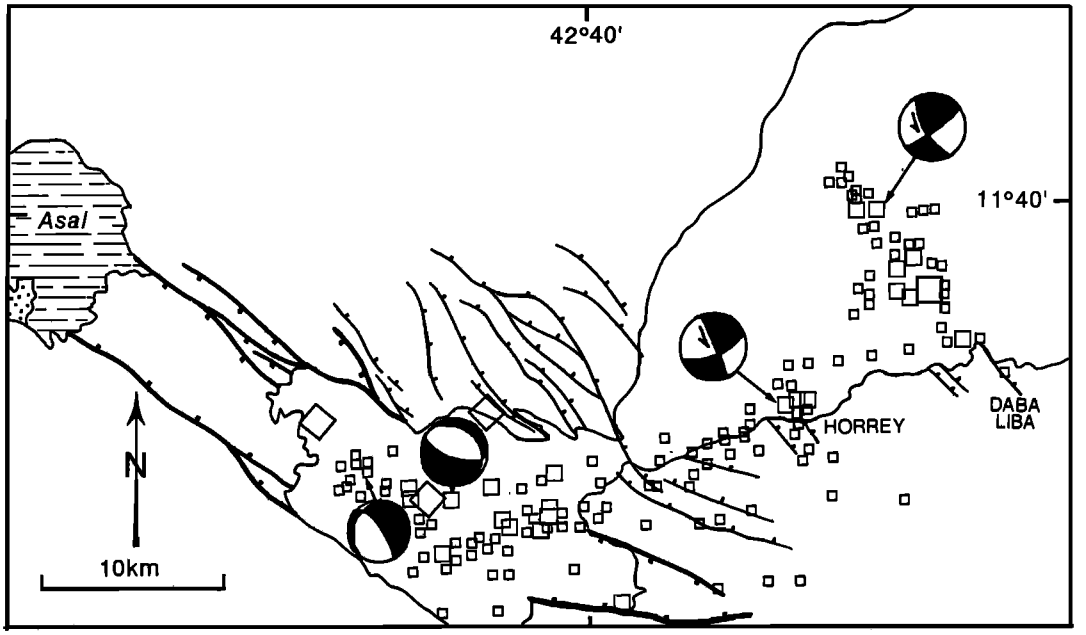

Figure 3. Distribution of seismicity from November 9 to December 31, 1978 [from *Lépine et al.*, 1980]. Faults are from *Manighetti* [1993]; the most recent swarms underly the Horrey and Daba Liba fault scarps; focal mechanisms are compatible with normal-left lateral slip on these faults.

at the southeastern edge of the overlap, along the Ali Sabieh block (Plate 2). These secondary faults strike ~150°-170°. They exhibit a straight, continuous trace over several tens of kilometers, with no or little vertical throw. Small, fresh-looking spatter cones are aligned en échelon along the fault traces, which usually curve counterclockwise at both ends, to join the 130° dominant fault systems. Such a geometry also suggests the existence of a left-lateral component of slip on these 150°-170° secondary faults.

The northwestern part of the overlap, west of a line that would join lake Uddummi (Ub in Plates 1 and 2) to northern Alol, exhibits a smoother overall topography. It is structured by a few approximately thousands of meters high scarps, antithetic, ~ 130° striking, fault systems that slice the Stratoid basalts into four major, horizontal blocks (Gamarri, Isso, Siyyarou, Amhera Rasu; Plate 1) with narrow full grabens in between (Dôbi, Immino, Ab'a). Most fault escarpments (except those bounding the Immino graben) are straighter and more continuous than farther east, and their cumulative geometry does not reveal any clear evidence of oblique movements. The curved trace of the Immino bounding faults and the lack of significant, kinematically related faulting in the surrounding blocks suggest that these latter faults formed with such a curved trace, maybe around a preexistent volcanic center (possibly marked by the Humbab rhyolitic outcrop [*CNR and CNRS*, 1975]). The northwestern part of the overlap therefore seems characterized by predominant normal faulting, without any clear evidence of left-lateral movements in the cumulative Quaternary geometry .

Between the eastern and western parts of the overlap lies an approximately NE trending, 20 km wide strip of closely spaced, more easterly striking (90°-120°), small, normal faults (vertical throws <100 m), running from lakes Uddummi and Gêra to the Alol basins ("Gamarri-Alol zone"; Plate 1 and inset, and Plate 2). These smaller faults connect the major eastern and western fault systems. Their finite geometry does not reveal any clear evidence of composite movements on them. Most exhibit light colored scarplets at the base of their free-face, suggesting they may have been the sites of earthquakes in the last few hundreds years [*Tapponnier et al.*, 1990] (Plate 2).

The cumulative Quaternary geometry of faulting therefore suggests that strain kinematics inside the AMI/MHG overlap is more complex than that expected for purely normal faulting and involves distributed oblique movements. Strain kinematics also seem to vary within the overlap between its southeastern and northwestern parts. In order to quantitatively assess the evolution of strain in that area we performed a detailed kinematic analysis of faults, wherever possible. As Ethiopia was then inaccessible for field work, we mostly worked in the Djiboutian southeastern part of the overlap. Our purpose was to solve, for the maximum number of faults, the following, related three questions: How have the faults been slipping in the last ~2 Myr? At what rates? Have these movements and rates changed with time? Such analyses could therefore only be performed on faults where the four following conditions were met: (1) At least one Quaternary marker clearly offset by the fault could be observed. (2) That offset marker was

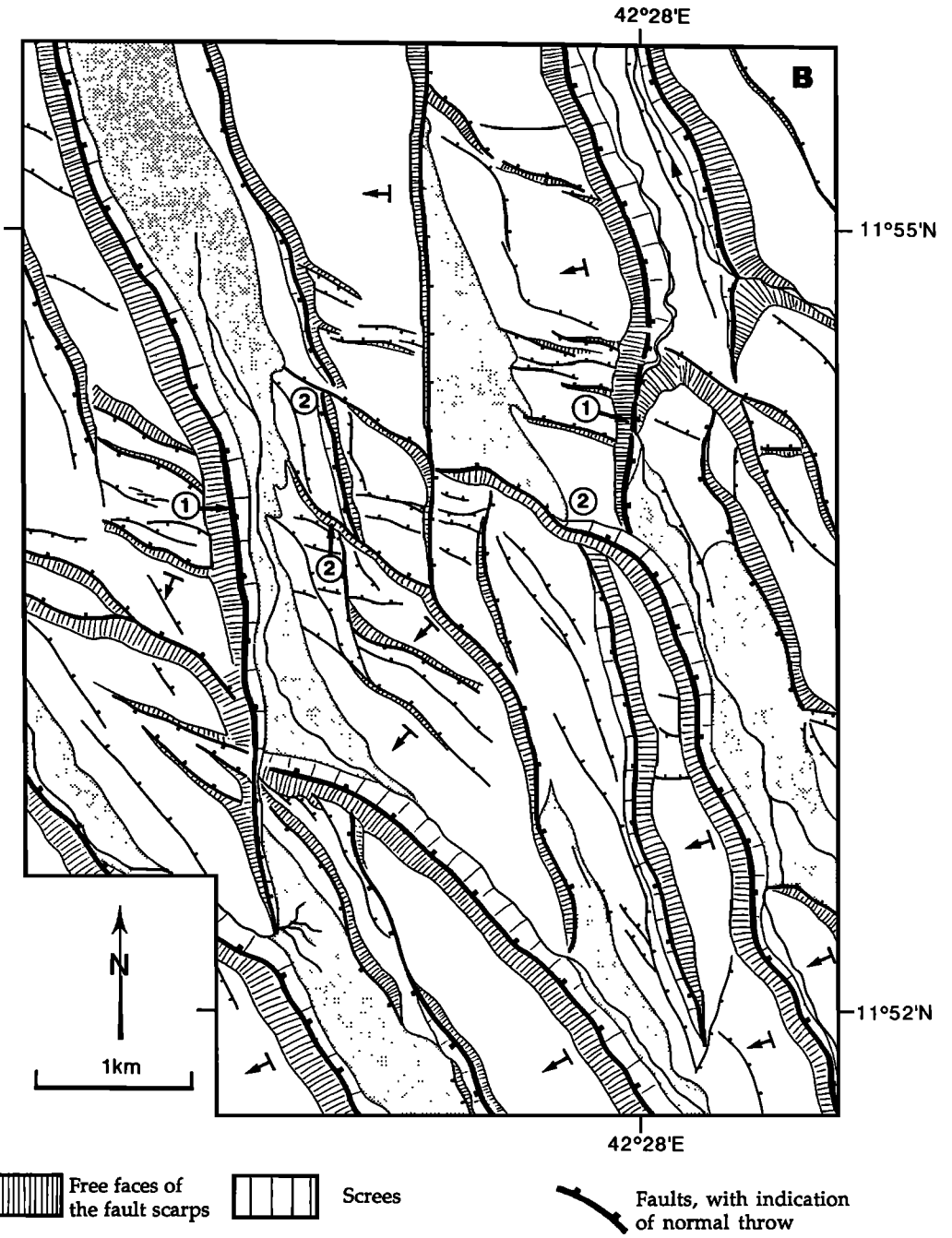

Figure 4. Tectonic map of central part of Mak'arrasou transfer zone based on aerial photo analysis. Most approximately N-S striking normal faults exhibit horsetail terminations indicating an additional left-lateral component of slip.

preserved in the present morphology on both sides of the fault scarp. (3) The marker could be dated. (4) Its offset could be precisely measured. The low rates of erosion and deposition prevailing in Afar make the surface of the Stratoid basalts a good first-order, dated Quaternary marker (1.8 ± 0.4 Ma), likely to provide a well-preserved record of subsequent Quaternary faulting. However, the hanging walls of most major faults are now buried under the sediments that fill the full or half-grabens developed at their base. This led us to search for other Quaternary markers subsequently offset by faults, such as alluvial fans, lacustrine deposits etc. As a result, only a limited number of faults could be subjected to detailed kinematic analyses.

3.3.1. Holocene kinematics. In the following, we present these kinematic analyses for five of the major faults or fault zones in eastern Afar.

3.3.1.1. Der'Ela fault: The Der'Ela fault forms a ~135° striking scarp <80 m high, separating the Der'Ela and the Gaggade depressions (Plate 2). The

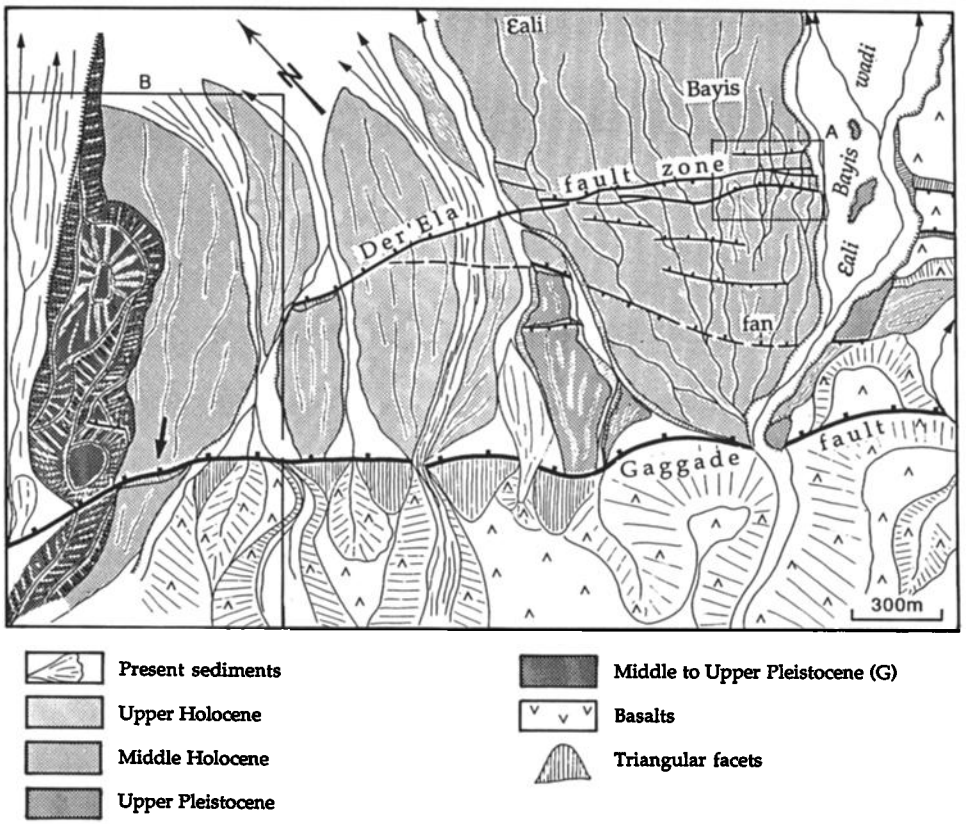

Figure 5a. Geological and structural map of the western termination of the Der'Ela fault (location indicated with black arrow in Plate 2), interpreted from aerial picture analysis. Box A is Figure 5b; box B is discussed in text.

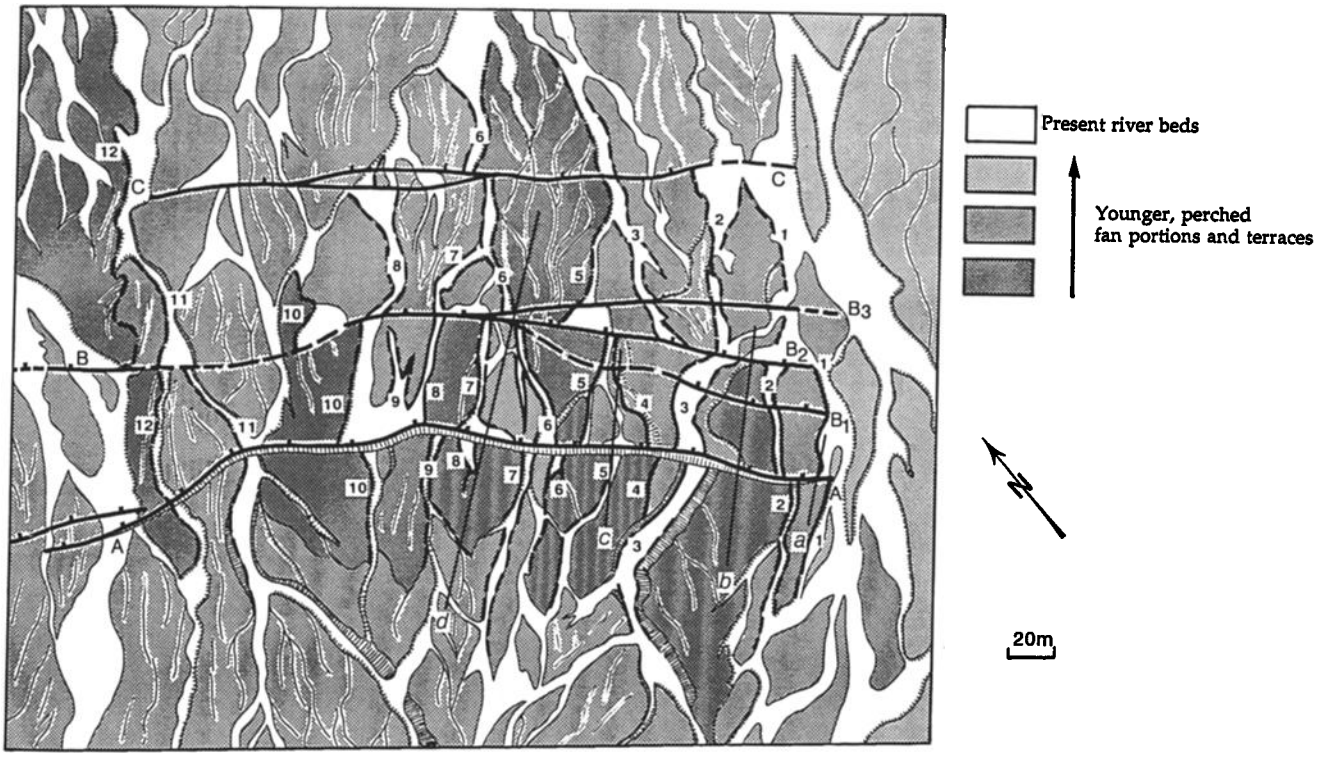

Figure 5b. Morphotectonic map of a close up of Eali Bayis fan portion (box A in Figure 5a), interpreted from aerial picture enlargement. A, B, C are fault scarps; numbers indicate identified river beds (general water flow toward NE); solid lines indicate leveled, topographic profiles, either transverse to scarps (a-d), or along river flanks; dashed lines outline unleveled river flanks.

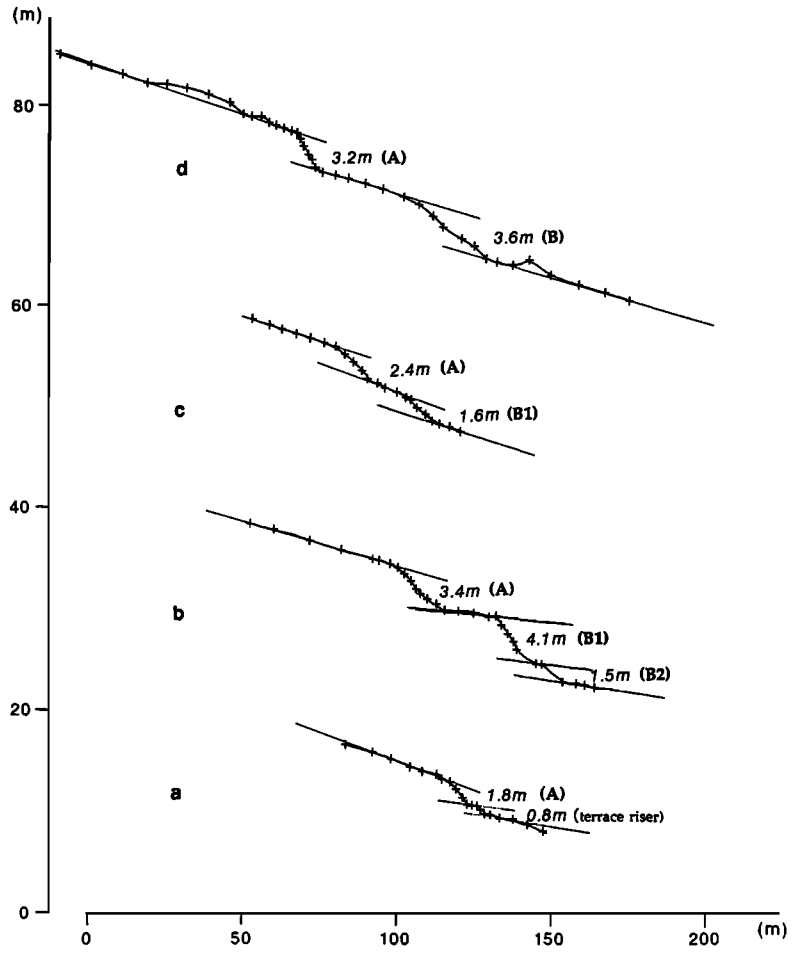

Figure 6a. Topographic profiles a-d perpendicular to A, B1, B2 Der'Ela fault segments (location in Figure 5b). Crosses are measurements; thin straight lines indicate mean terrace slopes; measured vertical offsets are in italic.

scarp is actually made of disconnected, en échelon, 125° ± 5° striking, normal fault segments, a geometry that may suggest a left-lateral component of slip on the Der'Ela fault. The segments join with the major, more northerly striking Gaggade fault farther to the west (Plate 2). For that reason, we refer to the fault zone as the "Der'Ela-Gaggade fault" at and north of that junction and as the "southern Gaggade fault" south of it. Figure 5a based on the analysis of air photographs at a scale of 1:15,000 shows that the westernmost Der'Ela segments offset at least four alluvial fan generations younger than Upper Pleistocene [*Gasse*, 1991] that were deposited at the base of the Gaggade escarpment. These segments form small scarps, the dips of which often reverse along strike, a feature usually observed along steep, strike-slip fault planes. They merge to the west into a unique fault trace.

Figure 5b, mapped from an air photo enlargement (box A, Figure 5a), focuses on a portion of the upper Pleistocene-Holocene Eali Bayis alluvial fan. The fan is cut by three main parallel, NE dipping, normal fault scarps (A, B, C) that strike 130°-135°, nearly perpendicular to the dry river runoff that dissects the fan surface. Most seasonal channels exhibit a left-lateral bayonet pattern as they cross the scarps. Some dry river beds incise the fault hanging walls, although no clear counterparts can be found in continuity in the footwalls. Such overall drainage pattern hence suggests that the channels and river beds have been offset by faults A, B, C, with a combination of left-lateral and normal slip. In order to estimate amounts and rates of such composite movements we leveled a series of topographic profiles across the main A and B scarps (a-d; Figures 5b and 6a) and along some of the offset terrace risers (continuous solid lines; Figure 5b), using a high-precision, digital-recording total station. Numbers 1-12 distinguish the different offset channels that we could identify. We were able to level numerical profiles along only nine of them (1-9; Figures 5b and 6b), following the base of their western banks (western edges are expected to be less eroded than eastern ones, according to the left-lateral sense of offset). Lateral and vertical offset amounts that we could measure across A, B, C, either on the leveled profiles and map (Figures 6a and 6b), or on the photo enlargement (Figure 5b), are listed in Table 2. The results can be summarized as follows:

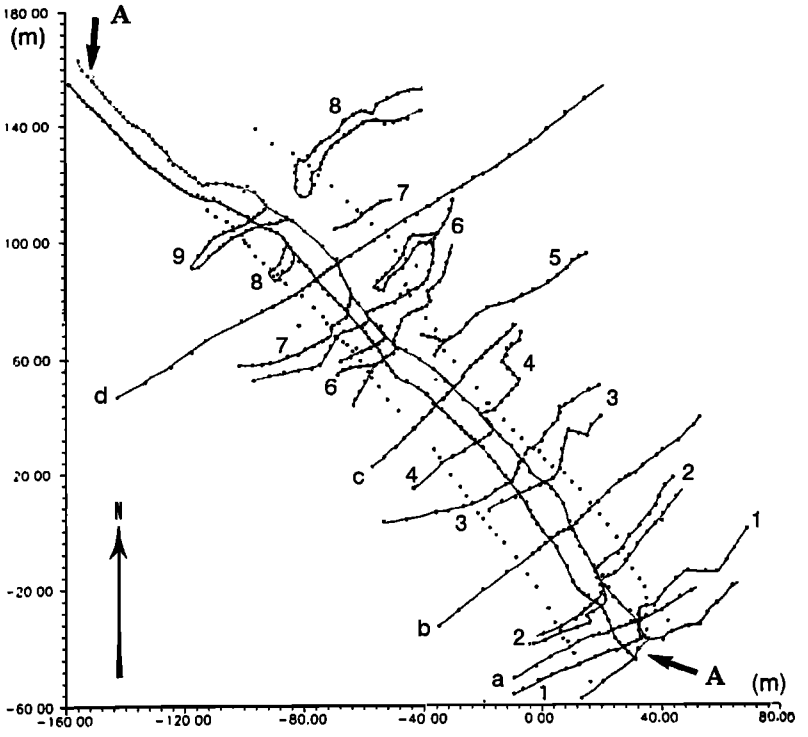

Figure 6b. All leveled profiles in map view (location in Figure 5b). Dots are measurements. Fault A top and base were leveled along strike; a-d are transverse profiles of Figure 6a; 1-9 are profiles leveled along river flanks as identified in Figure 5b.

1. The slip distribution is not uniform across the fault zone. Some segments are mostly dip slip with no clear left-lateral component (e.g., B1 and B3), while others show composite movements. B1 and B3, which splay from B, are likely to mark the near-surface partitioning of the oblique slip that is apparent on B [e.g., *Armijo et al.*, 1986]. For that reason, we only consider the cumulative slip on B.

2. Left-lateral offset amounts seem to vary with fault strike, with maximum lateral slip occurring across 130° striking sections of the scarps, and negligible lateral slip occurring across the more easterly striking sections.

3. Lateral offset amounts also vary along strike on 130° segments. The highest, oldest terraces are typically offset by the largest amounts. This attests to ongoing activity of the fault zone throughout the late Pleistocene-Holocene.

These measurements allow us to characterize slip on faults A and B only. Both faults display similar maximum slip amounts, of the order of 21-22 m and 3-6 m for the lateral and vertical components, respectively (the two ~30 m lateral offset values measured on B along profiles 8 and 10 are likely to be overestimated owing to the weathered pattern of the two channels). The Der'Ela fault segments are arranged en échelon at the regional scale (Plate 2), and the similarity of maximum offset amounts on A and B suggests that the latter are actually themselves arranged en échelon, so that both are likely to slip at the same rate, i.e., at the rate of the whole Der'Ela fault. Their maximum lateral slip amount is up to 4 times greater than their maximum normal one, which suggests that A and B are, at the surface, mainly left-lateral strike-slip faults. Concurrently, the long-term morphology of the Gaggade escarpment, <1 km farther south, with a cumulative, Quaternary vertical throw up to several hundred meters (Figure 5a), reveals that the latter is in contrast mostly normal. In box B of Figure 5a, an upper Pleistocene alluvial fan indeed appears vertically offset by the Gaggade fault (arrow) by a maximum of ~30 m (estimated from field observation), while no evidence of lateral displacement can be found. Note that the Gaggade fault strikes about parallel to the Der'Ela fault segments where it offsets the fan (arrow, Figure 5a). Together these observations suggest that slip around the Der'Ela-Gaggade junction is partitioned at the surface into two subparallel faults with different kinematics that would splay from one single master fault at depth (Der'Ela-Gaggade fault, Figure 6c). According to *Gasse* [1991], the two offset fans formed between ~18 and 12 ka. As offsets are unlikely to remain preserved in the morphology until the alluvial deposition period is over, we deduce that the cumulative offsets were built up in <12 kyr. Taking the measured maximum lateral and vertical offset amounts into account, Figure 6c illustrates a way to estimate the components of slip on the presumed 135° (local direction), single, Der'Ela-Gaggade fault plane at depth in the last 12 kyr [e.g., *Armijo et al.*, 1986]. Assuming that

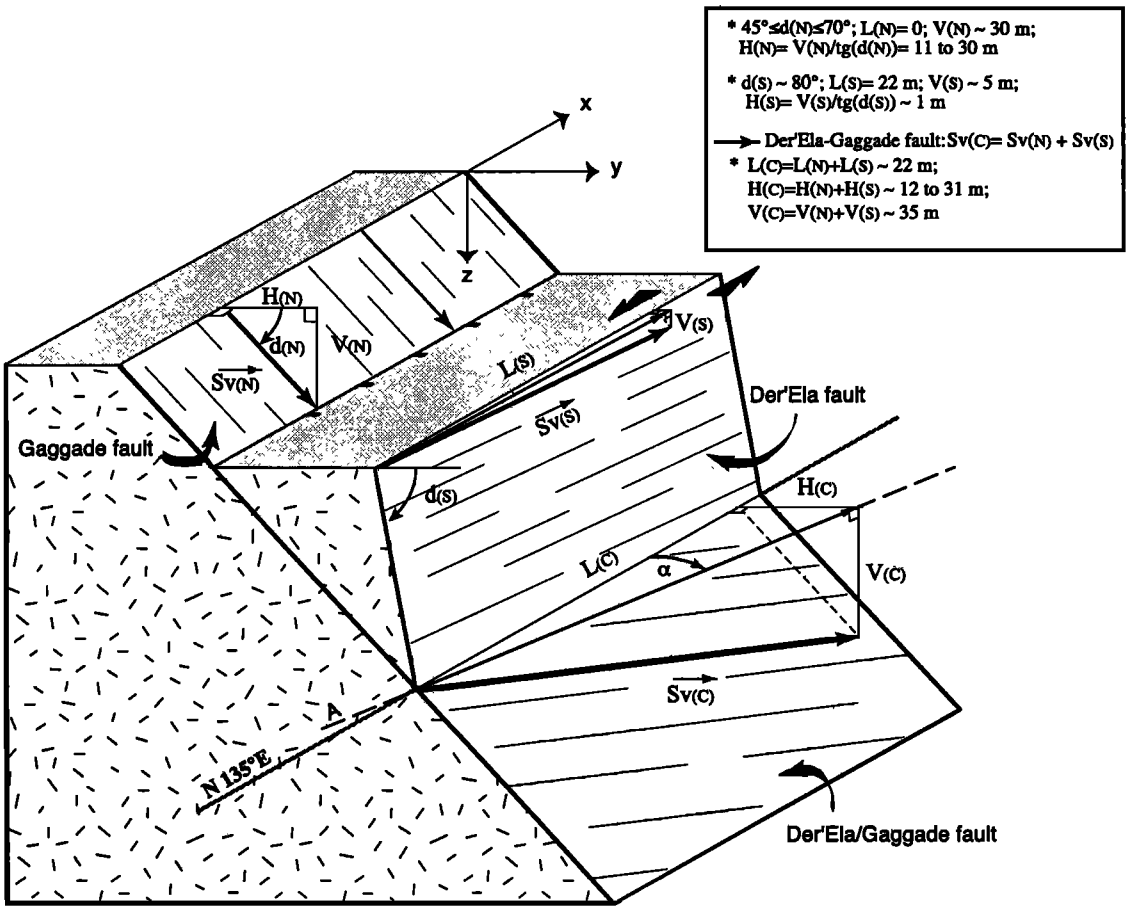

Figure 6c. Model of fault bifurcation [from *Armijo et al.*, 1986]. The coeval Gaggade and Der'Ela faults with parallel traces and different kinematics (normal and left-lateral slip, respectively) splay from single Der'Ela-Gaggade fault at depth. H, V, and L are for horizontal, vertical, and lateral components, respectively; (N), (S), and (C) are for normal, strike-slip, and composite fault, respectively; Sv is for slip vector (thick, solid arrow); d is for fault dip; N135°E is local fault azimuth strike; A is slip vector azimuth. Assumptions and calculations are indicated in the legend.

the dips of the fault plane at depth and of the splaying strike-slip Der'Ela fault plane closer to the surface are between 45°N and 70°N, and ~80°N, respectively (based on field observation), we deduce a slip vector azimuth ranging from N16°W to N10°E (Table 3). The corresponding, minimum, vertical and left-lateral slip rates estimated for the last 12 kyr on the locally 135° striking section of the Der'Ela-Gaggade fault are of the order of 3 and 1.8 mm/yr, respectively (Table 3). The left-lateral slip rate is thus >2 mm/yr on the overall, ~145° striking, Der'Ela-Gaggade fault. We conclude that the Der'Ela-Gaggade fault has been moving fast during the Holocene, with a mean lateral rate almost as great as its mean vertical rate, itself comparable to those measured on the most active faults in Afar [*Stein et al.*, 1991; *De Chabalier and Avouac*, 1994; *Manighetti et al.*, 1998] (Table 3).

3.3.1.2. Southern Gaggade fault: The southern Gaggade fault forms a huge cumulative Quaternary escarpment (several hundred meters to a thousand meters high) bounding the Gaggade depression to the SW over a 40 km length (Plate 2). The fault comprises 10-20 km long, disconnected, normal segments, disposed en échelon along its 145° ± 5° mean direction. In its southeastern section, several en échelon, normal fault scarplets emerge at the base of its cumulative escarpment. These scarplets offset several alluvial fan generations younger than ~30 ka [*Gasse and Fournier*, 1983; *Gasse*, 1991], with a throw which becomes smaller as the fans they offset become younger [e.g., *Manighetti*, 1993]. This attests to ongoing activity of the southern Gaggade fault during the Holocene. Figure 7a focuses on a site where one of the fault scarplets offsets two different fan generations. The older fans exhibit smooth glacis surfaces bearing subparallel traces, which have been identified as ~6 ka, lacustrine regression lines [*Gasse*,1983]. The younger fans do not exhibit leveled surfaces or shoreline traces, implying they were deposited less than 6 kyr ago. All fans appear vertically offset, with no evidence of lateral displacement.

Table 2. Vertical and Left-Lateral Offset Amounts Recorded by Dry River Beds of Figure 5b, Across Faults A, B, C[a]

Fault	River Beds											
	1	2	3	4	5	6	7	8	9	10	11	12
C	...	...	...	...	...	...	...	...	...	...	...	...
	...	...	(0)	...	(0)	(8.8)	...	...	...	...	...	(0)
B3	...	...	...	...	...	...	...	...	...	...	...	...
	(0)	(0)	(0)	...	(0)	...	...	...	...	...	...	...
B2	[1.5?]	[1.5]	[1.5?]	[1.5?]	...	...	...	...	...	...	...	...
	(16.6)	(21)	(22)	...	(21)	...	...	...	...	...	...	...
B1	[4.1?]	[4.1]	[2-4?]	[1.6]	[1.6]	...	...	...	...	...	...	...
	0	0	0	(0)	0	...	...	...	...	...	...	...
Total B	[≥ 5.6?]	[≥ 5.6]	[≥ 3.5-5.5?]	[≥ 3.1]	[~3.6?]	[3.6]	[~3.6?]	...	...	...	...	...
	(16.6)	(21)	(22)	(0)	(21)	(3.9)	(20.7)	(30)	...	(30)	(11.7)	(10.7)
A	[1.8]	[2-3?]	[2-3?]	[2.4?]	[2.4]	[2-3?]	[3.2]	[~3.2?]	[~3.2?]	...	...	...
	8.7	9.8	4.5	6.4	(12.6)	11	20.2	16	(21.4)	(9.7)	(0)	(0)

[a]All measurements are given in meters. Lateral offsets are given with a ± 1 m uncertainty, whereas vertical measurements are estimated at ± 0.5 m at most. River beds and faults are referred as in Figure 5b. Vertical offsets (measured from Figure 6a) are in brackets, left-lateral offsets measured from Figure 5b (aerial picture interpretation) are in parentheses, and left-lateral offsets measured from Figure 6b (numerical profiles) are remaining values. See text.

We leveled five topographic profiles perpendicular to the scarplet, three running on the oldest alluvial surfaces (1-3; Figures 7a and 7b), and the other two on the youngest (4-5). As the oldest fan surfaces are buried under sediments in the hanging wall of the fault, profiles 1 to 3 only allow to estimate a minimum value of the actual vertical throw of the scarplet across these fans. That actual throw would therefore be >26 m (Figure 7b). The fault offsets the younger alluvial fans with a smaller throw. Profile 5 crosses one single scarplet ~5.5 m-high, while profile 4, leveled along a small river bed, reveals three little steps above the expected fault trace (Figure 7b). The three steps exhibit comparable heights, of the order of 1.8 m each. The resulting cumulative throw reaches 5.4 m, a value identical to that obtained on profile 5. This is consistent with a single, continuous fault crossing the fan. The three steps could be the surface expression of three distinct seismic ruptures on the fault.

Gasse [1983] attributes the oldest fan generation to an alluvial deposition period that lasted between ~18 and 12 kyr. The ~26 m high scarplet therefore formed in <12 kyr. At the site of Figure 7, the scarplet appears as a sharp, steep, continuous wall slicing the fan surface. A narrow strip of sparse lacustrine shells (<2 m thick) underlines its upper part (Figure 7b). However, the blocks of basalt with shells scattered in between, as well as those exposed below the shell level, look fresh and unaltered. Stromatolites are nowhere apparent and the shell level does not coincide with any clear excavation level or flat bench which would attest to Holocene lake stagnation against the scarp. Finally, the shell level crops out both in the scarp and in a perpendicular river bank. Together these suggest that the shell strip is actually the apparent section of a shell level interbedded inside the fan rather than a superficial deposit that would have resulted from lake stagnation against the preexisting scarp. As the scarp looks particularly steep and fresh below the shell level (Figure 7b, profiles 1-2), we deduce that at least this ~12-18 m high portion of the scarp formed after the Holocene lake retreat that took place ~6 ka. This implies that the southern Gaggade fault has been moving in the last 6 kyr with a vertical slip rate >3 mm/yr, as the Der'Ela-Gaggade fault did farther north (Table 3). Such a rate implies that the whole, ~26 m high scarp formed in the last 9 kyr, in agreement with the estimated age of the older fans [*Gasse*, 1991]. The younger fans would have formed ~1.8 ka, during the last wet climatic stage identified by *Gasse* [1991].

If we consider that typical seismic events on the southern Gaggade fault make it slip vertically by ~1.8 m, we infer that such events occur on the fault every 600 years at most (Table 3). However, the maximum vertical offsets at the surface either measured or calculated following the few historical earthquakes known in Afar are much smaller, of the order of 0.4-0.8 m high

Table 3. Kinematic Analysis Results for Major Faults Discussed in Text[a]

	Mean Fault Strike	Vertical Rates, mm/yr		Lateral rates, mm/yr			Lateral/Dip Slip Ratio at the Surface	
		Last 1.8 Myr[b]	Last 10-12 kyr[b]	Last 1.8 Myr[b]	Last 1.8 Myr[c]	Last 10-12 kyr[b]	Last 10-12 kyr	Instantaneous (Seismic)
Der'Ela Gaggade	135°-145°	$\geq$ 0.7	$\geq$ 3[d]	($\geq$ 0.5)	2.4 $\pm$ 0.9	$\geq$ 2[d]	0.7[d]	
Southern Gaggade	145°	$\geq$ 1.1	$\geq$ 3[d]	($\geq$ 0.8)	2.4 $\pm$ 0.9	$\geq$ 2[d]	0.7[d]	
Hanle	130°-145°	$\geq$ 1.3 (SE) to 2 (NW)	$\geq$ 1.1 (NW)	?	2.4 $\pm$ 0.9	?		
Goba'ad	110°-120°	$\geq$ 0.6			2.4 $\pm$ 0.9			
Serdo (F1)	140°-153°				3.5 $\pm$ 1			~0.9[d]
Dôbi D1	130° $\pm$ 5°							
D3	125° $\pm$ 5°	$\geq$ 0.45			3.5 $\pm$ 1			0.1-0.2[d]
D5	135°							
Asal Rift Faults	130° $\pm$ 10°		1-4[d,f]			(0.2-1.2)		0.2-0.3

[a]Asal Rift faults indicated for comparison. Mean fault strike given with respect to north, going eastward. Numbers in parentheses are from assumptions discussed in text.
[b]From morphotectonics.
[c]From paleomagnetism.
[d]Best results.
[e]From *Jacques* [1995].
[f]From *Stein et al.* [1991].

Table 3. Continued

	Holocene or Instantaneous Slip Vector Azimuth	Inferred Holocene or Instantaneous Local σ_3 Direction	Age of Fault Scarp Initiation, Ma	Seismic Offsets, m		Recurrence Times, years
				Vertical	Lateral	
Der'Ela Gaggade	N16°W to N10°E[d]		~0.43 to 1.8 (0.22-0.26[d] at NWmost tip)			
Southern Gaggade	N21°W to N05°E[d]		~0.67 to 1.8 (~0.8[d] at SEmost tip)	$\leq$ 1.8	($\leq$ 1.2?)	~150-600
Hanle			1.2 (SE) to 1.8 (NW) (~1.8 to 0.2[d] from NWmost to SEmost tips)			
Goba'ad						
Serdo (F1)	N17°W[d]			0.75[d]	0.65[d] (surface) to 0.7[d] (depth)	200 $\pm$ 50[c]
Dôbi D1		N10°E (NW)		0.45-0.7[d]	?	
D3		to		0.4[d,e]	0.07[d,e]	
D5		N45°E (SE)[d]		0.3[d,e]	0.04[d,e]	
Asal Rift Faults		N20-45°E[d]		0.1-0.5[d,f] (on each fault) ~1.1[d](total synthetic slip)	0.2-0.3 (total slip)	230 $\pm$ 135[d,f]

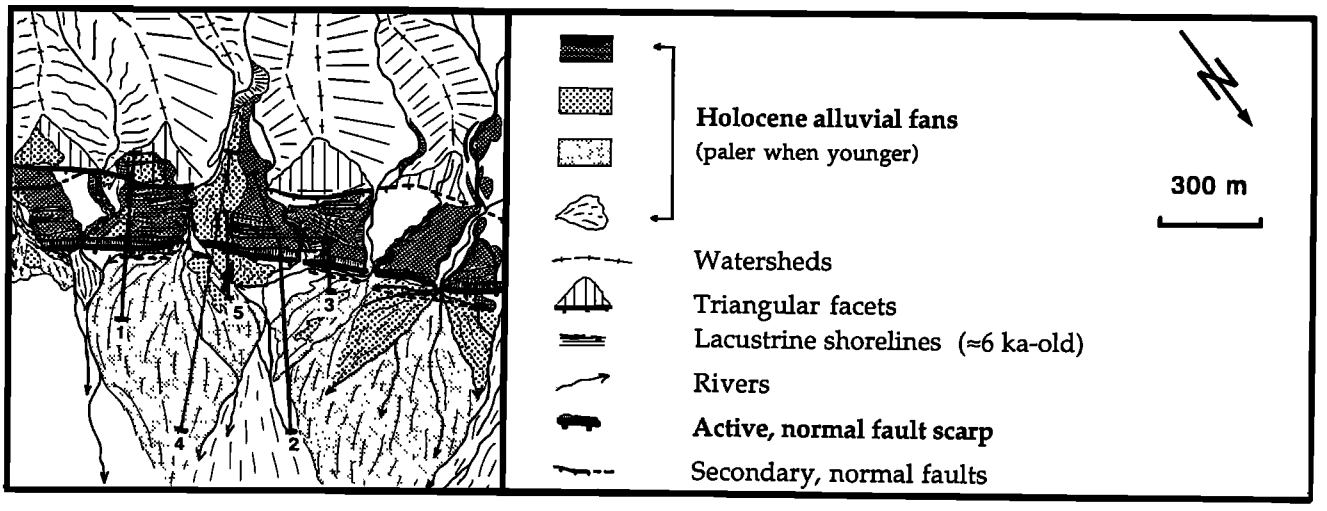

Figure 7a. Morphotectonic map of a portion of southern Gaggade fault, based on interpretation of aerial photos. Location is given in Plate 2; 1-5 are the numerical, topographic profiles that we leveled with a total station across the Holocene Gaggade scarp.

[e.g., *Jacques*, 1995] (Table 3). We therefore believe that smaller events, comparable to the historical ones, are more likely to occur on the southern Gaggade fault, following each other with a recurrence time of the order of 150-300 years. Moreover, our field observations reveal that the different late Quaternary scarplets which underline the whole Gaggade fault zone, were not active at the same time. For instance, the scarplets we could observe ~500 m east of Figure 7a and farther east clearly formed before the last lacustrine stage that subsequently weathered them and do not exhibit any evidence of subsequent Holocene activity. Distinct segments may have therefore been successively activated along the fault zone, making the recurrence time between seismic events probably even smaller at the scale of the whole Gaggade fault.

The covering of the Gaggade fault hanging wall by the present floodplain sediments prevented us from determining the left-lateral component of slip expected from the cumulative Quaternary geometry of the whole fault zone. However, our analysis of aerial photos reveals that lateral and dip-slip components are partitioned in that area along two parallel faults, one, mostly normal, emerging with the Holocene scarplet previously described at the base of the Gaggade cumulative escarpment, and the other, mostly strike-slip, that we observed running parallel, <1 km south of the former, across the escarpment flank (see *Manighetti* [1993] for more details). We measured left-lateral offsets of $\sim 40 \pm 5$ m on drainage channels and watersheds across this fault. Knowing that the oldest fans in the area were deposited between ~30 and 20 ka [*Gasse*, 1991], it is likely that drainage channels could only start incising the fans and then become offset ~20 ka. According to this hypothesis the Holocene, left-lateral slip rate on the uphill fault would be >2 mm/yr, as is the case farther north on the composite Der'Ela-Gaggade fault (Table 3). Considering that the mean dip of the Gaggade fault plane ranges between 60°N and 80°N, a slip vector compatible with both minimum vertical (3 mm/yr) and lateral (2 mm/yr) slip rates, would have an azimuth between N21°W and N05°E (Table 3). If the slip vector is thought to remain constant with time, the typical, maximum, seismic lateral slip on the Gaggade fault could reach 1.2 m (Table 3).

3.3.1.3. Hanle fault: The Hanle fault forms an escarpment that bounds the Hanle depression to the SW, several hundred meters to ~1 km high, and striking ~130° (Plate 2). Its hanging wall is blanketed under the present sedimentary fill of the Hanle plain, preventing detection of any lateral offset. At some places, a scarplet emerges at the base of the cumulative escarpment and offsets several late Quaternary alluvial fan generations. In the northwestern section of the fault, that scarplet forms a normal step dipping NE, appearing as a 130°-145°, straight, continuous, white trace between basalts and sediments (Figure 8, location in Plate 2). It offsets at least four alluvial fan generations, all younger than 30 ka [*Gasse*, 1983]. In particular, the fault offsets the Gadal fan (deposited between ~30 and 12-10 ka [*Gasse*, 1991]), with a normal scarp striking ~140°. Another scarp, smaller and more subdued, crosses the downstream, northeasternmost part of the fan (Figure 8). However, this smaller scarp strikes ~180°, parallel to the Holocene lacustrine shorelines and is likely to be a lacustrine erosion bench. The vertical throw of the 140° striking scarp, measured on a digital topographic profile levelled across the fan, is ~11 m, whereas that of the lacustrine bench is only 2.5 m. We deduce that the northwestern section of the Hanle fault has been moving in the last 10 kyr with a minimum vertical slip rate averaging 1.1 mm/yr (Table

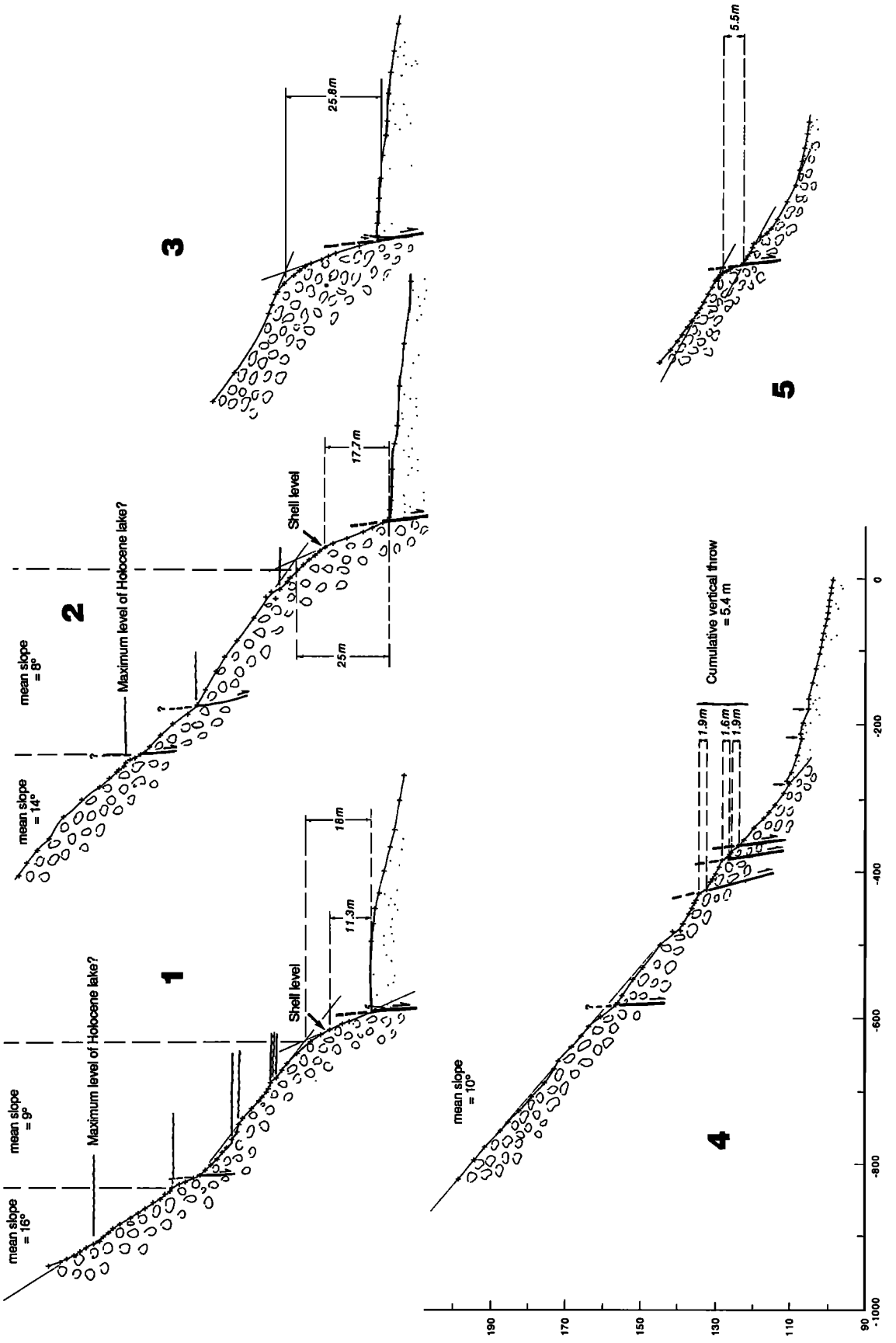

Figure 7b. Profiles 1 to 5 projected perpendicular to the Holocene Gaggade scarp. Crosses are measurements; thin lines indicate mean slopes; measured vertical throws are in italic; wavy lines indicate Holocene lake shorelines.

3). The Gadal fan does not seem to have recorded any evidence of left-lateral slip. SPOT image and air photo analyses reveal that this fault does not show any clear evidence of Holocene tectonic activity in its southeastern section (approximately SE of 42°E longitude; Plate 2).

3.3.1.4. Serdo fault zone: On the basis of field observations by *Gouin* [1979] and *McKenzie et al.* [1970], *Tapponnier et al.* [1990] showed that the 1969 Serdo earthquakes implied, at the surface, normal, left-lateral movements on at least two ~140° striking faults. However, the fault plane solutions of the two main shocks imply pure left-lateral faulting at depth, on near vertical planes striking 153°, ~15°-20° more northerly striking than the regional faults at the surface. Left-lateral and vertical offset amounts measured on the main, observed surface break (F1) [*Gouin*, 1979] are of the same order (65 and 75 cm, respectively; Table 3). Making the assumption that the 140° striking fault plane F1 dips ~70°N at the surface, we deduce that a compatible slip vector would have a N17°W azimuth (Table 3). If we suppose that most slip occurred on F1, then the total left-lateral seismic displacement on the 153° striking, near-vertical fault plane at depth had to be of the order of 70 cm (Table 3).

3.3.1.5. Dôbi fault zone: The Dôbi fault zone comprises two main antithetic, ~120°-130° striking normal fault systems that bound the Dôbi graben (D1-D2 to the SW, D3-D4 to the NE, according to *Jacques* [1995]), associated with numerous smaller ones striking slightly more easterly (~100-120° [e.g., *Jacques*, 1995]) (Plates 1 and 2). The two main bounding fault systems form high, steep escarpments (~600-800 m high, ~70°-80°-dip) bounding the Dôbi graben. The southwestern escarpment is composed of three main segments arranged in a left-lateral en echelon pattern with a mean trend of 140°. This escarpment is underlined in its SE section by a set of large recent alluvial fans that are, in some places, offset by scarplets likely to be the Holocene expression of the main fault. Unfortunately, we were unable to reach these scarplets in the field and therefore cannot specify the late Quaternary kinematics of the Dobi fault zone.

A series of destructive earthquakes, three with magnitude up to 6, occurred in that area in August 1989. The epicenters of the main shocks (August 20, 1989, 11.16 UT, m_s = 6.3; 13.26 UT, m_s = 6.1 and August 21, 1989, 01.09 UT, m_s = 6.2) and more than 600 recorded aftershocks spread over an area ~70 km long and 20 km wide, inside the strongly faulted zone extending between the southern Dôbi and Der'Ela-Gaggade bounding faults [*Jacques*, 1995; *Noir et al.*, 1997]. The earthquake sequence produced ground deformation that we could observe and analyze mostly in the SE half of the Dôbi graben. By combining detailed seismological (accurate epicentral relocations, focal mechanism determinations) and tectonic analyses (precise mapping and analysis of surface ruptures, overall tectonic study of the graben), together with Coulomb stress variation modeling, *Jacques* [1995] and *Jacques et al.* [1996] showed how seismic slip during the Dôbi sequence incremented long-term cumulative Quaternary deformation. They found that the two main shocks broke the two southeastern sections of the main SW Dôbi bounding fault (D1) by total vertical slip amounts estimated at depth as being ~45 cm (on D1a) and 70 cm (on D1b, Table 3). Slip on D1 was distributed, at the surface, on several, antithetic, parallel, smaller faults. The sequence also broke about a dozen other faults along the edges of, or inside, the graben, which, all in all, slipped vertically by ~25 to 80 cm. Among them, several 110°-120° trending, preexisting faults moved with a small component of right-lateral slip, while other faults with a strike greater than ~130° including D1, coevally slipped with a small component of left-lateral slip. Total vertical slip could be precisely measured on the northern Dôbi bounding fault (D3) and on the Eounda Dôbi fault (D5 for *Jacques* [1995], E. D. F in Plate 2), and the corresponding left-lateral component inferred from slickenside measurements (80°SE pitch) and slip vector determination, respectively [e.g., *Jacques*, 1995] (Table 3). The local extension directions average N10°-30°E and N30°-45° in the northwestern and southeastern parts of the Dôbi graben, respectively. On average, seismic normal faulting propagated ~35 km northwestward along the graben in ~20 hours.

3.3.2. Cumulative Quaternary kinematics. In order to understand the relationships between Holocene and Quaternary kinematics we measured three NE trending topographic sections across southeastern Afar (Plate 2 and Figure 9). Most major faults are associated with southwestward tilting of large blocks of Stratoid basalts. Assuming that the major fault dips (β) range between 45°N and 80°N at the surface (maximum value observed on the field) and that the tilt amounts (α) measured at the surface remain constant at depth, we obtain a first-order estimate of the true cumulative Quaternary vertical throws (T_t) of the major faults, where the profiles intersect them (Figure 9a). Cross section A-B suggests that the Der'Ela-Gaggade fault scarp is actually ~1200-1300 m high and is partly hidden by ~600-700 m thick sediments (Figure 9b). The southern Gaggade depression may be filled by ~1500 m thick sediments (section E-F), with an actual throw up to 2 km on the escarpment. Cross sections A-B and C-D suggest that the true vertical throw of the cumulative Quaternary Hanle escarpment may reach ~3.6 km toward the NW, and ~2.4 km in the SE. Up to 2 km of sediments fill the Hanle depression, making it the deepest in central Afar. Finally, Figure 9b suggests that the Goba'ad fault, along which no late Quaternary offset marker could be observed, may have a cumulative vertical throw ~1.1 km high, hence hidden by ~600 m thick sediments.

Knowing that all these cumulative throws have been built up in the last ~1.8 Myr (mean age of the Stratoid surface that they offset), we can use them to deduce

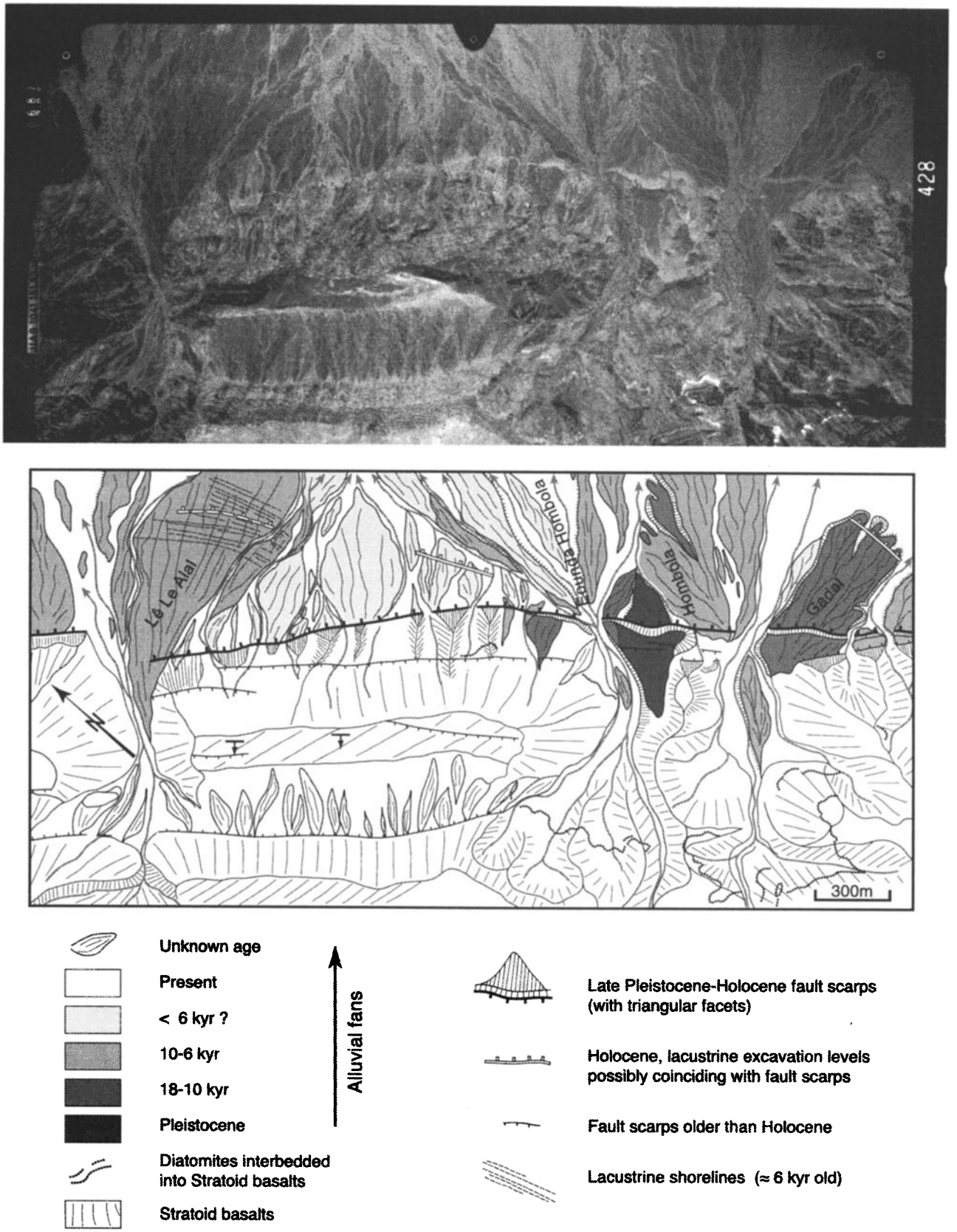

Figure 8. (top) Aerial photo of NW portion of Hanle fault escarpment (initial scale 1:15,000). (bottom) Morphotectonic interpretation of aerial photo above. See text.

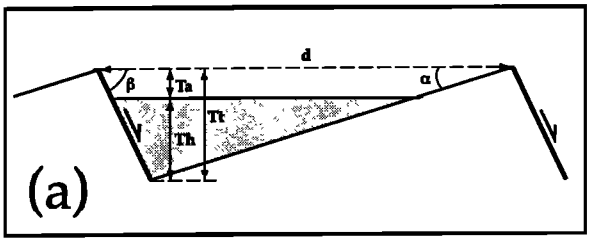

Figure 9a. First-order geometry of block tilting related to faulting in central Afar. Sediments are shaded; parameters used in calculations of Figure 9b are indicated; α is block tilt angle; β is fault dip; d is distance between successive faults; T_a is apparent vertical fault throw; T_h is hidden throw; and T_t is total vertical throw.

the minimum vertical rates at which the major faults must have been slipping for the last ~1.8 Myr in order to build them. We find that the Der'Ela-Gaggade and the southern Gaggade faults must have been slipping for that period of time with a minimum vertical rate of the order of 0.7 and 1.1 mm/yr, respectively, hence ~3-4 times slower than during the Holocene (Table 3). The Hanle fault would have been slipping at a faster rate, of 1.3 to 2 mm/yr from SE to NW, hence about twice as fast as during the Holocene. The Goba'ad fault would have been slipping at a minimum rate of the order of 0.6 mm/yr (Table 3). Finally, with apparent escarpments of ~600-800 m [*Jacques*, 1995] the major bounding Dôbi faults would have been slipping at rates much greater than 0.45 mm/yr. Furthermore, if we assume that the lateral-/dip-slip ratios remained constant with time, we

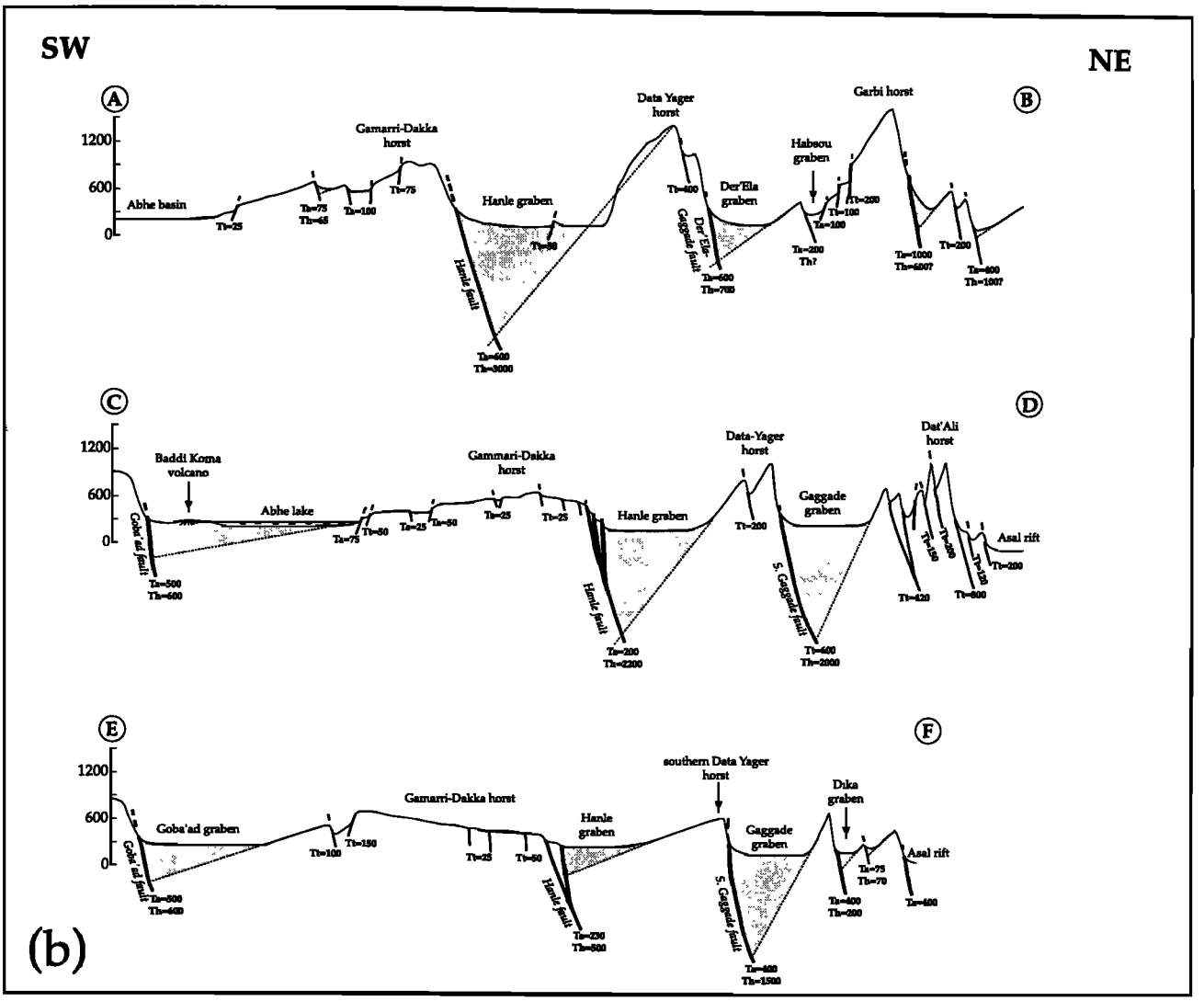

Figure 9b. Tectonic interpretation of topographic cross sections A-B, C-D, and E-F located in Plate 2 (based on Institut Géographique National (IGN), 1:100,000 topographic maps of Republic of Djibouti); vertical exageration is 10; symbols and parameters as in (a); thin dotted lines indicate mean slope of tilted block surfaces; thicker lines are faults; first-order throw values are given in meters.

deduce that the Der'Ela-Gaggade fault also slipped left laterally at a minimum average rate of ~0.5 mm/yr, producing a cumulative left-lateral offset of at least 900 m. Similarly, the southern Gaggade fault would have slipped left laterally by at least 1.4 km since 1.8 Ma, at a minimum rate averaging 0.8 mm/yr.

However, one may rather assume that slip rates remained constant with time, equal to the better estimated Holocene values. If so, we deduce that the Der'Ela-Gaggade and southern Gaggade faults (along cross sections A-B and E-F, respectively) have started to offset the Stratoid surface only ~430 and 670 kyr ago, respectively. The sharp, fresh morphology of the overall Der'Ela-Gaggade/southern Gaggade escarpment (i.e., the overall Gaggade escarpment) supports this assumption. The corresponding cumulative lateral offsets would average ~0.9 and 1.4 km, respectively. Similarly, the Hanle fault would have started to offset the Stratoid surface ~3 to 2 Myr ago at the earliest, from northwest to southeast. These ages being older than the mean age of the offset Stratoid surface, one may conclude that this assumption is unlikely. However, the estimated Holocene rate being a minimum value, we actually cannot reject it. To go further, we need to consider the fact that the highest, northwestern section of the Hanle cumulative escarpment must have been built in the last 1.8 Myr. This implies that this portion of the fault moved with a minimum vertical slip rate of the order of 2 mm/yr, comparable to the Holocene slip rate on the whole Gaggade fault system. If this rate kept constant along strike, we infer that the fault started to offset the Stratoid surface in its southeastern section (where cross section C-D intersects it) at about 1.2 Ma (Table 3).

Finally, we note that the small component of vertical slip measured on the predominantly strike-slip, Holocene Der'Ela fault scarp (~3-6 m in the last 12 kyr) would imply, with the assumption of constant slip rates, that the Der'Ela fault would have a Quaternary cumulative scarp ~100-200 m high, i.e., hardly higher than its present, apparent throw. The sediment thickness might therefore be strongly variable into the Der'Ela and the Gaggade depressions.

3.3.3. Synthesis and discussion Our kinematic analyses show that the eastern part of the overlap is sliced by several major, ~135° ± 10° striking faults which were both active and oblique during the Quaternary, characterized by left-lateral components of slip almost as important as their normal ones (lateral-/dip-slip ratios between ~0.7 and 0.9; Table 3). Vertical and lateral slip rates were fast, >0.45-3 mm/yr and >0.5-2 mm/yr, respectively (Table 3).

Holocene vertical and lateral rates are about the same on both the NW and SE sections of the overall Der'Ela-Gaggade/southern Gaggade fault, on average 3 and 2 mm/yr, respectively, which suggests that the overall fault has been slipping in the same way and at the same rates along its entire length, at least during the Holocene (Table 3). On the other hand, the Quaternary rates deduced from the assertion that the long-term escarpments must be younger than ~1.8 Ma appear as variable and systematically smaller than the Holocene rates. We see no way to account for this other than underestimation of slip rates. We therefore believe that slip rates could well have remained constant with time along the fault, equal to their better constrained Holocene values. This implies that the Gaggade fault escarpment becomes younger along strike in a northwestward direction, having started to offset the Stratoid surface at ~0.67 to 0.43 Ma, from cross section E-F to cross section A-B (Plate 2). We infer that the ~ 30-35 km long portion of the Gaggade fault between the two cross sections has propagated northwestward in a short time span of ~250 kyr, at a minimum rate averaging 12-15 cm/yr. This fast rate is comparable to the propagation rates estimated for some other faults and fault systems in Afar [e.g., *Manighetti et al.*, 1997, 1998, 2001]. If we consider that the whole Gaggade fault kept propagating in such a direction and at such a rate along its entire length, the fault would have started to offset the Stratoid basalt surface ~800 kyr ago at its southeastern tip (located ~15 km farther SE from cross section E-F), kept propagating northwestward in the following 550-600 kyr to reach its present length (~70-75 km), and then stopped propagating ~220-260 kyr ago. We note that although the Gaggade fault may no longer be increasing in length, it is still in the process of growing vertically. The slip partitioning that we observe between its normal and strike-slip Holocene components could be a consequence of the fact that this still active fault does not lengthen any more.

The Holocene vertical rate on the Hanle fault seems to be underestimated, since it would imply that the fault started to offset the Stratoid surface at ~3 Ma, whereas this surface is only ~1.8 Myr old. Hence, for that period of time and at least in its highest NW section the Hanle fault must have been slipping at a minimum vertical rate averaging 2 mm/yr. In keeping with the assumption that slip rates remained constant with time along the entire fault length, we infer that the ~20 km long portion of the fault between cross sections A-B and C-D (Plate 2 and Figure 9b) has been propagating southeastward from ~1.8 to 1.2 Ma, at a minimum rate averaging 3 cm/yr. If we assume that the whole Hanle fault kept propagating southeastward with time at such a rate, we infer that the fault initiated at its NW termination at ~3 Ma, and stopped propagating at ~1.2 Ma at its present SE termination (where the fault actually appears to be crosscut by a set of more oblique faults, see Plate 2). The inferred initiation age is again older than the Stratoid surface. This may suggest either that the fault propagated in both directions from a point located due west of cross section A-B or that the vertical slip rate of the Hanle fault was actually >2 mm/yr, which we believe instead. If we consider that the present total length of the fault (~50 km) results from its southeastward propagation in the last 1.8 Myr

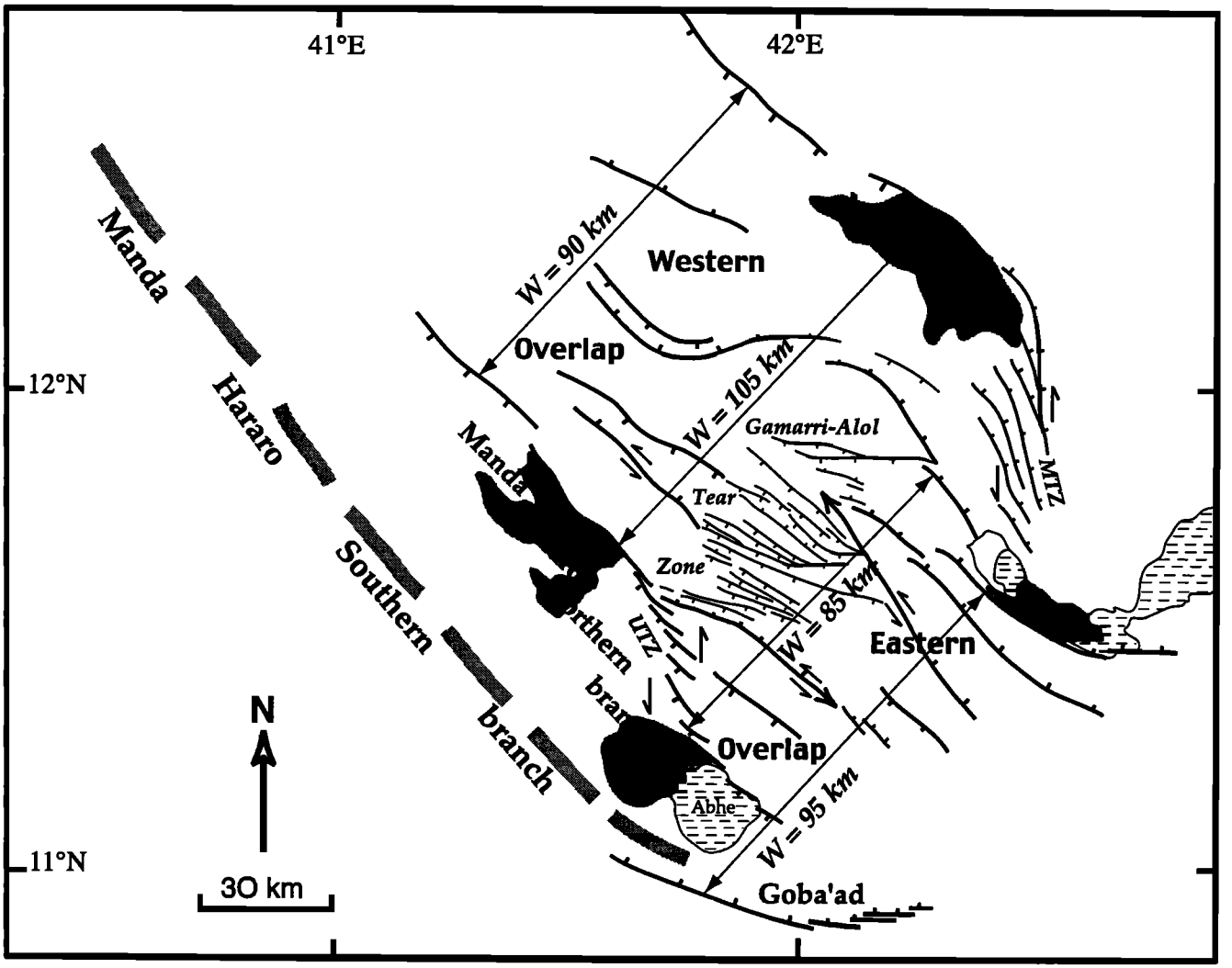

Figure 10. Tectonic sketch of Asal Ghoubbet-Manda Inakir/Manda Hararo-Goba'ad overlap. Rifts are shaded, darker where younger; both southwestern and northeastern edges of overlap are made with two active, volcano-tectonic segments (dark shading), separated by a northerly striking fault bundle forming a left-lateral echelon (UTZ for Uddummi transfer zone, and MTZ for Mak'arrasou transfer zone, respectively). Overlap width (W) remains constant between these two edges. Eastern and western faults are separated by the Gamarri-Alol tear zone. Double arrows indicate left-lateral components of slip where observed on major faults, and arrows on faults indicate their propagation direction.

at a rate of 3 cm/yr, we infer that the fault initiated at its present NW tip ~1.8 Myr ago, then kept propagating southeastwards to its present SE tip, where it stopped ~100-200 kyr ago.

In any case, the major Gaggade and Hanle faults, although close neighbors, propagated in opposite directions inside the overlap. In addition, the relative ages of the Gaggade and Hanle faults suggest a northward migration of tectonic activity inside the overlap, with present strain localization on the northernmost faults.

We have estimated the total Quaternary vertical throw accommodated by the major identifiable faults along the three NE striking topographic sections of Figure 9b. The summed throw averages 7.2, 7.7, and up to 5 km on the three sections, respectively, which leads to a similar minimum cumulative Quaternary vertical slip rate on the three sections of the order of 3-4 mm/yr. With an average fault dip of ~60°-70°N, this rate implies that the eastern overlap zone has been stretching since 1.8 Ma at an horizontal rate larger than 1-2.5 mm/yr. The overlap would have absorbed ~7 to 15% (and probably slightly more) of the total extension imposed at the plate boundaries (~16 ± 1 mm/yr [e.g., *Chu and Gordon*, 1998]) in the last 1.8 Myr.

The eastern part of the overlap has therefore been absorbing a constant, uniform, total strain amount in the last 1.8 Myr, but its distribution was not uniform within the overlap, either in time or space. Strain was distributed on several major NW striking parallel oblique faults, some of them grew and lengthened over sev-

eral tens of kilometers in opposite directions. Strain also migrated northward with time, so that most recent deformation now seems concentrated on the Gaggade fault. Finally, the great variability of local slip vector azimuths inside the overlap, which, all in all, appear more northerly striking than the Arabia-Nubia or the Danakil-Nubia plate motion vectors imposed at the plate boundaries [e.g., *Chu and Gordon*, 1998], implies that strain kinematics also varies within the overlap.

Figure 10, which sketches major faults and rifts in central Afar, shows that the width of the whole overlap remains approximately constant from east to west, of the order of 90-100 km. This suggests that the western part of the overlap has spread at the same horizontal rate than the eastern part. The geometry of the southern edge of the overlap ("Manda Hararo northern branch" and SW dipping bounding fault system) parallels that of its "Asal-Mak'arrasou-Manda Inakir" northern edge, both exhibiting a "Z" pattern made of two short rift segments (in dark shading) separated by an elongate, northerly striking, en echelon fault zone (UTZ for Uddummi transfer zone, and MTZ for Mak'arrasou transfer zone). Such a Z pattern also seems to characterize the geometry of faulting in central Afar, with the western faults appearing shifted northward with respect to the eastern faults, across the Gamarri-Alol zone. Along the Aden rifting zone, such a Z pattern has been shown to result from the ridge propagation process, which occurred through alternating phases of westward rift propagation and northward strain jumps [e.g., *Manighetti et al.*, 1998]. The Z distortion of the whole overlap suggests that the whole area has recorded the time-space evolution of the Aden propagator, the UTZ developing simultaneously with the MTZ, while the western faults were either forming farther north or being shifted northward, as a result of the overall northward migration of strain. In other words, faulting in the western part of the overlap seems to have migrated northward to "follow" the overall northward propagation of the "driving" Aden plate boundary. The "Gamarri-Alol zone" could be a tear zone, where the basaltic blocks and faults would have broken to accommodate their overall northward migration.

4. Paleomagnetism

Sites were selected based on their location inside the distinct deformation zones described above, on their accessibility in the field, and on field evidence that outcrops were both in place and unaltered. A total of 112 sites were sampled, representing a set of 163 distinct basaltic flows (Figure 11). In the following, each flow is taken as a statistical unit. However, in a very few cases where we have both strong stratigraphic and paleomagnetic (indistinguishable mean directions) arguments to ensure that some of the flows were extruded at almost the same time, we average these "similar" flows into a single unit.

Sampling was designed with two goals in mind: Dense spatial coverage was necessary to further constrain the geographical pattern and extent of rotational deformations discovered by *Courtillot et al.* [1984], and stratigraphical (temporal) coverage was necessary to ensure proper averaging of secular variation. Eighty-six sites (M01 to M36, I01 to I23, I43 to I47, BG01 to BG22) were sampled along tracks and trails, most of them at the base of fault scarps or deep canyons. At the top of the high fault scarps between Galafi and Bahlo, which is inaccessible by jeep, 19 sites (I24 to I42) were reached by helicopter. A succession of nine flows were sampled for magnetostratigraphic purpose along the steep wall of a canyon incising the Gamarri plateau (star, Figure 11). Six "supersites," gathering a total amount of 31 flows, were also sampled for magnetostratigraphic study, in the gulf basalts of the North Ghoubbet area (S1 to S6; note that only the analyses of supersites S2, S3, and S5 were performed for the present study).

At least four and up to eight cores (on average seven cores) were taken from each basaltic flow with a portable drill, over an area of a few tens of square meters. More than 1000 cores were collected. Whenever possible, cores were oriented both with a solar and a magnetic compass. For each core, and then for each flow, a local "bedding" surface was measured, both directly on flow surfaces and with combined measurements of apparent dips in the landscape. Air photo analysis usually helped decide whether tilt was original or tectonic (though this was not always easy; see discussion). Seventeen out of the 163 sampled flows belong to the Dahla basaltic series, 76 to the Stratoid basalts, 17 to the northern recent basalts, and 53 to the gulf basalts unit (see section 2 on ages).

4.1. Laboratory Work

The experimental procedure essentially follows that already used by *Courtillot et al.* [1984] and is discussed in some detail by *Manighetti* [1993]. At least two (more often three) specimens of standard size were cut from each core in the laboratory. Magnetic measurements were carried out in the magnetically shielded room at the Institut de Physique du Globe de Paris, with a computerized Molspin Spinner magnetometer. The alternating field (AF) demagnetizations were done with a GSD1 Schönstedt demagnetizer, and the thermal demagnetizations were done with a laboratory-built furnace. A pilot study, involving detailed stepwise thermal and alternating field demagnetization of selected specimens, was undertaken in order to specify the components of magnetization, to determine the nature and properties of the carriers of these components, and to develop a routine paleomagnetic analysis scheme for the large number of remaining samples. All samples were analyzed using principal component analysis. Data analysis techniques are as given by *Courtillot et al.* [1984], with the addition of the great circles analysis of *McFadden and McElhinny* [1988] in some cases.

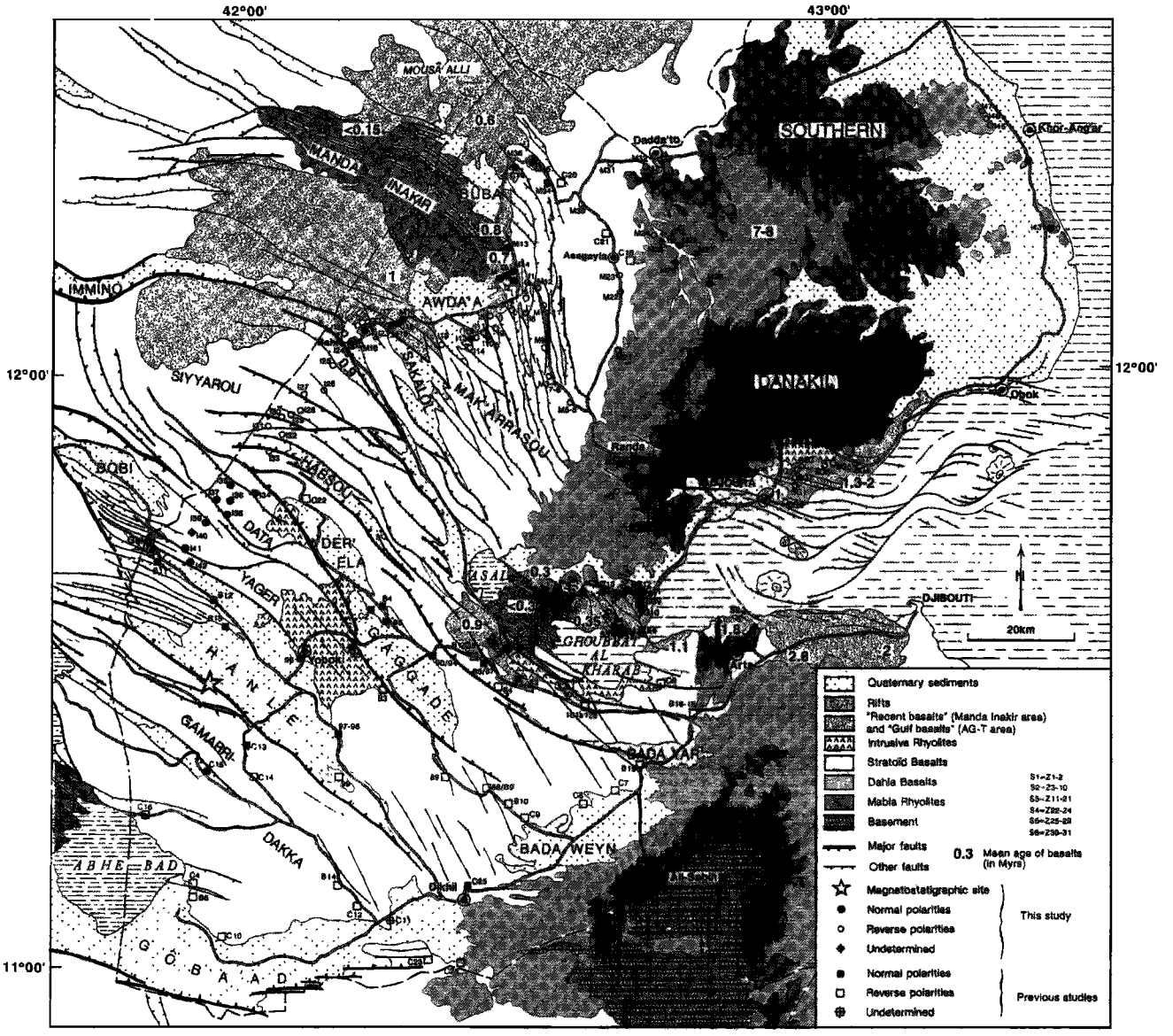

Figure 11. Simplified geological and structural map of eastern Afar, showing all paleomagnetic sites sampled by us and by *Courtillot et al.* [1984]. Ages are averages, most from present study.

Selected cores yielded two specimens, allowing direct comparison of AF and thermal demagnetization (Figure 12).

Samples can be divided in two groups, according to their behavior during thermal demagnetization. For most specimens having a natural remanent magnetization (NRM) intensity close to 5 A/m (overall NRM average value), distinct magnetic components could be isolated. In more than half of these samples, a soft, apparently random component was removed by 120-400°C, followed by univectorial demagnetization up to 575 or 580°C (see MO5-08A, Figure 12). For the remainder, there was overlap of two components, up to the highest temperature steps (see M33-03A, Figure 12). For specimens having a high NRM intensity (>15 A/m), thermal demagnetizations often did not succeed in isolating the different components. Most of the time, only a single high unblocking temperature component could be isolated (I23-07B, Figure 12). However, the intensity and random direction of that component suggest that it might be due to lightning. In one out of five cases, however, two components with overlapping blocking temperature spectra could be identified (M31-08A, Figure 12). AF demagnetizations generally confirmed and in some cases complemented the thermal demagnetizations. AF demagnetizations often led to less noisy diagrams and allowed better separation of components. This is particularly clear in the cases of sample M33 and I23 (Figure 12) where the large normal overprint totally masked a small reverse underlying component in the thermal treatment. As a result of the pilot study, most remaining samples were subjected to alternating field demagnetization only.

The distribution of NRM intensities, computed for

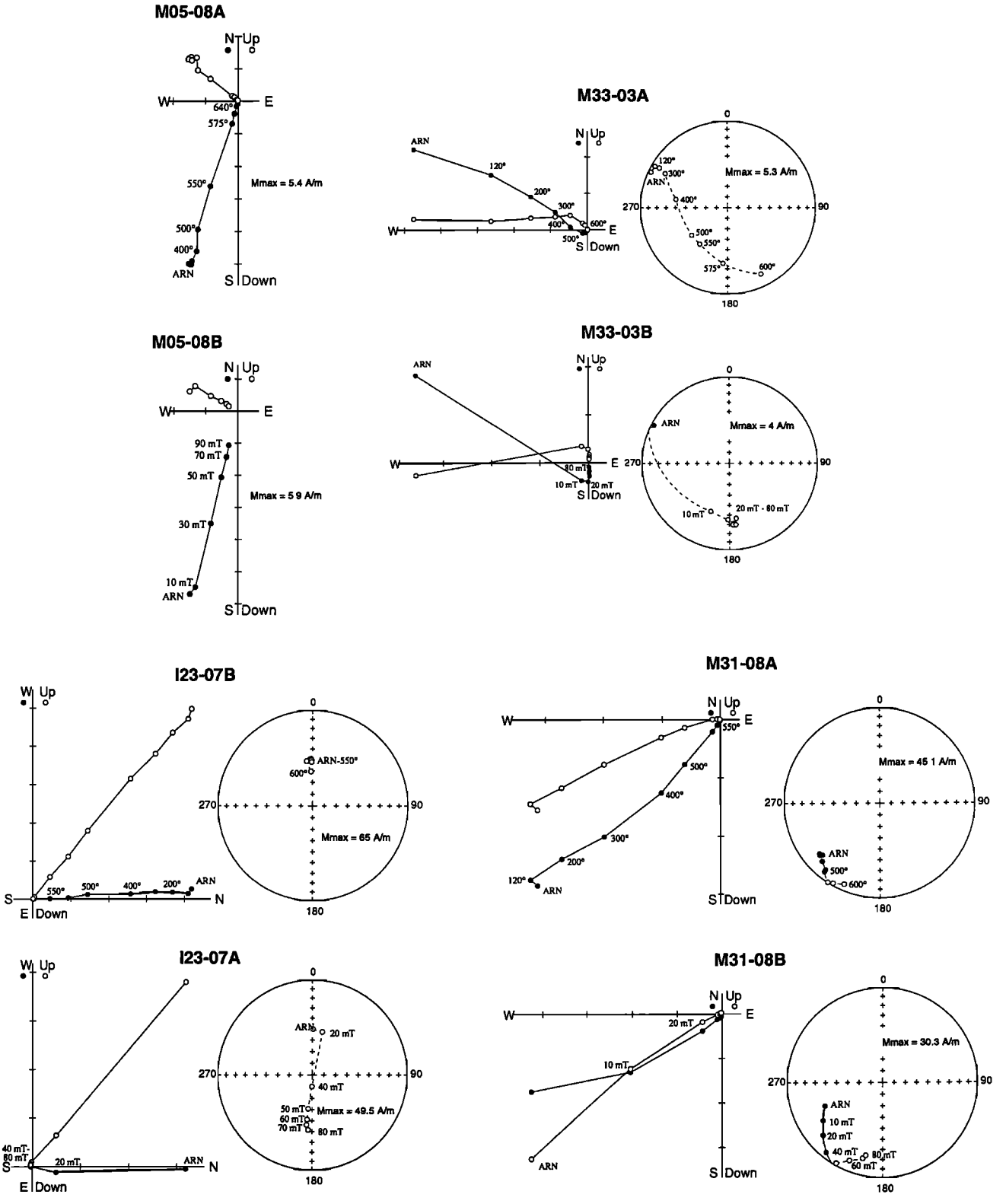

Figure 12. Vector plots of pilot demagnetizations for four selected specimens. Top part of each panel is for thermal demagnetizations (steps in degrees Celsius), and bottom part is for alternating field demagnetizations (steps in milliteslas); each column is for two specimens from the same core. Mmax, maximum natural remanent magnetization.

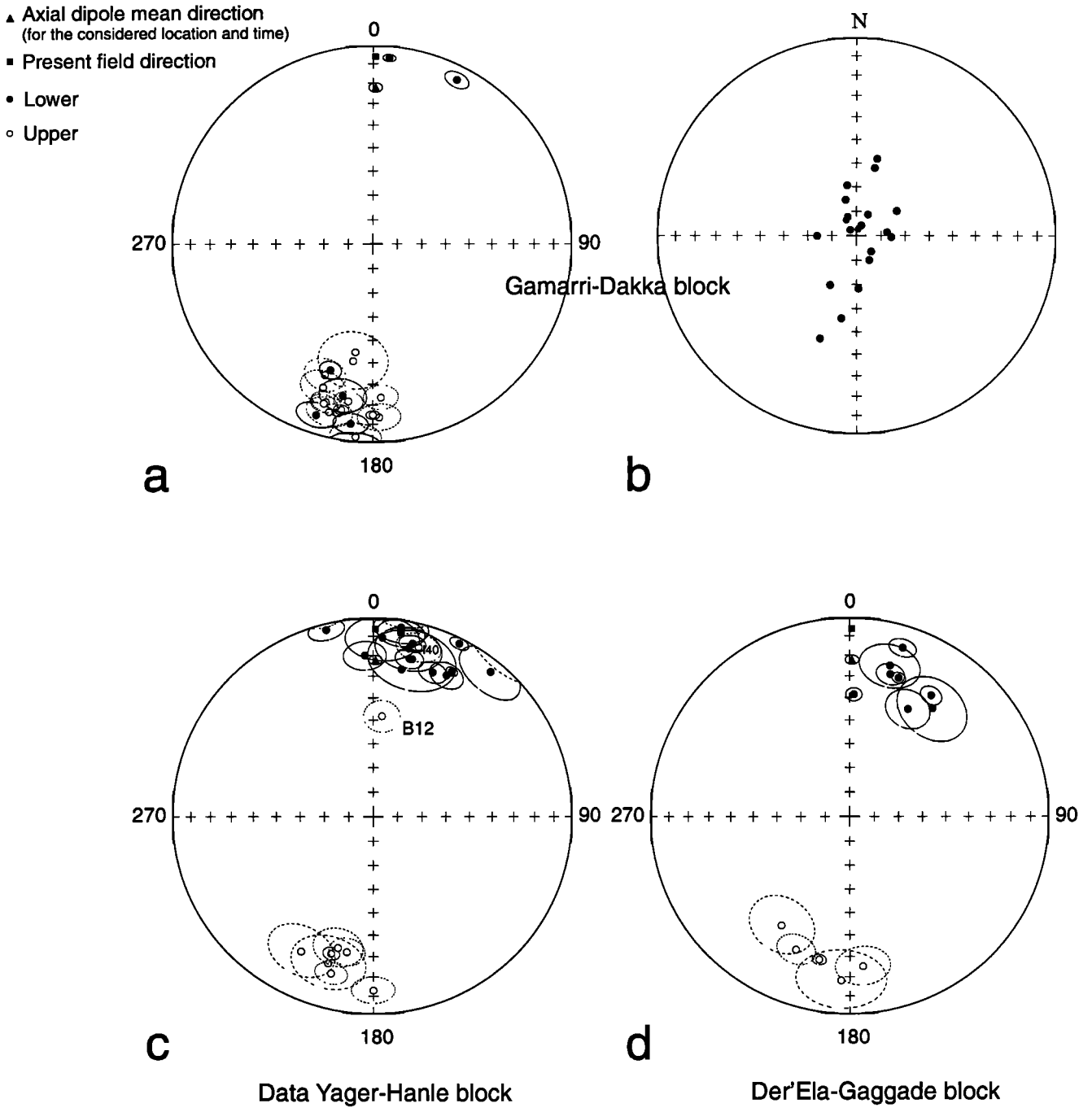

Figure 13. Equal-area projections of mean flow directions (with their α_{95} circle of confidence) for first-order blocks in AMI/MHG overlap. Axial dipole mean direction is interpolated from *Besse and Courtillot* [1991]. (a) Gamarri-Dakka block; (b) same as Figure 13a, but directions are projected in a plane perpendicular to their vector average; (c) data Yager-Hanle block; and (d) Der'Ela-Gaggade block.

each type of basalts, does not fit the expected lognormal population [e.g., *Irving*, 1964], being biased toward higher values. Many samples exhibit NRM intensities 10 to a few hundred times higher than the average value estimated for continental basalts (~4 A/m [*Prévôt and Grommé*, 1975]). Most of these strongly magnetized samples have been sampled at the top of high reliefs. High NRM intensities often occur in the upper (surface) part of the core and strongly decrease downcore (going into the flow). These strong intensities, which are largely removed in the first stages of AF demagnetization (~20 mT), are likely due to lightning. After "magnetic cleaning" (20 mT), the distributions of NRM intensities are approximately lognormal for each basalt

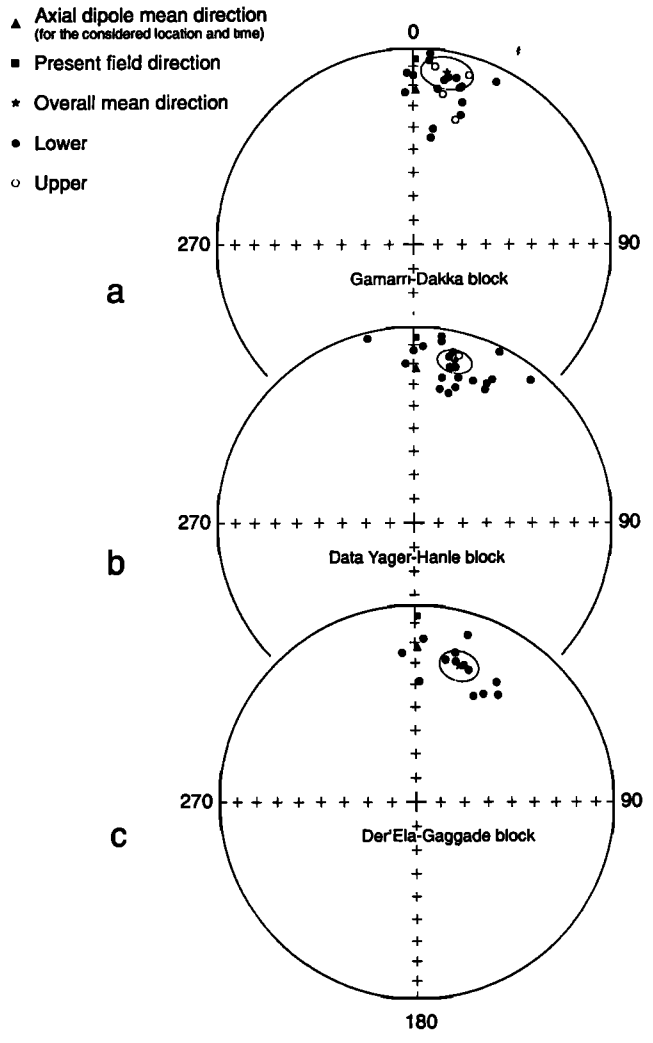

Figure 14. Equal-area projections of final mean directions (with their α_{95} circle of confidence) for (a) Gamarri-Dakka block; (b) Data Yager-Hanle block; and (c) Der'Ela-Gaggade block.

population. Averages are of the order of 3.5 A/m (range 1.3/9.9), similar to those obtained on a heterogeneous population of continental basalts (3.6 A/m [*Prévôt and Grommé*, 1975]) or, for instance, for the Deccan basalts (3.4 A/m [*Vandamme et al.*, 1991]), i.e., apparently typical of subaerial basalts, regardless of age.

The above analysis confirms previous conclusions that the main carrier of magnetization in Afar lavas is magnetite [*Courtillot et al.*, 1984]. Acquisition of isothermal remanent magnetization (IRM) shows that saturation is achieved in fields of ~0.3-0.4 T, consistent with a magnetic mineralogy dominated by magnetite. However, a slight increase is sometimes observed in fields higher than 0.3 T. To better characterize magnetic carriers, we have therefore thermally demagnetized a composite IRM as described by *Lowrie* [1990]. This confirms that magnetization is dominated by magnetite with low to medium coercivity, with little evidence for higher-coercivity minerals.

4.2. Mean Flow Directions

AF demagnetization diagrams generally allowed us to clearly isolate a characteristic component in each core. The 95% confidence angles obtained for each mean flow direction are small, 90% of them <10°, on average of the order of 4°, thanks to good clustering of sample directions. Mean flow directions with a 95% confidence angle larger than 15° were rejected from the following calculations, which resulted in a total of <3% of our sites being rejected. Tectonic corrections were applied to several tilted basaltic flows, with rotation axes striking parallel to the faults that bound them. The difficulty in determining the original orientation of a volcanic flow surface may result in large uncertainties in the corrections. Because the rotation axes often strike almost perpendicular to the mean paleomagnetic directions, the uncertainty related to the amount of tilt will affect inclinations more than declinations.

All paleomagnetic results (both "in situ" or "geographic", and "tilt corrected" or "stratigraphic" directions) are listed separately (electronic supporting Tables A to L[1]) for each first-order tectonic block or unit as identified in the previous section (the sampling distribution and paleomagnetic resolution allow only first-order analyses, which cannot reach the level of detail revealed by fault analysis). The relevant results from *Courtillot et al.* [1984] have been included for completeness and are also used when computing the overall means. We now discuss each of these units.

4.2.1. Asal-Manda Inakir/Manda Hararo-Goba'ad overlap. *Courtillot et al.* [1984] sampled 11 randomly distributed flows in the Gamarri-Dakka block, which we supplemented with the magnetostratigraphic sampling of nine successive flows (star, Figure 11). Mean directions for all flows are listed in Table A and shown in Figure 13a. Two have normal polarity, and 18 are reversed. The directions do not follow a Fisherian distribution. When projected in a plane perpendicular to their vector average (Figure 13b), they appear as an elongate cloud. This unusual scatter (with rather tightly grouped declinations) is largely due to four flows with high inclinations (Table A). Flow B14, with an inclination of -40°, has the lowest precision parameter and the largest uncertainty (α_{95} = 13°), close to the 15° threshold beyond which data are considered unreliable. Flow C11 (I = 33.5°) has by far the largest tectonic correction, with a dip of 28° that might have been misinterpreted in the field. We have no straightforward explanation for the other two values (-44° in S03 and 23° in P04), which come from the series of nine reversed flows. The latter might be a transitional

[1]Supporting Tables A-L are available via Web browser or via Anonymous FTP from ftp://kosmos.agu.org, directory "apend" (Username = "anonymous", Password = "guest"); subdirectories in the ftp site are arranged by paper number. Information on seraching and submitting electronic suplements is found at http://www.agu.org/pubs/esupp_about.html

Table 4. Synthesis of Paleomagnetic Analysis Results for the Different, Identified First-Order Blocks and Areas

Block or Region Names	Table[a]	N[b]	ΔD,[b] deg	ΔI,[b] deg	Maximum Age[b] of Basalts, Ma
Asal-Manda Inakir/Manda Hararo-Goba'ad Overlap					
Gamarri-Dakka	A	20	10.2 ± 7.1	-10.3 ± 7.4	~1.8
Data Yager-Hanle	B	23	13.3 ± 5.1	-6 ± 5.7	~1.8
Der'Ela-Gaggade	C	13	16.9 ± 6.6	5.9 ± 6.5	~1.8
Siyyarou	D	9	?	?	~1.8
Bahlo-Sakalol	E	10	1.1 ± 10.1	-4 ± 10	~1.8
Northern recent basalts	F	15	-6.2 ± 4.3	-0.1 ± 4	≤ 0.8
Outer, Northeastern Margin of the AMI/MHG Overlap					
	G	7	8.9 ± 10.2	-11.1 ± 10.3	~1.8
Mak'arrasou Transfer Zone					
Central part	H	10	-0.7 ± 6.6	-5.1 ± 6.9	~1.8
Northern termination	I	14	19.7 ± 6.6	-19.5 ± 7.1	~1.8
Tadjoura/Asal-Ghoubbet Overlap					
Overlap interior	J	34	13.4 ± 3.4	0.3 ± 3.2	~0.35
Outer margins	K	19	1.4 ± 3.3	-10.6 ± 3.2	~0.8-1
Danakil Block					
	L	40	-10.7 ± 4	-13.5 ± 4.9	~7 ± 1

[a]Available as electronic supporting material.

[b]N is number of mean flow directions considered for final mean calculation; ΔD is declination difference between final mean declination and that of axial dipole field at the considered latitude and age (from [*Besse and Courtillot*, 1991]; ΔI is inclination difference between final mean inclination and that of axial dipole field at the considered latitude and age. Maximum ages of basalts come from dating discussed in text.

field direction. Because of their peculiar arrangement, the four unusual directions do not significantly alter the location of the mean. This mean direction is $D = 11.1°$, $I = 11.9°$ ($\alpha_{95} = 8.5°$, $N = 20$; the reversal test of *McFadden and McElhinny* [1990] is positive class I; Figure 14a; note that in the following mean directions are always given as normal polarities). The angular standard deviation (ASD) calculated for the corresponding VGP distribution [e.g., *Merrill and McElhinny*, 1983] is 13.1°, consistent with the mean value expected at latitude 12°N in the last 5 Myr (13° ± 1° [*McFadden et al.*, 1991]). This suggests that the flows probably have properly sampled secular variation of the geomagnetic field (despite the elongate distribution). The overall mean direction is statistically different from the axial dipole mean direction expected for stable Africa at the location of Afar (latitude ~12°N, longitude ~42°E), at ~1.8 Myr ($D = 0.9° \pm 2.3°$, $I = 22.2° \pm 4.1°$; the corresponding reference paleomagnetic pole is linearly interpolated from the curve of *Besse and Courtillot* [1991]; error estimates are from *Demarest* [1983] (Figure 14a). The declination difference suggests a 10.2° ± 7.1° horizontal clockwise rotation of the Gamarri-Dakka Stratoid block with respect to stable Africa, in the last 1.8 Myr (Table 4, all error estimates from *Demarest* [1983] and *Acton et al.* [1991]). Inclination appears to be too shallow with respect to that expected from either the present dipole ($D = 0°$, $I = 23°$) or that expected for stable Africa ~1.8 Myr ago, by 10.3° ± 7.4° for the latter (Table 4). It happens to be closer to that of the present field in Afar ($D = 0.7°$, $I = 6.1°$; Figure 14a).

A total of 24 flows were sampled through the Data Yager-Hanle block, from the Ethiopian border to Dikhil-Bada Weyn (Figure 11). All mean directions are listed in Table B and shown in Figure 13c. All directions but two (B12 and I40, Figure 13c) cluster in two groups with opposite polarities for which the normal and reversed means are antipodal within statistical uncertainty (reversal test of *McFadden and McElhinny* [1990] is positive C when B12 and I40 are removed from the data set). Thus, after elimination of flow B12, which is the only one to have an abnormal (transitional?) inclination (I40 does not seem to us abnormal enough to be removed), all flows can be combined in a single population to yield an overall mean direction $D = 14.2°$, $I = 16.2°$ ($\alpha_{95} = 5.8°$, $N = 23$, Figure 14b). The cor-

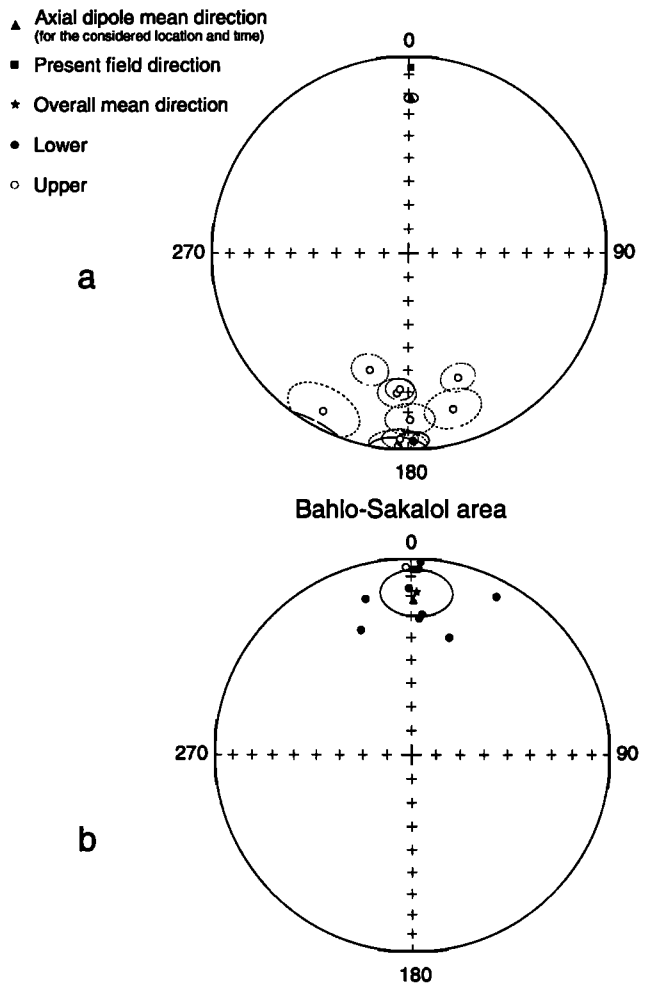

Figure 15. (a) Equal-area projection of mean flow directions (with their α_{95} circle of confidence) for Bahlo-Sakalol area. (b) Equal-area projection of corresponding, final mean direction, with its α_{95} circle of confidence.

responding VGP angular standard deviation is 12.8°, again close to the value expected from secular variation. Inclination is consistent with that expected, but there is a large declination difference of 13.3° ± 5.1°, indicating a statistically significant clockwise rotation by that amount with respect to stable Africa in the last ~1.8 Myr (Table 4).

A total of 13 flows were sampled through the Der'Ela-Gaggade block, from the Ethiopian boundary to Bada Weyn-Bada Yar (Figure 11). All mean directions are listed in Table C and shown in Figure 13d. Directions cluster in two groups with opposite polarities, for which normal (eight) and reversed (five) means are antipodal within statistical uncertainty (reversal test positive C following *McFadden and McElhinny* [1990]). The overall mean direction is $D = 17.8°$, $I = 28.1°$ ($\alpha_{95} = 7.1°$, $N = 13$; Figure 14c). The corresponding ASD of VGP is 13.3°, suggesting a proper secular variation record, though the number of VGPs is relatively small. Inclination after tilt correction is consistent with that expected for stable Africa, but there is a large declination difference of 16.9° ± 6.6°, again compatible with significant clockwise rotation (Table 4).

We sampled nine flows at the top of the Siyyârou block, along the Ethiopian border. Problems with access prevented more extensive sampling further to the SE. Flow mean directions are listed in Table D. It appears that at least five out of the nine flows have the same direction, suggesting they were emplaced in a same brief period of time, perhaps belonging to a single very large flow. Our data therefore cannot be used to recover the magnetic field direction in the Siyyârou block for lack of proper averaging of secular variation.

Some Stratoid basalts are exposed between the Asal-Bahlo fault system and the Sakalol depression, south of the "northern recent basalts" coming from the Inakir range (Figure 11). We sampled 11 flows in that Bahlo-Sakalol area, with mean directions listed in Table E and shown in Figure 15a. All flows have reversed polarity. Even though directions as a whole are somewhat scattered, they are compatible with a Fisherian distribution. The mean paleomagnetic direction for this population is $D = 2.0°$, $I = 18.2°$ ($\alpha_{95} = 12°$, $N = 10$, Figure 15b). The corresponding ASD of VGP is larger than expected (16.1°), suggesting that dispersion may include a component in addition to secular variation.

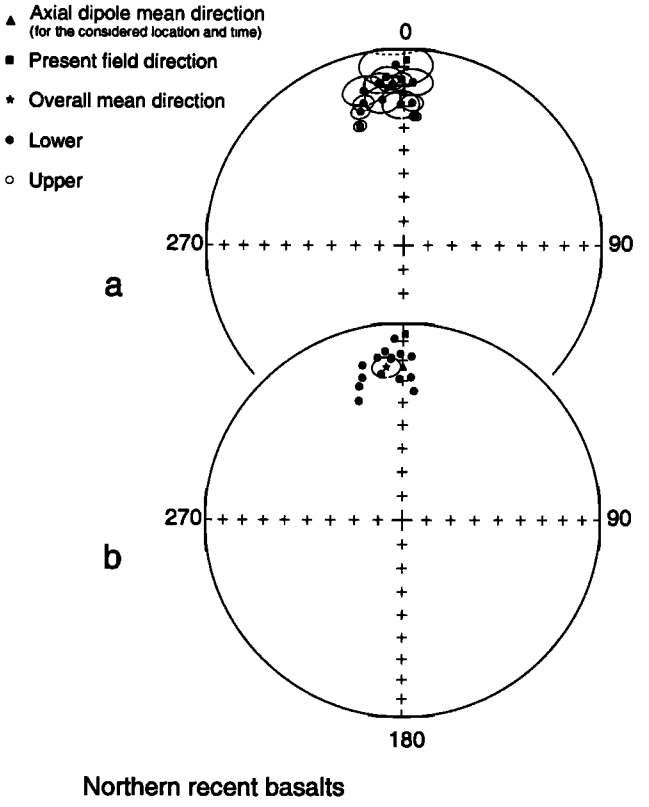

Figure 16. (a) Equal-area projection of mean flow directions (with their α_{95} circle of confidence) for northern recent basalts. (b) Equal-area projection of the corresponding, final mean direction, with its α_{95} circle of confidence.

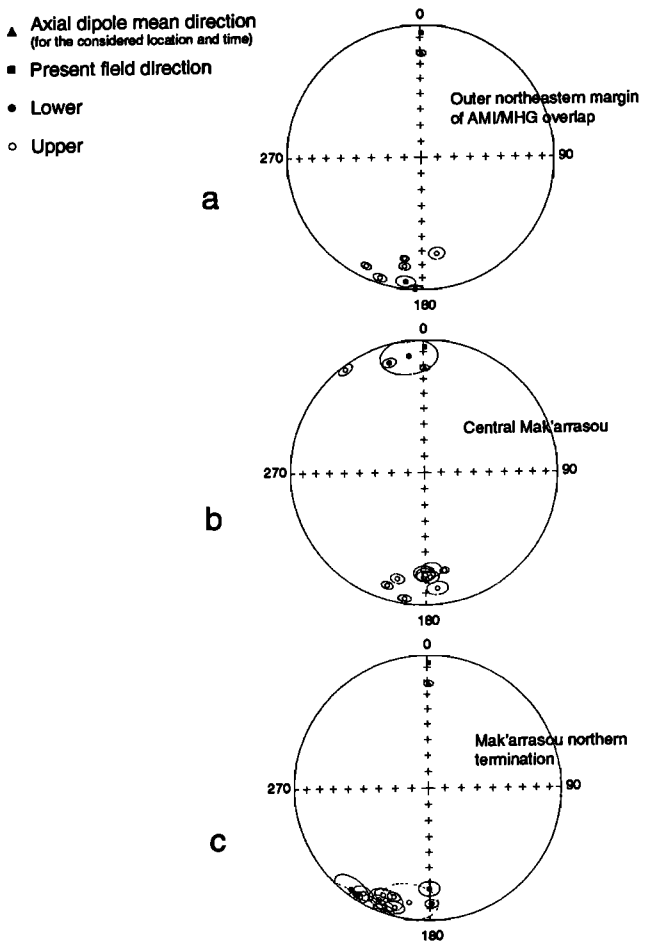

Figure 17. Equal-area projections of mean flow directions (with their α_{95} circle of confidence) for (a) outer northeastern margin of AMI/MHG overlap; (b) central Mak'arrasou; and (c) Mak'arrasou northern termination.

The overall mean direction is, however, similar to that expected for stable Africa, suggesting that the Stratoid basalts exposed northeast of Bahlo are not rotated significantly (Table 4).

Farther north, the Stratoid series is overlain with the northern recent basalts (<1 Ma, Table 1) erupted from the Inakir volcanic rift and the Moussa Alli volcano (Figure 11). We sampled 17 flows in those basalts, mostly south and east of the Manda Inakir rift, to which we added site C19 sampled by *Courtillot et al.* [1984]. Mean directions for all flows are listed in Table F and shown in Figure 16a. All flow directions cluster in a single population with normal polarity (Figure 16a), consistent with emplacement during the Bruhnes normal epoch, in the last ~0.8 Myr. They can be combined to yield an overall mean direction $D = 353.8°$, $I = 22.9°$ ($\alpha_{95} = 5.0°$, $N = 15$; Figure 16b). The corresponding ASD of VGP is 8.9°, smaller than the value expected for adequately sampled secular variation. It is worth noting, however, that this expected value is an average estimation for the last 5 Myr, whereas the "northern recent basalts" are only a few 100 kyr old. Hence the long-term average model proposed by *McFadden et al.* [1991] may not apply on shorter scales or for the most recent times. The pattern of the direction distribution actually suggests that the flows may have properly sampled secular variation of the geomagnetic field. The overall mean direction is different from the present field direction in Afar. Its inclination is consistent with that of the present axial dipole, but there is a small declination difference of $6.2° \pm 4.3°$, suggesting a possible slight counterclockwise rotation of recent basalts with respect to stable Africa (Table 4).

4.2.2. Outer northeastern margin of the Asal-Manda Inakir/Manda Hararo-Goba'ad overlap. Eight flows were sampled due NE of the overlap, one belonging to the Dahla series and the others to the Stratoid basalts (Figure 11). The final mean directions are listed in Table G and shown in Figure 17a. All flows have a reverse polarity. Two ($M31_1$ and $M31_2$) were clearly part of the same cooling unit and were averaged together. The mean paleomagnetic direction is $D = 9.8°$, $I = 11.1°$ ($\alpha_{95} = 12.6°$, $N = 7$; Figure 18a). The corresponding ASD of VGP is 13°, suggesting a proper secular variation record, though the number of VGPs is small. The mean direction has a shallow inclination and a declination that seems to be slightly rotated clockwise by $8.9° \pm 10.2°$ (Table 4).

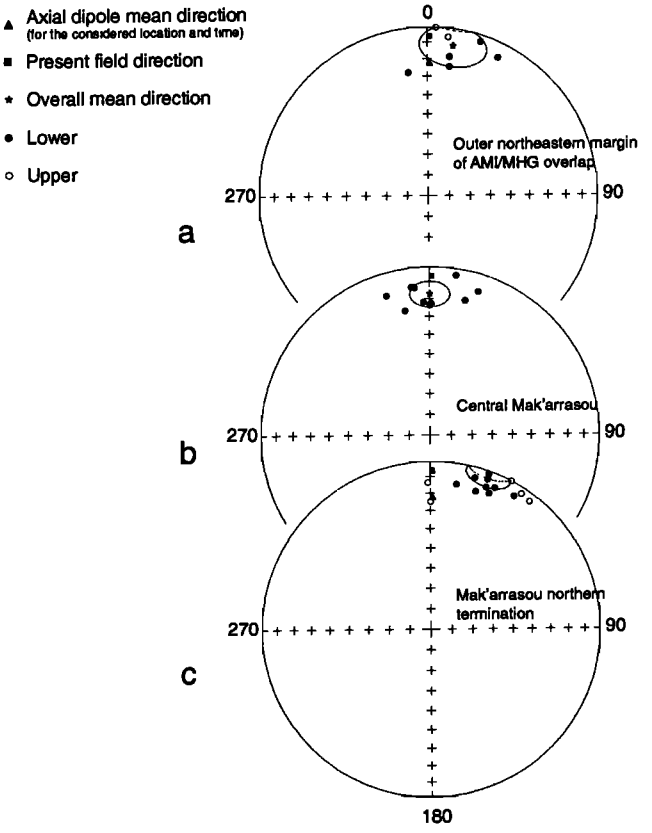

Figure 18. Equal-area projections of final mean directions (with their α_{95} circle of confidence) for (a) outer northeastern margin of AMI-MHG overlap; (b) central Mak'arrasou; and (c) Mak'arrasou northern termination.

4.2.3. Mak'arrasou transfer zone. We sampled 13 flows in the Stratoid basalts of Central Mak'arrasou (Figure 11). Mean directions are listed in Table H and shown in Figure 17b. Most flows have a reversed polarity. Three (M03, $M10_1$, and $M10_2$) yield directions which are clearly offset with respect to the others. If we assume that the three directions result from secular variation, we obtain a mean direction $D = 357.1°$, $I = 9.3°$ ($\alpha_{95} = 11.7°$, $N = 13$, reversal test as above, positive I). The corresponding ASD of VGP is 16.6°, suggesting that there may actually be another source of dispersion beyond normal secular variation. As a matter of fact, the three directions might reflect transitional directions during a reversal, or a remagnetization effect [*Valet et al.*, 1998]. This is likely to be the case for flow M03, which has a direction intermediate between that of a lower flow with normal polarity (M04, Table H) and two upper flows with reversed polarity (M07-M08, Table H). If we eliminate the three anomalous directions, the remaining 10 flow directions follow a Fisherian distribution and yield an overall mean direction $D = 0.2°$, $I = 17.1°$ ($\alpha_{95} = 7.7°$, $N = 10$, reversal test positive C; Figure 18b). The corresponding ASD of VGP becomes 11.7°, closer to the value expected from secular variation. The latter direction is not statistically different from that expected for stable Africa, suggesting that the Stratoid basalts that crop out in the central part of Mak'arrasou are not rotated significantly. The fact that both ASD of VGPs and mean inclination are consistent with field models after removing the three anomalous flow directions but not before supports the hypothesis that they are indeed anomalous.

We sampled 16 flows in the Stratoid basalts offset by the faults of the Mak'arrasou northern termination (western branch, Figure 11). Mean directions are listed in Table I and shown in Figure 17c. Most directions cluster in the SW quadrant of the stereogram, following a distribution that is not Fisherian. Two abnormal flow directions (I10 and $I13_1$), characterized by a reverse declination with high positive inclination, are clearly separate from the others. If we consider that these two directions reflect intermediate directions during a reversal (or are for some other reason unreliable) and can therefore be excluded from data, the mean paleomagnetic direction is $D = 23.9°$, $I = 6.3°$ ($\alpha_{95} = 5.6°$, $N = 12$). However, the corresponding angular standard deviation of VGP (8.6°) is on the low side, suggesting that secular variation of the field might not have been averaged out. If, on the other hand, we consider that the two directions result from secular variation of the geomagnetic field, the mean direction obtained from all data becomes $D = 20.6°$, $I = 2.7°$ ($\alpha_{95} = 8.0°$, $N = 14$, Figure 18c). The corresponding ASD of VGP is 12.8°, indeed close to the value expected from secular variation. The latter calculation leads to a significant declination difference (19.7° ± 6.6°) with that expected for stable Africa, which may result from the clockwise rotation of Stratoid basalts at the northern termination of Mak'arrasou. However, inclinations are in all cases too shallow and much closer to that of the present field rather than the expected one for the Stratoid series. This suggests caution when interpreting these data.

4.2.4. Tadjoura/Asal-Ghoubbet overlap zone. We sampled 34 flows in the gulf basalts exposed in the interior of the Tadjoura/Asal-Ghoubbet overlap (Figure 11 and Table J), and 10 flows in the gulf basalts exposed just outside the overlap, on its outer northern and southern margins, that can be combined with the nine flows previously sampled by *Courtillot et al.* [1984] in the same area (Figure 11 and Table K). Note that flows Z03-Z10, Z11-Z21, and Z25-Z29 were respectively sampled in succession at three supersites. For that reason, only a small number of cores (two to four) were taken through each individual flow. As a consequence, although some of the angles of 95% confidence obtained for individual flows are larger than 15°, their corresponding mean directions are not rejected from the overall calculations.

Figure 19a shows that the 34 flow directions obtained inside the overlap (Table J) cluster in a group with normal polarity, which seems to follow a Fisherian distribution. Thus all flows can be combined in a single population to yield an overall mean direction $D = 13.4°$, $I = 23.3°$ ($\alpha_{95} = 4°$, $N = 34$; Figure 20a). The ASD of

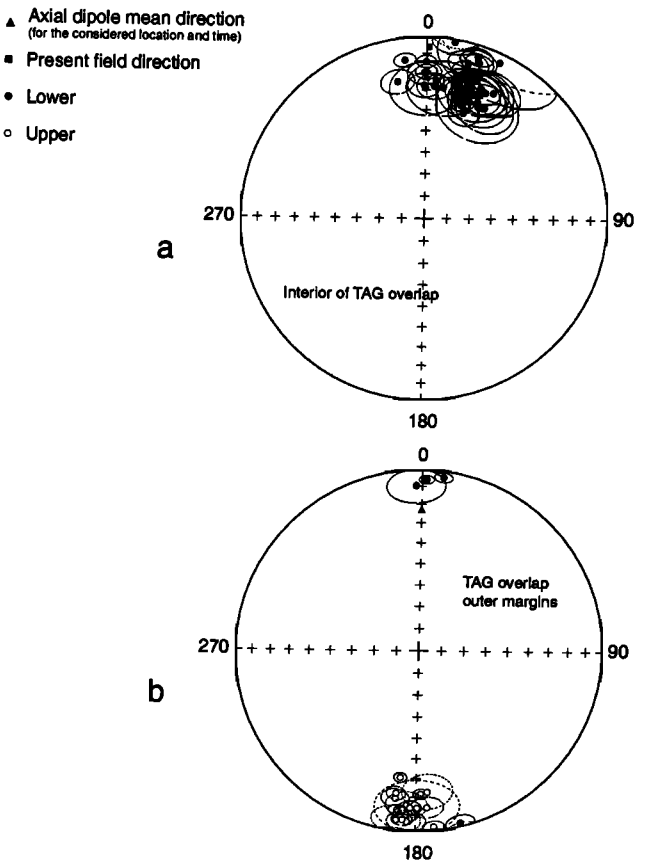

Figure 19. Equal-area projections of mean flow directions (with their α_{95} circle of confidence) for (a) interior of TAG overlap; and (b) outer overlap margins.

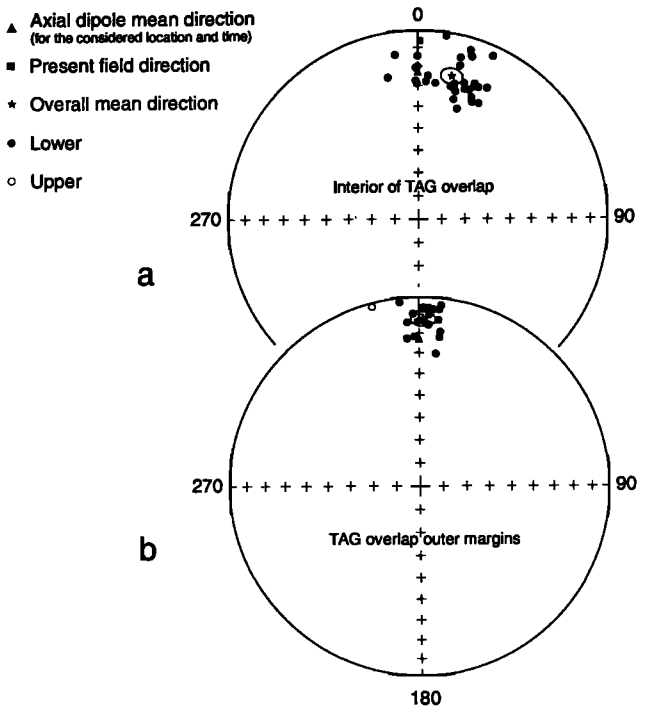

Figure 20. Equal-area projections of final mean directions (with their α_{95} circle of confidence) for (a) interior of TAG overlap; and (b) outer overlap margins.

VGP is 11.4°, suggesting a proper record of secular variation. Inclination is consistent with that of the present axial dipole field, but there is a large declination difference, suggesting that the gulf basalts exposed inside the overlap were rotated clockwise by 13.4° ± 3.4° with respect to stable Africa in the last 350 kyr (Table 4).

Most flows analyzed on the overlap outer margins have a reverse polarity (Figure 19b, Table K), suggesting they were probably emplaced during the Matuyama chron, between ~780 ka and 1 Ma. Figure 20b shows that all flow directions cluster in a single population (reversal test positive C), with mean paleomagnetic direction of $D = 1.4°$, $I = 12.4°$ ($\alpha_{95} = 4.1°$, $N = 19$). The corresponding ASD of VGP is 7.2°, similar to the value obtained for the "northern recent basalts" (with a similar age). For the same reason, we consider that the direction distribution has properly recorded secular variation. The overall mean declination is consistent with that of the present axial dipole field at that latitude (Table 4), suggesting that the gulf basalts exposed just outside the overlap, on both outer rift margins, are not rotated significantly with respect to stable Africa. In contrast, there is an inclination difference ($\Delta I = -10.6° \pm 3.2°$), that might be associated with undetected tectonic tilt of the basaltic blocks.

4.2.5. Danakil block. Evidence for a counterclockwise rotation of the Danakil block or microplate comes from a paleomagnetic analysis performed by *Schult* [1974, 1975] on 27 Dahla basaltic flows ($D = 353.9°$, $I = 8.5°$; $\alpha_{95} = 3.5°$, N=26). However, the mean inclination found from all flows is abnormally low, while the corresponding ASD of VGP (~8.0°) is smaller than expected for the period 6-8 Ma (15.5° ± 3.5° [*McFadden et al.*, 1991]). This suggests that the mean paleomagnetic direction found by *Schult* [1974, 1975] might not have sufficiently averaged out secular variation.

In order to extend the database we performed additional sampling of 13 Dahla basaltic flows in the southern termination of the Danakil block, between Tadjoura, Asagayla and Khôr-Ang'âr (Figure 11). The C17 flow sampled by *Courtillot et al.* [1984] is added to these data, as well as three more flows (M22, M23, C18, Figure 11), which, although sampled in the Stratoid series, structurally belong to the Danakil block. The final mean directions are listed in Table L (together with the Schult directions) and shown in Figure 21a. Flows are dominantly of reversed polarity, some of them having abnormal inclinations. Directions do not follow a Fisherian distribution; when projected in a plane perpendicular to their global Fisherian mean (Figure 21b), they cluster in two groups. Note that the cluster of flows with anomalous inclinations (M25, M26, M27, M29, C17), except I44, was sampled along the same canyon incising flat lying Dahla flows, which we followed for more than 20 km (Figure 11). It is therefore possible that these belong to the same volcanic unit.

We can first consider that the six "anomalous directions" correspond to large oscillations of the magnetic field but are part of secular variation. The overall mean direction is then $D = 351.5°$, $I = 4.3°$ ($\alpha_{95} = 9.3°$, $N = 17$, reversal test positive I). The corresponding ASD of VGP is 12.8°, which would suggest proper recording of secular variation, despite a peculiar distribution. Another possibility is to exclude these anomalous directions, considering them to represent transitional directions during a reversal. The overall mean direction becomes $D = 353.2°$, $I = 17.1°$ ($\alpha_{95} = 6.2°$, $N = 11$, reversal test positive C). ASD of VGP is now 9.1°, suggesting insufficient averaging of secular variation. However, the inclination becomes compatible with the expected dipole direction, suggesting that the new average may actually be a better estimate of the paleofield direction.

The 95% confidence intervals obtained by Schult and by ourselves (from sites separated by more than 100 km) intersect (whether we exclude the six anomalous directions or not), although the intersection does not include either mean. The two complete data sets can therefore be combined to yield an overall mean paleomagnetic direction $D = 352.9°$, $I = 6.8°$ ($\alpha_{95} = 4.4°$, $N = 40$, reversal test positive C; Table L and Figure 21c). The corresponding ASD of VGP is 10.4°, still on the low side, suggesting incomplete secular variation recording. The problems described above make us think that the mean inclination is not accurately constrained. In contrast, we think that the mean declination is a good first-order estimate of that actually recorded by the Danakil Dahla basalts. There is a large difference

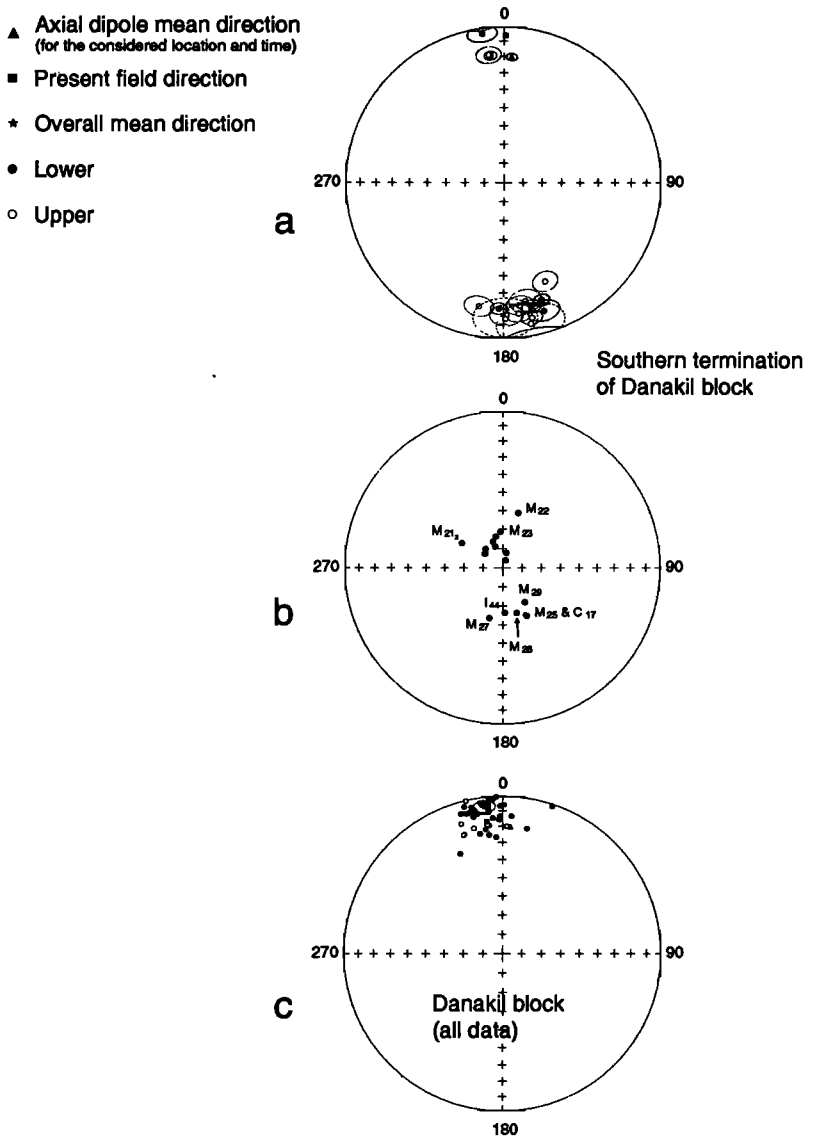

Figure 21. (a) Equal-area projections of mean flow directions (with their α_{95} circle of confidence) for samples taken by us in southern termination of Danakil block. (b) Same as Figure 21a, but with directions projected in a plane perpendicular to their vector average. (c) Equal-area projection of final mean direction (with its α_{95} circle of confidence) for all flows sampled by *Schult* [1974, 1975] and us in Danakil block.

between that declination and that of the axial dipole field at that latitude at 7 ± 1 Ma (D = 3.6° ± 2.3°, I = 20.3° ± 4.2°; deduced from *Besse and Courtillot* [1991], as above), suggesting that the Danakil block was rotated counterclockwise by 10.7° ± 4° with respect to stable Africa, in the last 7 Myr (Table 4).

5. Mechanisms of Strain Transfer

Figure 22 combines our paleomagnetic results (mean declination per block or region, as synthesized in Table 4) with main Quaternary faulting. Note that although our paleomagnetic data did not allow us to identify and characterize rotating blocks or units smaller than those represented in Figure 22, the large number of faults that dissect the overlap (see Plates 1 and 2) leaves no doubt that such smaller rotating blocks exist, associated with or part of the larger first-order blocks/units sketched in Figure 22.

In any case, Figure 22 shows that southeastern Afar did not deform homogeneously in the Quaternary, parts of it having rotated in the horizontal plane while others remained stable. All rotations except that of the Danakil block occurred either between the overlapping Asal-Manda Inakir and Manda Hararo-Goba'ad rifting zones or between the overlapping Tadjoura and Asal-Ghoubbet rifts. Both overlap areas, the former ~3 times larger than the latter, are cut by a network of steep, near rift-parallel, normal-left-lateral, active faults. Thus rotations occurred between rifts and rifting

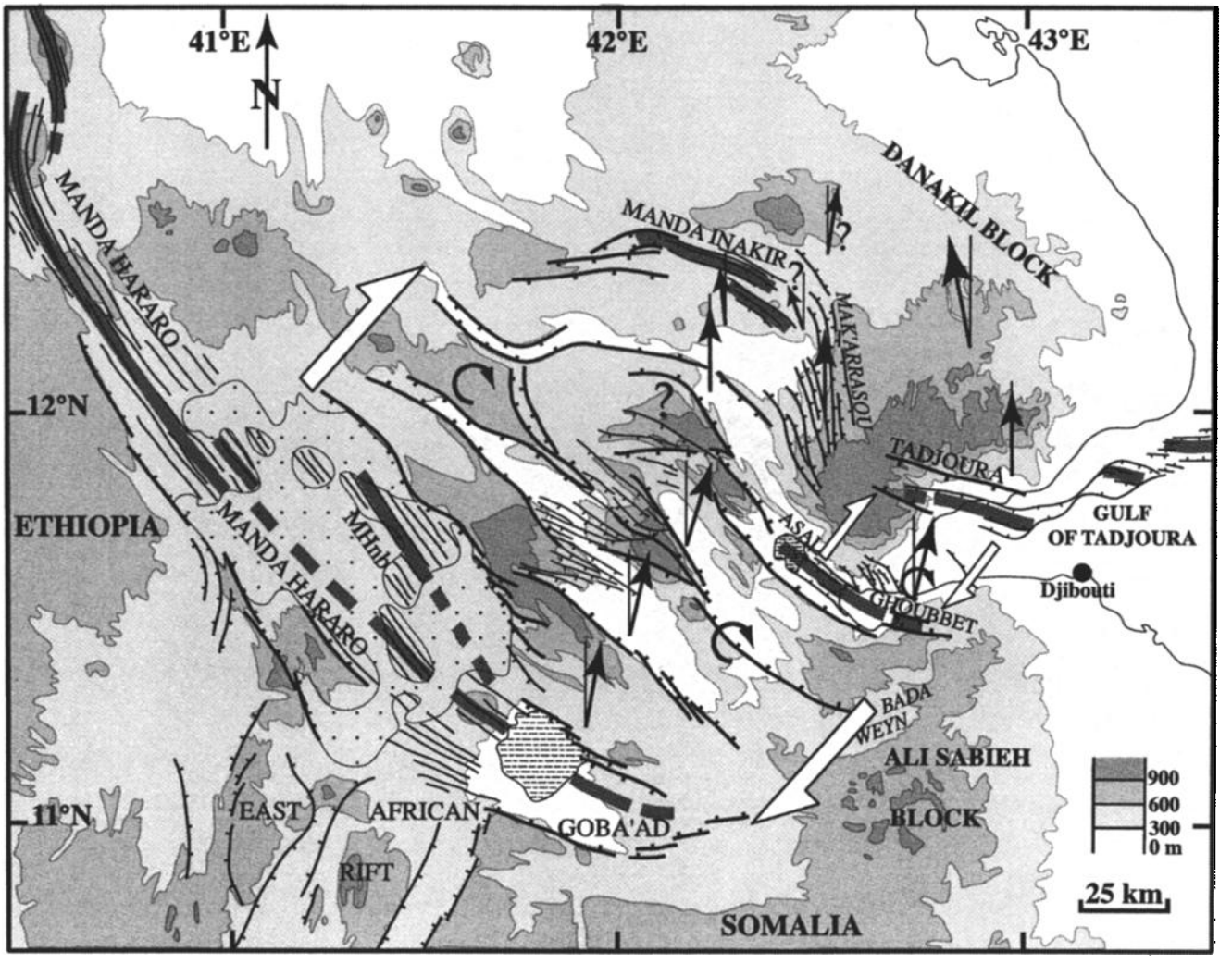

Figure 22. Simplified, synthetic structural map of central Afar, showing measured paleomagnetic rotations. Only major faults and first-order blocks are represented. Active rifts are shaded; MHnb, Manda Hararo northern branch. Solid arrows indicate the measured declination anomaly (from Table 4) relative to north (vertical thin line), curved arrows indicate zones where blocks are currently rotating, and open half arrows indicate shear due to simultaneous opening of facing, disconnected rifts.

zones that overlap and end without being connected by transform faults. Outside such overlap zones, as well as between rifts that do not overlap, basalts show no rotation.

Courtillot et al. [1984], followed by *Acton et al.* [1991], first interpreted the ~14.5° clockwise rotation they found for the southern Stratoid basalts between the Goba'ad (eastern termination of Manda Hararo rift) and Asal rifts, as reflecting the rotation of a single crustal block or microplate between the stable Ali Sabieh block to the SE and an undefined boundary to the NW. However, the assumption of a rigid microplate between the Asal-Manda Inakir and the Manda Hararo-Goba'ad rifting zones is inconsistent with the observation that faulting is distributed in the whole overlap area and accommodates a significant part (at least 7-15%) of the total amount of extension imposed by plate-driving forces. The microplate model also would imply compression on the northwestern boundary of the rotating block, and none of the effects that one would expect from such a compression are observed. Finally, the microplate/Arabia rotation pole proposed by *Acton et al.* [1991] (located near the present Asal-Ghoubbet propagating tip) would make the supposed "Bada Weyn rift" open at a rate of ~7 mm/yr, in a 135°-170° direction, in the last ~1 Myr. Such a rifting rate, as large as the Nubia/Somalia or the Danakil/Arabia separation rates in the last few million years [e.g., *Manighetti*, 1993; *Manighetti et al.*, 1997; *Chu and Gordon*, 1998], would imply significant seismotectonic and volcanic activity, as is observed along the East African Rift and the Bab El Mandeb Strait, with the development of NE striking active faults, open fissures and magnetic anomalies west of the Ali Sabieh block. None of these are actually

observed [*CNR and CNRS*, 1975] (field observations; Plates 1 and 2, and Figure 22). In contrast, the NW to WNW regional extensional fabric of the area, and the magnetic anomalies found in the aeromagnetic map [*Courtillot et al.*, 1980; *Gruzsow*, 1992] appear to continue under the Bada Weyn-Bada Yar flats, into the Ali Sabieh western boundary (Plates 1 and 2, and Figure 22). Therefore rotation of one large microplate cannot account for observations.

Acton et al. [1991] proposed a second model, which they prefer, in which the southern part of the overlap is divided into three rotating rigid microplates which roughly coincide with our three southernmost first-order blocks (compare Acton et al.'s Figure 13 at 0 Ma to our Figure 22). In this model the three microplates are supposed to start rotating clockwise about vertical axes at ~1.8 Ma, as the Aden rifting zone starts enlarging and propagating into Afar (according to the authors). The resulting total rotation amounts predicted by the model are comparable to those we measure in the three blocks and farther north, although the paleomagnetic uncertainties are such that they actually allow a broad range of comparisons. In any case, despite this agreement between model predictions and paleomagnetic measurements, the second model of *Acton et al.* [1991] has two problems. First, it demands that the rotation of the three microplates be accommodated by the opening of rifts taken to lie at the emplacement of the Hanle, Gaggade, and Bada Weyn basins, whereas no deformation is supposed to occur within the rigid microplates. Again, this is inconsistent with observations that show that the entire overlap is dissected by a dense network of active faults, while active rifting (i.e. volcano-tectonic) is lacking. The Hanle, Gaggade, and Bada Weyn basins are not rifts but simple normal fault-bounded basins. Second, the model has rotations starting at 1.8 Ma, while we showed that the overlap, as well as the major block-bounding faults, did not develop before ~0.9 Ma. Thus such a localized deformation model is not supported by observations either.

We propose to account for horizontal rotations and oblique faulting between overlapping rifts and rifting zones in southeastern Afar with a distributed strain model implying bookshelf faulting rotations, as first proposed in Afar by *Tapponnier et al.* [1990] (followed by *Acton et al.* [1991] who proposed a third model with three pinned, rigid, rotating blocks) (Figure 23), and elsewhere by many authors [*Macdonald et al.*, 1984; *McKenzie and Jackson*, 1986; *Nur et al.*, 1986; *Mandl*, 1987; *Kleinrock and Hey*, 1989b; *Phipps Morgan and Kleinrock*, 1991; *Wetzel et al.*, 1993; *Martinez et al.*, 1997]. The finite length of the zone along which the two rifts or plate boundaries overlap in Figure 23 requires dextral shear of this zone. Such shear implies left-lateral motion on the NW striking, rift-parallel, normal faults that allows faulted crustal slivers to rotate clockwise by the same amount about vertical axes. Following *Acton et al.* [1991] (third model) and *Sigmundsson* [1992],

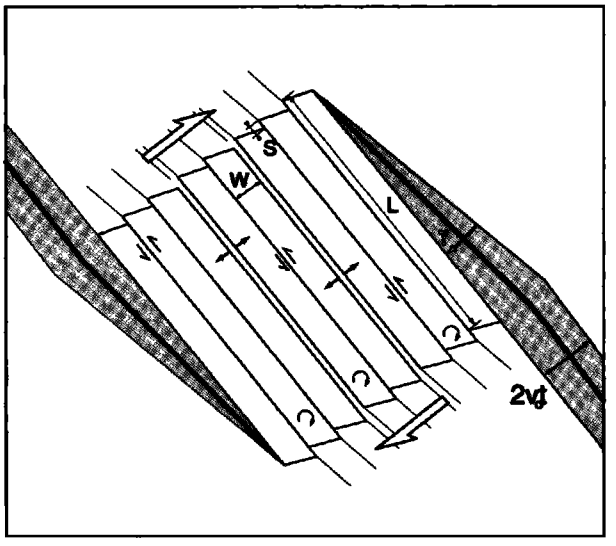

Figure 23. Bookshelf faulting model, modified from *Tapponnier et al.* [1990] and *Sigmundsson* [1992]. Overlapping rifts (or plate boundaries) are shaded. Blocks are bounded by normal-left lateral faults (double arrows); open arrows for shear due to coeval opening of rifts; curved arrows for horizontal rotation; $2V_0$ is total amount of extension resulting from plate driving forces; residual extension accommodated within the overlap (~7-15%) is represented by small solid arrows associated with space between some of the blocks; γ is rotation angle; L, block length; W, block width; S, total, left-lateral slip. Note that this model applies at two different scales (~120 and 30 km in length).

the residual extension accommodated within the overlap zone is also taken into account. Even though shear is distributed within the overlap, the bookshelf faulting model involves a finite number of rotating blocks. Although the density of paleomagnetic sampling of our study was not sufficient to test for second-order block rotations, Plates 1 and 2 show that there are clearly more than five major faults which bound blocks between the Asal-Manda Inakir and the Manda Hararo-Goba'ad rifting zones, and possibly seven or eight. Hence seven or eight blocks might have rotated in the overlap, as suggested by *Tapponnier et al.* [1990].

With our new data and observations, we further test models that incorporate strain localization, rift propagation, and bookshelf faulting, both at a large scale, for the ~100 km wide Asal-Manda Inakir/Manda Hararo-Goba'ad overlap (AMI/MHG) and at a smaller scale, for the ~3 times smaller (~35 km wide) Tadjoura/Asal-Ghoubbet overlap (TAG), where rotation rates are expected to have been ~3 times faster. Because the Aden rifting zone has been propagating northwards into Afar in the last ~900 kyr (whereas the Red Sea continuation, the Manda Hararo-Goba'ad rifting zone, was already localized [e.g., *Manighetti et al.*, 1998]), the length of the AMI/MHG overlap is expected to have increased with time. Figure 24a sketches the situation of south-

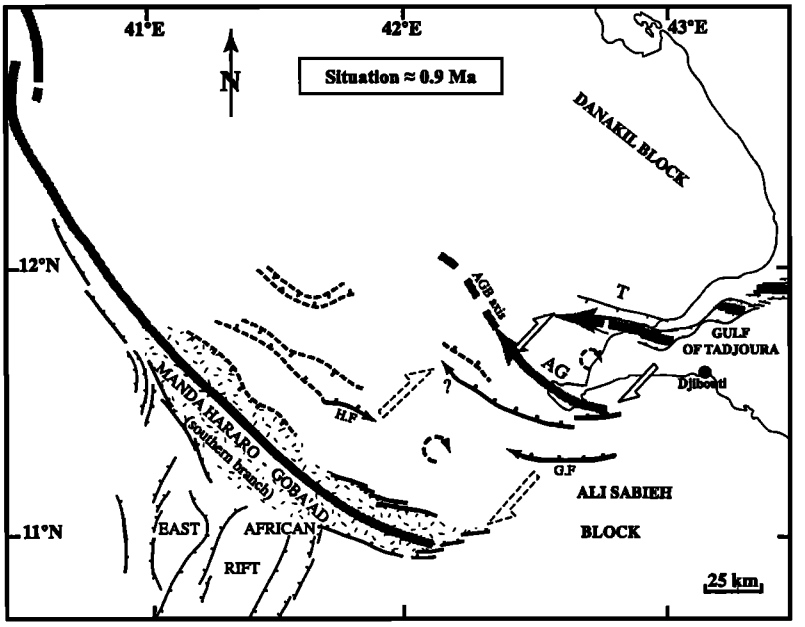

Figure 24a. Situation of central Afar ~0.9 Ma. Active rifts are shaded lines, solid where strain localization is associated with volcanism localization, and stippled where strain localization is not associated with volcanic activity. "Eastern faults" are represented by thick black lines, and "western" by thick dotted grey lines. Onset of shear and rotations is indicated by stippled half and curved arrows, respectively. About 0.9 Ma, both Tadjoura and Manda Hararo-Goba'ad (southern branch) rifts are active, while strain just starts localizing along Asal-Ghoubbet-Bahlo axis (AGB), with associated volcanic activity in the SE half of the latter (AG). As the Tadjoura and Asal-Ghoubbet rifts overlap, fault and block rotations can start between them. Similarly, rotation of some eastern faults and blocks start between SE part of Manda Hararo and Asal-Ghoubbet. To recover the fault geometry at ~0.9 Ma, eastern faults have been rotated back by the amounts synthesized in Table 5; Gaggade and Hanle faults (GF and HF, respectively) are represented just starting growing and propagating, as found in section 3. Note that obliquity between Asal-Ghoubbet axis and eastern faults suggests that AG might have also rotated clockwise in the last 0.9 Myr. Western faults have been at once rotated back by the amounts predicted by the bookshelf faulting model (~3° in the last 0.2 Myr), and shifted back southward across the Gamarri-Alol tear zone to lie in continuity with eastern faults. The best fit is found for a southward shift of ~30 km. The Manda Hararo rift then recovers a classical rift structure (stippled). Western faults are represented with dotted lines because some of them might not have developped yet 0.9 Myr ago.

ern Afar at ~900 ka. At that time, both the Manda Hararo-Goba'ad and the Tadjoura segments were active volcano-tectonic rifts. By contrast, strain was just beginning to localize along the Asal-Ghoubbet-Bahlo fault zone, while gulf basalts were erupting at its southeastern end [*Manighetti et al.*, 1998]. The onset of rifting along the Asal-Ghoubbet-Bahlo axis induced dextral shear of the two overlapping zones that were now laying, on one hand between the Asal-Ghoubbet and the Tadjoura rifts and, on the other hand, between the Asal-Ghoubbet-Bahlo and the Manda Hararo-Goba'ad rifts.

Within the latter overlap the WNW to NW striking normal faults ("eastern faults") inherited from previous, ongoing regional extension, were forced to start rotating clockwise and slip with a left-lateral component (note that all previous models have rotations starting around 1.8 Ma; the finite rotation amounts these models predict are therefore twice as large as they should be). Note that, if we assume constant rotation rates, the rotation amounts we measured for the different eastern, first-order blocks are such that ~900 kyr ago, most eastern faults had to strike more easterly than now, about 120° ± 10° (Figure 24a). This direction is perpendicular to the ~N30° Danakil/Somalia motion vector at that time [*Manighetti et al.*, 1997]. This supports the idea that central Afar faults first formed as pure normal faults before being subsequently rotated and activated with an oblique, normal-left lateral slip. Moreover, the propagation history that we inferred in section 3 for the Hanle and Gaggade faults, suggests that these two faults were just initiating 900 kyr ago, so that the surface of southeastern Afarwas still hardly faulted (Figure 24a).

Although we do not know much about the growth and propagation history of the "western faults" (i.e., faults west of the ~900 ky-overlap), we note that when the present major western faults are shifted southwards by

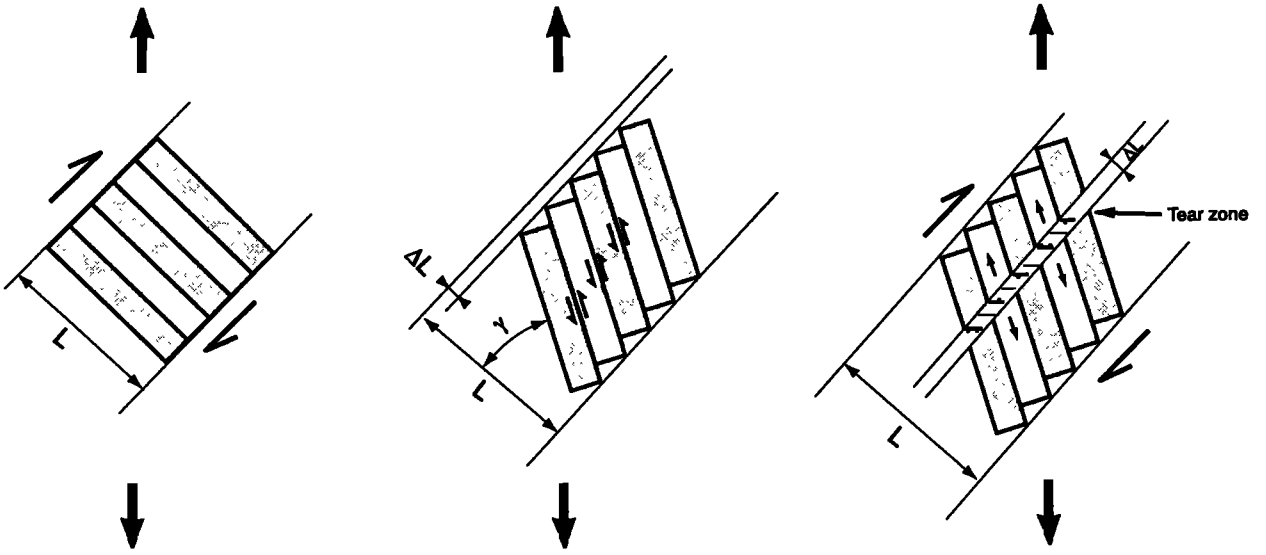

Figure 24b. Mechanism of block tearing as a result of rotation. L is initial block length. Because blocks are fixed at both extremities, they need to tear to compensate the "length decrease (ΔL)" that results from their rotation by angle γ. Faults in the tear zone are not rotated and strike perpendicular to regional direction of extension. Gamarri-Alol would be such a tear zone.

~30 km along the Gamarri-Alol zone, they happen to be in continuity with the major eastern faults (compare Figures 22 and 24a). In particular, the Manda Hararo-Goba'ad rift is then seen to be bounded to the NE by a rather continuous, south dipping fault zone which, together with the north dipping fault system that bounds the rift to the south, forms a more typical rift structure than the present one, with two facing normal fault systems bounding a narrow inner floor (~25-30 km wide, stippled in Figure 24a). This suggests that most major western faults might have been already partly developed ~900 kyr ago, as continuations of the eastern faults.

However, 900 kyr ago, the eastern faults were forced to start rotating clockwise, while the western ones were not. We therefore expect the rotating faults and blocks to have broken along the western boundary of the overlap to accommodate such a kinematic difference. By contrast, the present bending of fault strike from WNW to NW away from the Ali Sabieh block (Plates 1 and 2 and Figure 22), suggests that the eastern faults, although rotating, remained anchored to the latter at their southeastern extremities. The bookshelf faulting mechanism implies that the length of the zone where faults and blocks are rotating (L, measured parallel to initial fault strike; Figure 24b) must decrease by ΔL after a certain amount of rotation (as discussed by *Phipps Morgan and Kleinrock* [1991]) (Figure 24b). In eastern Afar, such a decrease in length was not possible, since the rotating zone, i.e., the overlap length, had to remain fixed between the Ali Sabieh anchoring zone to the SE and the ~N30-trending boundary joining to the NW the northern tip of the Asal-Ghoubbet-Bahlo axis to the Manda Hararo-Goba'ad rifting zone (Figure 24a). As a consequence, the rotating blocks must have been stretched along strike as they were rotating, to increase their length by the mechanically necessary ΔL (Figure 24b). Hence the rotating blocks tore and broke. We interpret the "Gamarri-Alol zone" to be such a tear zone, where the rotating eastern blocks broke at their western extremities under such a rotation-related stretching. This would explain why faults are shorter, smaller and denser in the Gamarri-Alol zone, as well as striking more easterly and dominantly dip-slip (no clockwise rotation).

Plate 3 sketches the overall pattern of faulting in southeastern Afar ~200 kyr ago, when the overall northward migration of the Aden rift was completed, the Mak'arrasou transfer zone was almost entirely formed, and rifting was newly starting in the Manda Inakir segment [*Manighetti et al.*, 1998]. This shows that in the ~700 kyr time span that separates Figure 24a and Plate 3, the eastern faults rotated clockwise by total amounts varying from ~8° to 15° from SW to NE (assuming constant rotation rates, see Table 5), while the western faults migrated northward by ~30 km across the Gamarri-Alol tear zone, without rotating. The western faults only started to rotate clockwise when rifting had become fully localized on the Manda Inakir segment, i.e., less than 200 kyr ago. From that time on, both eastern and western fault systems are rotating together, as sketched in Figure 22.

If, following *Tapponnier et al.* [1990], we assume the total rotation of the eastern faults and blocks to have resulted from the separation between the Danakil and Somalia plates ($2V_o = 16 \pm 1$ mm/yr, minus ~15% absorbed within the overlap, in the ~N30° direction [e.g.,

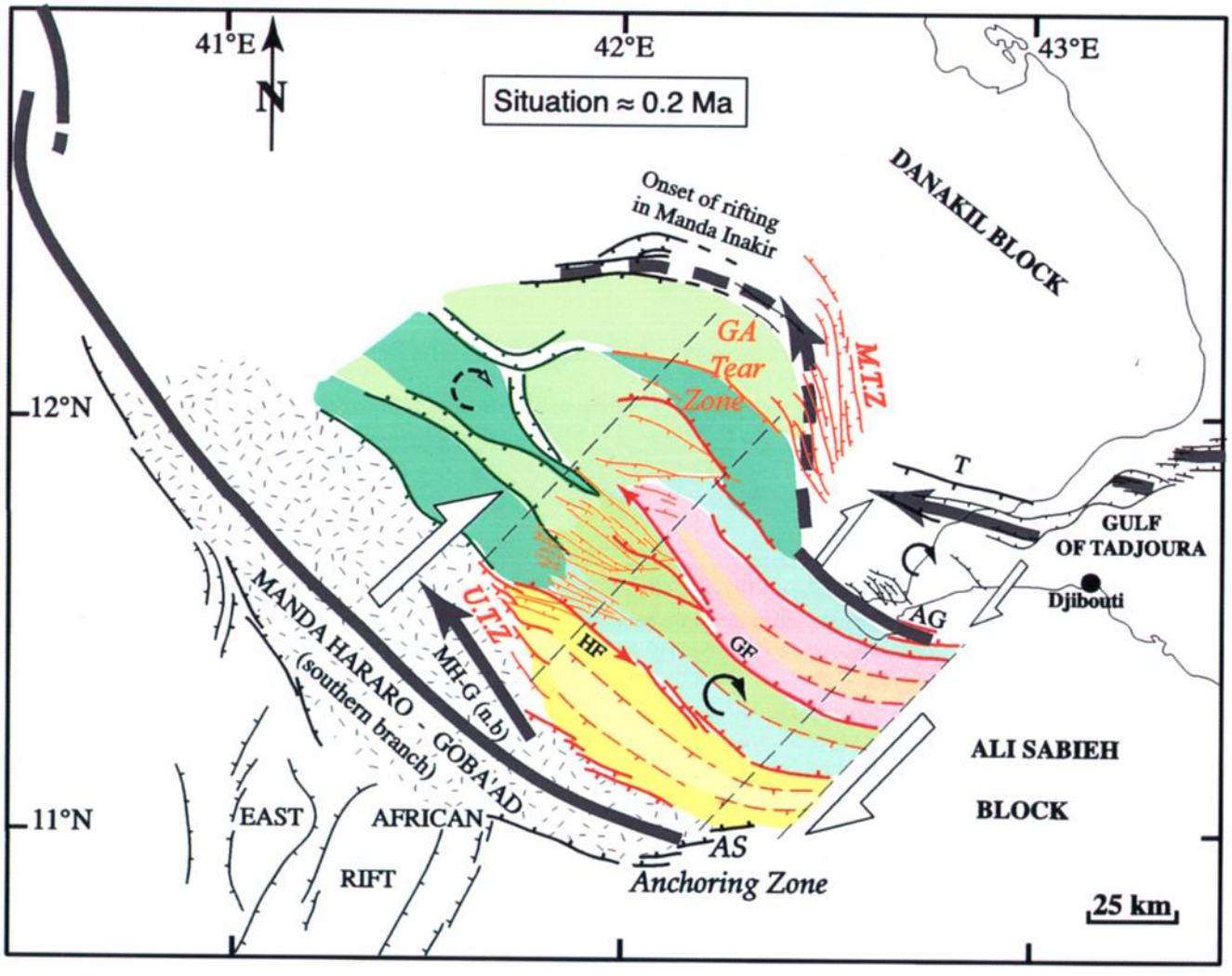

Plate 3. Situation of central Afar ~0.2 Myr ago. Rift representation as in Figure 24a. First-order and possible second-order rotating blocks are distinguished by colors, western blocks only are in greenish tones. Extension accommodated between blocks is not represented for clarity. Black, dotted lines mark limits of Ali Sabieh (AS) anchoring zone and Gamarri-Alol (GA) tear zone. In the 0.9-0.2 Myr time span, "old" faults between Tadjoura and Asal-Ghoubbet probably rotated by > 25°, whereas faults younger than ~350 kyr only rotated by ~6° ; eastern faults (red) of AMI-MHG overlap rotated by 8° to 15° (Table 5). While rotating, they kept anchored at their SE ends (AS) and broke at their NW ends (GA). Also while rotating, the Hanle and Gaggade faults propagated in opposite direction. Western faults (green) of AMI-MHG overlap migrated northward by ~30 km across the GA tear zone. They only started rotating clockwise when strain ended to localize along Manda Inakir, i.e., ~0.2 Myr ago. The Manda Hararo northern branch (MH-G (n.b)) would have developed as a result of overall strain northward migration, led by Aden rift propagation.

Table 5. Kinematic Implications of Paleomagnetic Results in AMI-MHG Overlap[a]

Block Name	Names of the Block-Bounding Faults	Mean Block Width, km	Measured, Horizontal Rotation Amount, deg	Maximum Age of Cumulative Offset, Hence Rotation, Ma	Mean Rotation Rate, deg/Myr	Inferred, Cumulative, Left-Lateral Offset, km	Inferred, Total, Left-Lateral Slip Rate, mm/yr
Gamarri-Dakka	Goba'ad and Hanle	30	10.2 ± 7.1	0.9	11 ± 8	5.4 ± 3.8	~6
Data Yager-Hanle	Hanle and Gaggade broad sense	20	13.3 ± 5.1	0.8	15-17 ± 6	4.7 ± 1.8	~6
Der'Ela-Gaggade	Gaggade broad sense and Habsou	16	16.9 ± 6.6	0.8	19-21 ± 8	4.9 ± 2	~6

[a]Measured rotation amounts and rates appear higher for narrower blocks; for Data Yager-Hanle and Der'Ela-Gaggade blocks, two values of rotation rates are given, considering rotation occurred either in the last 0.9 or 0.8 Myr, respectively; cumulative, left-lateral offsets are deduced from bookshelf faulting model ($S = W_b \tan\gamma$, see text); maximum ages of cumulative offsets are maximum ages of faults, as found in section 3.

Manighetti et al., 1997]) in the last ~0.9 Myr (t), given the length of the rotating eastern blocks ($L = 60 \pm 10$ km; Plate 3), the bookshelf faulting model predicts a total clockwise rotation ($\gamma = \arctan(2V_o\alpha t/L)$, where $\alpha = 0.85$) of 11.5° ± 2°, in agreement with the paleomagnetic rotation amounts that we measured for the first-order blocks (overall mean is 13.5° ± 6°; Table 5). Considering that the overlap width ($W_o = 80 \pm 10$ km, Plate 3) is sliced in approximately seven to eight major rotating blocks, we deduce a mean block width W_b of 11 ± 2 km. This in turn results in a mean left-lateral offset on each bounding fault ($S = W_b \tan\gamma$) of 2.2 ± 0.8 km. The predicted strike-slip rate on these eastern faults in the last 0.9 Myr would thus be 2.4 ± 0.9 mm/yr, in agreement with the late Quaternary lateral rates measured on the Gaggade fault (Table 3).

At a more detailed level we note that the width of the eastern first-order blocks decreases from south to north (Plates 1 and 2), whereas their measured rotation amounts seem to concurrently increase (Figure 22, and Table 5). Taking these concurrent variations into account, we can calculate the cumulative left-lateral offset amounts expected on each block-bounding major fault. Table 5 reveals that these cumulative strike-slip amounts are similar on all faults, as predicted by the proposed bookshelf faulting mechanism, averaging 5 ± 2.5 km. This shows that the eastern overlap is actually sliced in first-order blocks of different sizes that rotate at different rates while accommodating a constant, total, left-lateral displacement. As oblique slip is supposed to have started only ~0.9 Myr ago, and even more recently on the Gaggade fault (the escarpment of which would have started to offset the Stratoid surface only ~0.8 Myr ago; Table 3), the cumulative lateral slip amounts that we obtain would imply that the major bounding faults have been slipping left-laterally in the last 0.8-0.9 Myr at similar rates, averaging 6 mm/yr (Table 5). Such rates are obviously too high to be related to single, although major, faults. They actually indicate that several additional smaller faults must exist and accommodate a significant part of the combined left-lateral slip/clockwise rotations. This confirms that the bookshelf strain transfer mechanism involves distributed faulting. Considering that all the rotating faults slipped in a left-lateral sense at rates comparable to the Holocene rates obtained in section 3 (~2 mm/yr), we deduce that each first-order block may actually be sliced by about three rotating faults, what would make a total of about nine fault-bounded rotating blocks within the eastern part of the AMI/MHG overlap. Such a number is similar to the one independently deduced from fault mapping (approximately seven to eight, see Plates 1 and 2).

The AMI/MHG overlap zone lengthened up to its present size only ~200 kyr ago. While the eastern blocks were rotating between the Ali Sabieh anchoring zone and the Gamarri-Alol tear zone at an overall mean rate of 15°/Myr (mean rate measured per block ~11° to 21° ± 8°/Myr, see Table 5; mean predicted rate is 13° ± 2°/Myr), the western blocks just started to rotate between the Gamarri-Alol tear zone and a N30°-trending boundary joining the northern tip of the Manda Inakir rift to the Manda Hararo-Goba'ad segment (Plate 3 and Figure 22). Hence the Gamarri-Alol tear zone started to act as a joint between the eastern and western rotating blocks. Note that this is precisely the time when we infer that both the whole Gaggade and the Hanle faults stopped increasing in length. Assuming that the

western overlap is sliced by about four to five major rotating blocks (see Plate 1), the mean length and width of which are $L = 60 \pm 10$ km and $W_b = 16 \pm 2$ km, respectively, the bookshelf faulting model predicts that the western blocks rotated clockwise by $2.6 \pm 0.5°$ in the last ~0.2 Myr (i.e., from Plate 3 to Figure 22). A paleomagnetic test of our predictions has been recently performed in the western Ethiopian part of the overlap: indeed, preliminary paleomagnetic results in the western overlap apparently fail to detect any significant rotation [*Kidane*, 1999 ; G.D. Acton, personal communication, 1994].

The model also predicts a mean left-lateral, total offset amount of 0.7 ± 0.2 km on each western fault, implying a mean strike-slip rate of 3.5 ± 1 mm/yr on the latter, similar to the lateral rates both measured and predicted along the eastern faults. If we suppose that the Serdo earthquake reactivated one of these western faults, we infer a recurrence time of 200 ± 50 years for comparable seismic events (Table 3). Such a recurrence time is similar to that estimated in the Asal-Ghoubbet rift by *Stein et al.* [1991].

Let us now consider the ~3 times smaller overlap between the Asal-Ghoubbet and the Tadjoura rifts. Within that zone, the gulf basalts, the surface of which has been dated at 350 ± 40 ka, appear to have rotated clockwise about a vertical axis by $13.4° \pm 3.4°$. In contrast, the older gulf basalts exposed on either side of the overlap show no rotation. The bending of the fault strikes from NNW to NW as one goes southeastward away from the central part of the overlap suggests that the rotating faults are anchored along the SE side of the overlap (Figure 1). Given the length of the rotating blocks ($L = 27 \pm 3$ km), the bookshelf faulting model predicts a clockwise rotation of $12° \pm 2°$ since 350 ± 40 ka, in agreement with the measured rotation ($13.4° \pm 3.4°$). The corresponding rotation rate (both measured and predicted) is very fast, of the order of 38°/Myr (more than double the fastest rate estimated for microplate rotation in ocean [e.g., *Naar and Hey*, 1991; *Schouten et al.*, 1993], slightly more than twice as fast as that measured in the twice as long, eastern half of the Asal-Manda Inakir/Manda Hararo-Goba'ad overlap (~15°/Myr). First-order blocks, the mean width of which is 0.7 ± 0.3 km, can be delineated in Figures 1 and 2b. Such a width would imply a total, left-lateral offset amount of 160 ± 100 m on each major fault. That amount is comparable to the cumulative, left-lateral offsets that we could measure along some of the faults in Figure 2b (~100 m, see *Manighetti* [1993] for details). We infer that the major faults that bound the first-order rotating blocks might have slipped left laterally in the last 350 kyr, at a rate of 0.5 ± 0.2 mm/yr. The seismic lateral offsets that could be measured or estimated along some of these faults [*Jacques*, 1995] being of the order of 20-35 cm, we deduce that such faults may break every 400-700 years, i.e., ~2-3 times less frequently than the bounding Asal-Ghoubbet rift faults.

Going back in time, measured rotation amounts imply that the two main fault sets that presently slice the overlap ($150° \pm 10°$ striking left-lateral faults and $115° \pm 5°$ striking normal faults; see section 3) were striking more easterly ~350 kyr ago, being $135° \pm 10°$ and $100° \pm 5°$, respectively. We note that the $100° \pm 5°$ direction is that of present open fissures, as observed in Figure 2b: The current local σ_3 azimuth within the overlap is close to ~N10°E. The azimuth of σ_3 therefore remained constant with time inside the overlap since 350 ka, striking more northerly than the Danakil/Somalia motion vector. The present $150° \pm 10°$ striking left-lateral faults are underlined by small recent spatter cones: Being the only ones to guide lavas up to the surface, they may be deeper, steeper and older than any other faults. The bookshelf faulting model assumes that rotations start as soon as the rifts overlap. Since extension started to localize along the Asal-Ghoubbet-Bahlo axis ~900 kyr ago (Figure 24a), the Tadjoura/Asal-Ghoubbet overlap is expected to have existed, and rotations are expected to have occurred since that time. Assuming that the mean rotation rate remained constant with time (~38°/Myr), we infer that the present $150° \pm 10°$ striking left-lateral faults might have been striking $115° \pm 10°$E, ~900 kyr ago. Such an initial direction is almost perpendicular to the Danakil/Somalia motion vector at ~900 ka (~N30°E [*Manighetti et al.*, 1997]), which suggests that these faults might have first formed as pure normal faults, before being rotated and activated in an oblique, left-lateral sense. They subsequently were blanketed by Gulf basalts, at ~350 ka, when their strike was averaging $135° \pm 10°$.

The bookshelf faulting model therefore accounts quite well for all structural, paleomagnetic, and geochronological data acquired inside the overlap zones, both at large and small scales. Hence, although the overlap zones between rifts and rifting zones in Afar cannot be modeled as single rotating rigid bodies, a description of the strain field in terms of small rigid block motion may be adequate at any given moment in time. Such block motion results from bookshelf faulting, which accommodates transfer of strain between rifts or plate boundaries that do not meet and overlap. The geometry of both the TAG and the AMI/MHG overlaps somewhat resembles classical "overlapping spreading centers" (OSC) found along the East Pacific Rise and the Mid-Atlantic Ridge [e.g., *Macdonald and Fox*, 1983; *Lonsdale*, 1983; *Sempéré and Macdonald*, 1986a,b; *Fox et al.*, 1991], except that the overlap to offset ratio is ~1 (as in work by *Martinez et al.*, 1997] instead of the common value of 3 [e.g., *Macdonald et al.*, 1984; *Sempéré and Macdonald*, 1986a,b]. The size of the AMI/MHG overlap makes it comparable to the largest OSCs described in the oceans [e.g., *Klaus et al.*, 1991; *Hey et al.*, 1995; *Martinez et al.*, 1997]. The overlap length defines the length of the blocks which rotate through the bookshelf faulting mechanism and, hence, their rotation rate (which also depends on block width). In contrast, wherever rifts

fail to overlap, transfer of strain seems to occur without any block rotation. Even though the Mak'arrasou faults have a left-lateral component of slip in addition to their normal one, they do not rotate clockwise (see central part; Table 4). This is perhaps because they form a narrow fault bundle trending highly oblique to both rifts (~45°) and bound blocks with lengths ~20 to 40 times their widths. We think that the Mak'arrasou fault bundle more likely acts as an oblique transfer zone between the Asal-Ghoubbet and the Manda Inakir rifts and that its overall rooster tail geometry is a consequence of the stepwise propagation of the Aden ridge [e.g., *Manighetti et al.*, 1998]. We suggest that the clockwise rotations found at the northern termination of the Mak'arrasou western branch, which developed as the first kinematic junction between the Asal-Ghoubbet rift and the Inakir subrift [e.g., *Manighetti et al.*, 1998], may be related to local horsetail faulting.

Finally, our data agree with the proposal that Danakil is a rigid microplate which rotated counterclockwise, at least in the last 6-8 Myr, at a mean rate of 1.5 ± 0.6°/Myr. Note that this rate is similar to the rate independently determined by *Chu and Gordon* [1998] (1.220°/Myr) from regional plate kinematic analyses. If we assume that the present ~30° angle between the western Danakil edge and the main Ethiopian escarpment (Plate 1 and inset) results from the counterclockwise rotation of Danakil at this constant rate, we infer that the Danakil microplate started to break away from the Ethiopian plateau and to rotate ~20 Myr ago. This age coincides with the arrival of the Aden rift on the Shukra-El Sheik discontinuity and with the onset of stretching in Afar [*Manighetti et al.*, 1997; *Audin*, 1999]. We infer that the Danakil microplate might have started to rotate in unison with westward propagation of the Aden ridge into the soft, faulted, thinned and warmed Afar lithosphere because of the previous Afar hot spot activity [e.g., *Manighetti et al.*, 1997]. The Ali Sabieh block, the western edge of which strikes more than 90° more northerly than the Somalian escarpment (Plate 1), could be another microplate that might have rotated clockwise concurrently with the Danakil, but faster, at a rate inferred to be greater than 4.5°/Myr, contributing to general opening of the Afar depression in a "saloon doors" mode [*Manighetti*, 1993; *Audin*, 1999]. We also think that during the ~13 Myr when the ridge stalled on the Shukra-El Sheik discontinuity [e.g., *Manighetti et al.*, 1997], there was an attempt to transfer strain from the Aden ridge to the southernmost part of the Afar depression (north of Dire Dawa): The existence of approximately E-W trending magnetic anomalies and normal faults [*Hall and Girdler*, 1970; *Gruszow*, 1992] may be thought to be related to an ancient zone of localized rifting [*Audin*, 1999]. Clockwise rotations would have occurred during that strain transfer attempt, possibly involving the Ali Sabieh microplate and faults, the present signature of which could be the unexplained 160 ± 10° left-lateral faults underlined with small recent spatter cones all along the western edge of the Ali Sabieh block (Plates 1 and 2).

6. Discussion

The Afar region offers a unique opportunity to directly observe and measure all the processes that have been and still are contributing to the birth and development of a single, divergent plate boundary between Arabia and Africa. In particular, the mechanisms allowing strain transfer at large scale between the two present "arms" (Aden and Red Sea) of the future unique plate boundary can be observed in central Afar, and their evolution in space and time can be depicted in detail from their onset to present. At smaller scale, one can also analyze the evolution of rifting and of strain transfer mechanisms along an actively propagating plate boundary (here the Aden arm). It appears that three distinct strain transfer mechanisms are currently operating along the short western portion of the Aden rift (~100 km between Obock and Manda Inakir). A classic transform fault (Maskali), parallel to the Arabia-Somalia motion vector, transfers rifting from the Obock to the Tadjoura segment [e.g., *Manighetti et al.*, 1997; *Audin*, 1999] (Plates 1 and 2). Due west, strain transfer from the Tadjoura to the Asal-Ghoubbet rift segment occurs through a bookshelf faulting mechanism implying the rotation and oblique slip of rift-parallel faults. Farther west, the oblique transform Mak'arrasou fault zone accommodates strain transfer between the Asal-Ghoubbet and the Manda Inakir rift segments, through the normal left-lateral slip of a dense bundle of faults, strongly oblique to both the rifts and the plate motion vector. What could be the reasons for such significant changes in the strain transfer mechanisms along the western Aden rift?

A common idea in the literature is that subtle changes in the direction of plate motion may cause the ridge to break up into small en échelon segments, separated by offsets, with different sense, sizes, geometries and hence mechanisms [e.g., *Hey et al.*, 1980; *Phipps Morgan and Sandwell*, 1994]. However, *Manighetti et al.* [1997] showed that the Danakil-Somalia motion vector did not change since 2 Ma, during which the Aden rift propagated from the Obock segment to the Manda Inakir rift. Several authors [e.g., *Naar and Hey*, 1989] propose that there is a speed limit, either for slip or propagation rates, to ensure the stability of discontinuities, so that some forms (such as transform faults) become unstable at faster rates and can be replaced by other forms (such as overlapping spreading centers), with different strain mechanisms. However, both the opening and the propagation rates remained constant along the western Aden rift [e.g., *Manighetti et al.*, 1997], slow for the opening (~1.2-2 cm/yr), faster for the propagation (~10-15 cm/yr): Therefore the idea of a speed limit does not apply.

Manighetti et al. [1997, 1998] proposed that the Aden

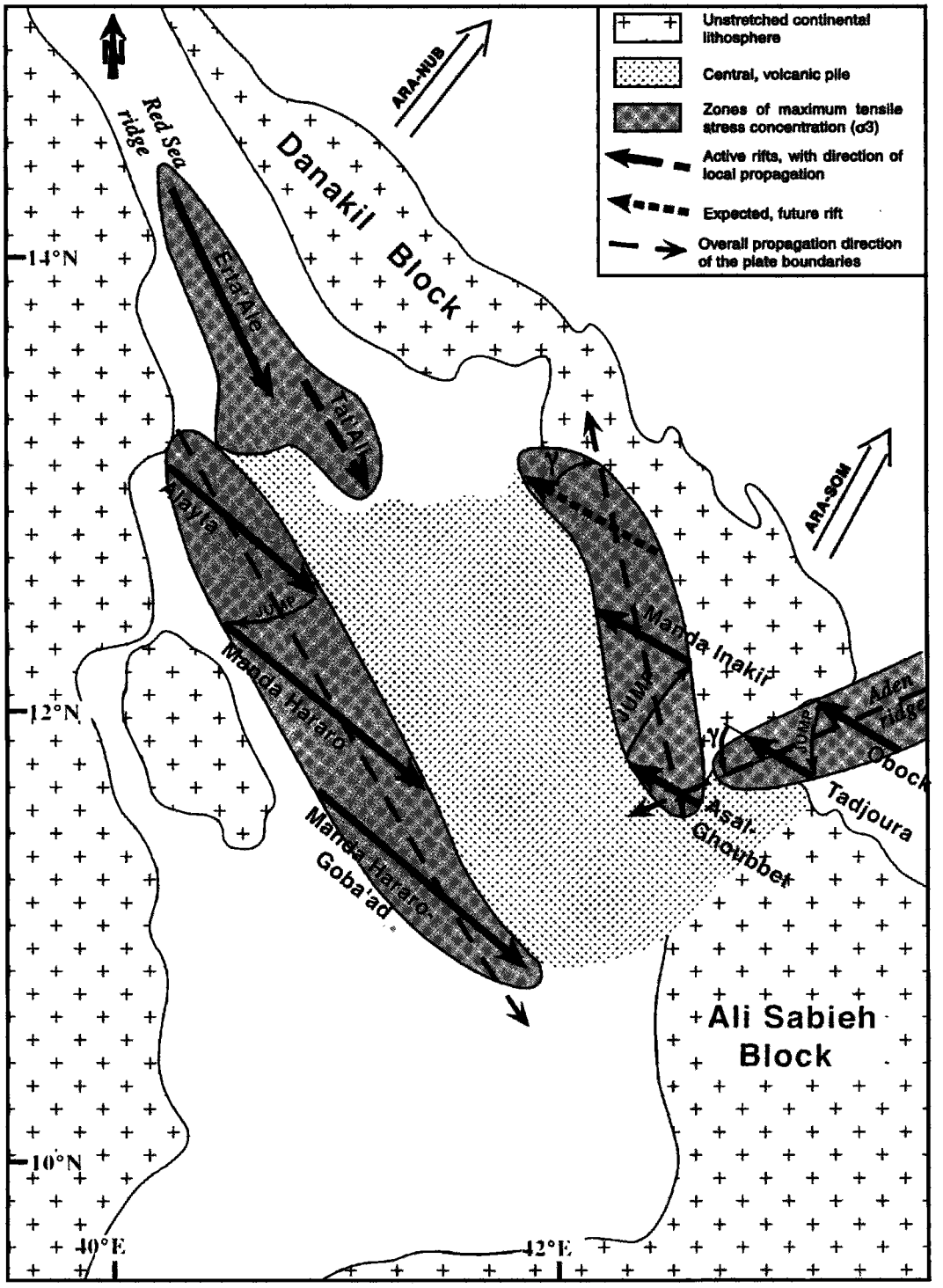

Figure 25. Pattern of rift and plate boundary propagation in Afar (modified from *Manighetti et al.* [1998]. Aden and Red Sea ridges localized and propagated in opposite direction on either side of central Afar volcanic pile, where lithosphere is thinnest and tensile stress concentration maximum. Rifts grew and propagated within these zones, perpendicular to ARA-SOM (Aden rifts) or ARA-NUB (Red Sea rifts) plate motion vectors. Here γ is angle between direction of overall plate boundary propagation and local rift propagation. Such a pattern of rift localization, propagation and jump allows prediction of the future development of a new rift north of Manda Inakir.

ridge localized and propagated at large scale inside zones of maximum tensile stress concentration, the existence of which depends on the initial three-dimensional (3D) geometry and rheology of the Arabia-Africa plate. The Aden ridge propagated in an overall WSW direction through the Gulf of Aden/Gulf of Tadjoura to cross the plate in its narrowest, and hence its weakest section in map view. Then it veered northward from Asal-Ghoubbet into Afar, to break the lithosphere where it was thinnest in cross section, i.e., along the eastern edge of the thick central Afar volcanic pile (Figure 25). However, individual rifts kept propagating northwestward, perpendicular to the direction of σ_3 resulting from plate driving forces, inside these large-scale, mechanically imposed lithospheric necking zones. Such a geometry, where rift propagation remained oblique to the overall plate boundary propagation, forced the rifts to jump, first southward throughout the Gulf of Aden/Gulf of Tadjoura, then northward along the eastern edge of Afar. We propose that the obliquity angle γ between the direction of rift propagation and that of overall plate boundary propagation is a major governing parameter as regards the nature and geometry of transfer zones between the propagating rifts and hence the mechanisms of strain transfer (see Figure 14 of *Manighetti et al.* [1998] and Figure 25). Where γ is small, rifts tend to propagate farther, being closely spaced. Within transfer zones this may lead to the development of long normal faults striking perpendicular to σ_3, forming an échelon inside the imposed lithospheric necking zone. Such a geometry, reminiscent of the Mak'arrasou oblique transfer zone, corresponds to the more common "leaky transfer zones." Where γ is high, rifts tend to be shorter and clearly separated from each other. Within transfer zones this may lead to the development of long transfer faults striking parallel to σ_3, connecting successive rifts. Such a geometry is reminiscent of transform faults, such as the Maskali transform and other predominant faults along the length of the oceanic Aden ridge. Intermediate γ values may lead to the development of overlap transfer zones (equivalent to OSCs).

The existence and geometry of transfer zones along the Aden ridge, and the related strain transfer mechanisms, therefore appear to be governed by ridge propagation processes, which themselves strongly depend on the relation between the initial 3-D geometry of the Arabia-Africa plate and the plate driving forces. This holds at the larger scale: In central Afar, the Aden and Red Sea ridges localize and propagate in opposite direction along the two facing edges of the central Afar volcanic pile, where tensile stress concentration is maximum (Figure 25). As a consequence, the two propagating plate boundaries cannot meet within Afar, since their respective rifts keep jumping farther away from each other. Such dynamic evolution, where the two ridges are forced to propagate simultaneously in opposite direction and bypass each other along two imposed, distinct paths, leads to the development of a growing overlap zone between them, where bookshelf faulting operates to transfer strain. The development of an overlap zone between the two ridges therefore seems to be a simple consequence of the initial 3-D geometry of the African plate before the onset of rifting.

In oceans the existence of discontinuities along ridges is often thought to be related to the along-axis distribution of magmatism. As recalled by *Martinez et al.* [1997], *Rea* [1978] proposed that the outer faults of a rift segment may intersect a magma chamber and capture magmatic flow, contributing to local shift of the location of the spreading center axis and inducing the development of a discontinuity and the onset of strain transfer (with a mechanism that will depend on the geometry of the discontinuity). *Macdonald et al.* [1984] relate the variation in geometry of discontinuities and strain transfer mechanisms to the existence of local, along-axis magmatic pulses that either succeed or fail to meet head on. Although some of these local magmatic processes may well play a role in Afar, we believe, together with *Macdonald et al.* [1984] and *Martinez et al.* [1997], that a more fundamental factor is the strength of the lithosphere being rifted. As is the case in Iceland, the AMI/MHG overlap developed where the central Afar lithosphere had been previously weakened by the Afar hot spot (thermal thinning plus local volcanic thickening through underplating and lava emplacement; see discussions by *Manighetti et al.* [1998] and *Courtillot et al.* [1999]).

The model shown in Figure 25 has implications for OSC-type transfer zones. First, in Afar, OSC transfer zones operate between two facing rifts or rifting zones, both of which are currently active and propagating. In contrast with what is usually described in oceans [e.g., *Hey*, 1977; *Hey et al.*, 1989; *Macdonald et al.*, 1984; *Kleinrock and Hey*, 1989*a*, 1989*b*; *Perram and Macdonald*, 1994], no doomed or failing rifts are observed [*Courtillot*, 1982]. This may be because processes are younger than the ones observed in the ocean and have not yet reached the stage when strain transfer is completed in such a way that one rift takes over the other one (as in Iceland [see *Gudmundsson* 1995]). OSC transfer mechanisms actually operate in Afar between rifts (or rifting zones) that are propagating either in the same sense (Tadjoura and Asal-Ghoubbet) or in the opposite sense (Aden and Red Sea rifting zones). Another consequence seen in Figure 25 is that the width of the OSC transfer zones is determined either by the width of the large-scale zones of maximum tensile stress concentration where rifts are forced to remain (in the Gulf of Tadjoura), or by the relative location of these zones (in central Afar). This may explain why the AMI/MHG overlap zone is wider than most OSCs observed in the oceans. The offset between the Aden and Red Sea propagating rift zones is so large that it demonstrates that the distributed, rotating faults within the overlap cannot have been created along the rift zone axes, as suggested elsewhere [e.g., *Phipps Morgan and Kleinrock*,

1991]. The fact that the width of the Afar OSCs is determined by initial conditions (initial 3-D geometry of the lithosphere) also explains why the width versus length ratios of these OSCs do not fit the 1:3 ratio usually measured in the oceanic OSCs, being instead close to 1:1. The $W : L$ ratio of the AMI/MHG overlap was even higher when the overlap started to form about 0.9 Myr ago, of the order of 1.5. Indeed, while the width of the Afar overlap zones is initially fixed, their length is not, since they lengthen in time as their bounding rifts or rifting zones propagate. This was one of the main ingredients in the original propagating rift model of *Courtillot* [1980], who pointed out the fundamental difference between initial, transient propagation during continental breakup, and equilibrium propagation of a preexisting plate boundary in the oceanic case. This situation is reminiscent of the migrating extensional relay zone model proposed by *Phipps Morgan and Kleinrock* [1991], as well as the growing overlap zones described by *Macdonald et al.* [1986, 1987, 1988], *Carbotte and Macdonald* [1992], and *Perram and Macdonald* [1993].

Strain transfer processes in Afar, and in particular bookshelf faulting, are necessarily transient, as are the processes of continental breakup, rift propagation and strain jumps recognized as dominant in this region [e.g., *Courtillot*, 1980; *Tapponnier et al.*, 1990; *Stein et al.*, 1991; *Manighetti et al.*, 1997, 1998]. These processes cannot last more than a few 10^5 or 10^6 years (and even less, according to *Macdonald et al.* [1991] and *Perram and Macdonald* [1993]) before the geometry of faulting changes so much that new deformation systems must be activated (see also *Bird et al.* [1999] for mid-ocean ridges). Thus, the real situation may neither be described by steady state plate tectonics nor continuous flow. At any moment in time, a description of the strain field in terms of small rigid block motion may be adequate, but it is governed by the hierarchy and organisation of the structures. Over longer periods of time the changes in the hierarchy and organization must be deciphered, through a detailed analysis of all faults. Each has a particular behavior, or role, that needs to be accurately determined. Any averaging of the strain field, as for instance that attempted by *Souriot and Brun* [1992] and *Rouby et al.* [1996], would result in losing the precious and rich information that any individual fault of any size holds on its evolution. Also, any spatially "static" vision of faulting would be wrong.

Can the way transient bookshelf faulting processes will evolve in space and time between the Aden and Red Sea ridges be predicted, until eventually Arabia and Africa are fully separated? Although the bookshelf faulting process involves small rigid block motions, active faulting is clearly distributed within the overlap, so that the overlap zone, despite its large size and 1:1 overlap to separation ratio which both make it comparable to most identified microplates in the ocean [e.g., *Martinez et al.*, 1997], cannot represent the initial stage of formation of a new microplate, as has been suggested elsewhere [e.g., *Acton et al.*, 1991; *Hey et al.*, 1995; *Martinez et al.*, 1997]. Although the Aden and Red Sea rifting zones curve toward one another (as observed in all oceanic OSCs [e.g., *Macdonald and Fox*, 1983; *Lonsdale*, 1983; *Macdonald et al.*, 1984]), we do not observe any evidence of oblique faulting within the overlap that would actually suggest either that one of the rifting zones is in the process of breaking through into the other one (as observed by *Sempéré and Macdonald* [1986a, 1986b]), or that a transform fault that would eventually join the two rifting zones by cutting through the overlap and truncating their tips, is in the process of developing (as described in the Woodlark Basin by *Taylor et al.* [1995, 1999]). This implies that an overlapping nontransform offset zone as large as $\sim 100 \times 120$ km^2 may persist, with bookshelf faulting operating for at least ~1 Myr. New fault sets are expected to form when older ones have rotated sufficiently away from the direction of optimal failure [*Nur et al.*, 1989], as suggested by our observations.

The organization in the propagation/transfer processes imaged in Figure 25 suggests that the Aden ridge is likely to continue to propagate northward within the large-scale lithospheric necking zone which runs along the western side of the Danakil microplate (Figure 26). It is unlikely to curve to the south, toward the Manda Hararo segments that form the southern termination of the Red Sea ridge propagation onland, or to cut through the overlap. We propose that the Aden ridge will eventually join the southern tip of the Red Sea ridge under water by cutting through the Bidu-Dubbi area where the Danakil microplate is already faulted and the site of active fissuring and volcanism [*CNR and CNRS*, 1975]. The distance separating the present northern tip of the Aden rift from the southern termination of the underwater Red Sea ridge being ~200 km and the propagation rate of the western Aden rift being >100 mm/yr [e.g., *Manighetti et al.*, 1998], we predict that a continuous waterway, floored with extended continental crust, will separate Arabia (including the southern half of the Danakil microplate) from Africa in <2 Myr. It should then give birth, ~2-3 Myr later (a time span deduced from *Manighetti et al.* [1997]), to a real ocean floored with oceanic crust. The geometry of the offset between the onland Aden rift and the underwater Red Sea southern termination is such that one might expect a new overlap transfer zone to develop between the two rifting zones, inducing counterclockwise block rotations in between (Figure 26).

7. Summary and Conclusions

The following are the main findings and conclusions of the present work.

1. As suggested in section 1, deformation mechanisms and strain distribution in Afar vary with observation scale (in space and time):

At a scale of several hundred kilometers and probably

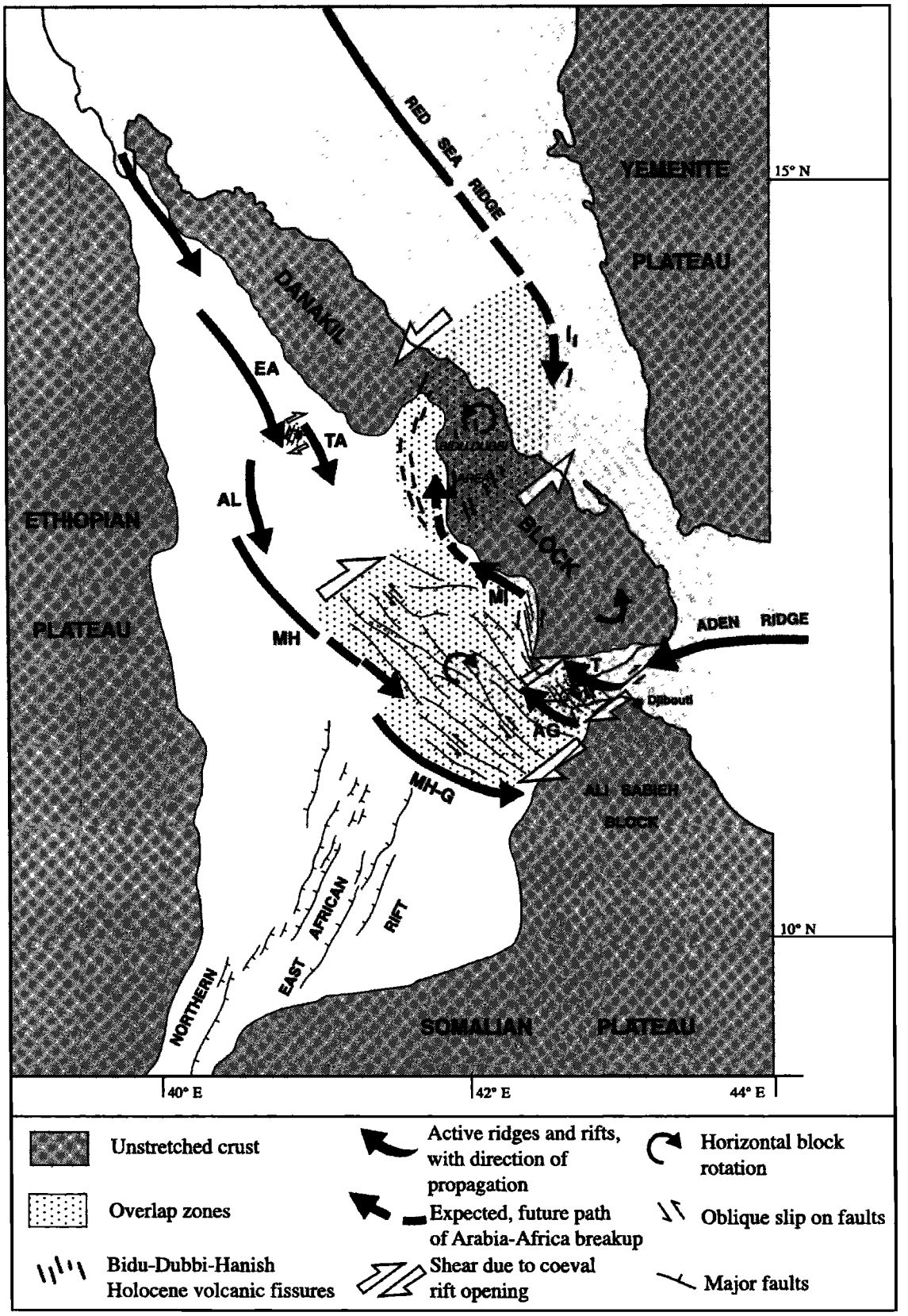

Figure 26. Model of current strain distribution and dynamics in Afar. Ridges and rifts are in black, with direction of propagation: EA, Erta'Ale; TA, Tat'Ali; AL, Alayta; MH, Manda Hararo; MH-G, Manda Hararo-Goba'ad; T, Tadjoura; AG, Asal-Ghoubbet; MI, Manda Inakir. Microplate and block rotations are indicated with curved arrows. Strain dynamics is such that it allows to predict path of final Arabia-Africa breakup, through Danakil block. EA-TA and Bidu Dubbi overlaps are predicted from rift and fault geometry.

~20 Myr, the Afar depression opened as the Danakil microplate was rotating counterclockwise. Paleomagnetic data demonstrate this rotation for the last ~7 Myr, at a mean rate of 1.5° ± 0.6°/Myr, similar to that deduced from regional plate kinematics [*Chu and Gordon*, 1998].

At a smaller scale of ~100 km and a few million years, the Afar depression mainly broke along two narrow, long rifting zones, localized along the two opposite edges of the central Afar volcanic pile. These two zones mark the penetration and propagation on land of the two Aden and Red Sea rifts/ridges.

At an even smaller scale of several tens of kilometers and less than 1 Myr, strain distribution and kinematics vary within Afar: Most strain (~85%) imposed by plate driving forces is localized within a series of disconnected rift segments, which are presently opening and propagating through the growth of numerous, closely spaced active normal faults, open fissures, and volcanic activity. These rifts are zones where crustal and lithospheric necking occurs (crustal thickness is ~2-3 km [e.g., *Lépine and Hirn*, 1992]). The residual extensional strain (~15%)is accommodated between the rifts and rifting zones by a dense network of thousands of distributed, active, normal faults of different sizes, the growth of which is not associated with any volcanic activity. The crust is ~10-12 km thick in these zones of distributed faulting [*Lépine and Hirn*, 1992].

2. The two Aden and Red Sea rifting zones overlap in eastern Afar (in the Arabia-Africa direction) over more than 120 km in length and 100 km in width (AMI/MHG overlap). At a smaller scale the Tadjoura and Asal-Ghoubbet rifts of the Aden rifting zone also overlap, over ~30 km in length and width (TAG overlap), while the other rifts do not.

3. The two overlap zones, in which strain transfer occurs, exhibit different scales but similar structural characteristics: Both are equidimensional; their surfaces are offset by a dense network of distributed, parallel, active, normal-left-lateral faults, oblique both to the bounding rifts and to the Arabia-Somalia motion vector, by ~20° and 70°, respectively. These faults slice the overlap zones into elongate, parallel blocks of different widths.

4. The kinematic measurements we performed on some of the major faults within the larger AMI/MHG overlap show that (1) these faults have been slipping rapidly in the Quaternary, with similar lateral and vertical rates of the order of 2-3 mm/yr, (2) their slip rates seem to have remained constant both in time and along fault strike over the last 1 Myr, (3) such fast rates imply that the major faults in the overlap initiated recently, <1 Myr ago. They subsequently grew and propagated, at rates we estimate to be of the order of 30-150 mm/yr, in directions sometimes opposite to that followed by their neighboring major fault, and (4) although strain distribution and kinematics obviously vary within the AMI/MHG overlap, it appears that the overlap keeps accommodating a constant, total amount of extension.

5. The paleomagnetic analyses we performed within the two AMI/MHG and TAG overlaps show that (1) some of the faults and the blocks that they limit have rotated clockwise about vertical axes, at least since the emplacement of the basaltic series that the faults offset; the total rotation amounts average 13.5° ± 6° and 13.4° ± 3.4° in the AMI/MHG and TAG overlaps, respectively, (2) whether we consider the rotations to have occurred since the emplacement of the surface lavas (1.8 ± 0.4 Ma and 350 ± 40 ka in AMI/MHG and TAG overlaps, respectively) or since the initiation of the major block-bounding faults (~0.8 and 0.35 Ma, respectively), the rotation rates are fast, of the order of 8°-17°/Myr and 38°/Myr in the AMI/MHG and TAG overlaps, respectively, (3) despite the large paleomagnetic uncertainties, it seems that within the AMI/MHG overlap the blocks did not all rotate at the same rate.

6. The paleomagnetic analyses that we performed either outside the two overlaps or between rifts that do not overlap show no rotations. Extension of observations into Ethiopian Afar to the west is in preparation.

7. A bookshelf faulting model, modified from *Tapponnier et al.* [1990], appears to account well for all structural, paleomagnetic, and geochronological data acquired inside the overlap zones, both at large and small scales. The model is basically a distributed strain model. The major modifications from that of *Tapponnier et al.* [1990] is that our model takes into account the residual extensional strain within the overlaps (as by *Sigmundsson* [1992]) and the variation of their spatial geometry (lengthening) with time. For the AMI/MHG overlap where the data are more numerous, the model integrates the new following points: (1) about seven to eight blocks, delineated on our structural maps, are taken to rotate; (2) rotations are taken to start only ~0.9 Myr ago, when the Asal-Ghoubbet rift starts opening into Afar; (3) between ~0.9 and 0.2 Ma, only eastern faults rotate between the opening Manda Hararo and Asal-Ghoubbet rifts; (4) the kinematic difference between eastern and western faults, the former being rotating while the latter are not, makes the eastern blocks tear and break at their western ends, generating the Gamarri-Alol tear zone; and (5) around 0.2 Ma, the overlap lengthens as the Aden rifting zone propagates farther north through the opening of a new rift segment (Manda Inakir); the western faults start rotating clockwise.

8. In both overlaps, the modified bookshelf faulting model allows important inferences: (1) the model predicts that the western faults (in AMI/ MHG) started rotating too recently for paleomagnetic studies performed farther west in Afar to reveal significant rotations, (2) although the data show that blocks with different widths rotate at different rates in eastern Afar, the model predicts that the faults bounding these blocks keep slipping at constant rates, and (3) the strike-slip rates deduced from the model are so high (~6 mm/yr

on each major fault bounding each first-order blocks and supposed to ensure its overall rotation) that they confirm that many other faults must participate to the block rotations within the overlap.

Independent of any preferred model, the block and fault rotation rates and the fault slip and propagation rates that we measure are so fast that they imply that strain transfer processes are transient. They obviously cannot last more than a few 10^5-10^6 years before the geometry of faulting changes significantly. However, despite these rapid changes, faults remain remarkably organized: Although, within the overlaps, they slip, propagate, and rotate at their own rates, which are generally different from those of their neighboring faults, they all seem to combine in a organized fashion to allow the overlap zones to stretch at constant overall rates. These constant rates are themselves a consequence of the strain distribution which prevails at a larger scale, while, in return, this larger scale strain distribution is dictated by the 3-D geometry of the plate.

Acknowledgments. We thank the Institut National des Sciences de l'Univers (INSU, Paris, France) for the financial support without which this work could not have been accomplished. In particular, SPOT satellite imagery was acquired through TECTOSCOPE program (INSU), cosponsored by the Centre National d'Etudes Spatiales (CNES, France). We also thank the Institut Supérieur d'Etudes et de Recherches Scientifiques et Techniques (ISERST) of the Republic of Djibouti, particularly its director M. Anis Abdallah, for his constant collaboration and scientific and logistic support. We thank the French Defense Ministery and the French Army based in Djibouti for their constant, precious logistic support without which a large part of this work could not have been accomplished. We are grateful to L. Audin, J.P. Avouac, Y. Gaudemer, S. Gruszow, J.P. Valet, and D. Vandamme for fruitful discussions. Most of our paleomagnetic calculations were done with the software "paleomac" written by J.P. Cogné, who we particularly thank (information on the software can be obtained from J.P. Cogné at cogne@ipgp.jussieu.fr). Our manuscript was improved by the helpful comments provided by J. Freymueller, G. Acton, and an anonymous reviewer. Special thanks to Y. Gaudemer for his constant help, and G. Aveline and A.C. Morillon for the illustrations. This is IPGP contribution 1739.

References

Abbate, E., P. Passerini, and L. Zan, Strike-slip faults in a rift area: A transect in the Afar triangle, East Africa, *Tectonophysics*, *241*, 67-97, 1995.

Acton, G.D., S. Stein, and J.F. Engeln, Block rotation and continental extension in Afar: A comparison to oceanic microplate system, *Tectonics*, *10*, 501-526, 1991.

Armijo, R., P. Tapponnier, J. L. Mercier, and H. Tong-Lin, Quaternary extension in southern Tibet: Field observations and tectonic implications, *J. Geophys. Res.*, *91*, 13,803-13,872, 1986.

Audin, L., Pénétration de la dorsale d'Aden dans la dépression Afar entre 20 et 4 Ma, Ph.D. thesis, Inst. de Phys. du Globe de Paris, 1999.

Audin, L., I. Manighetti, P. Tapponnier, F. Métivier, E. Jacques, and P. Huchon, Fault propagation and climatic control of sedimentation on the Ghoubbet rift floor: Insights from the Tadjouraden cruise in the western Gulf of Aden, *Geophys. J. Int.*, *144*, 391-413, 2001.

Barberi, F., and J. Varet, Nature of the Afar crust: A discussion, in *Afar Depression of Ethiopia*, edited by A. Pilger and A. Rösler, pp. 375-378, E. Schweizerbart'sche, Stuttgart, Germany, 1975.

Barberi, F., and J. Varet, Volcanism of Afar: Small-scale plate tectonics implications, *Geol. Soc. Am. Bull.*, *88*, 1251-1266, 1977.

Barberi, F., H. Tazieff, and J. Varet, Volcanism in the Afar depression: Its tectonic and magmatic significance, *Tectonophysics*, *15*, 19-29, 1972.

Barberi, F., G. Ferrara, R. Santacroce, and J. Varet, Structural evolution of the Afar triple junction, in *Afar Depression of Ethiopia*, edited by A. Pilger and A. Rösler, pp. 38-54, E. Schweizerbart'sche, Stuttgart, Germany, 1975.

Besse, J., and V. Courtillot, Revised and synthetic apparent polar wander paths of the African, Eurasian, North American and Indian plates, and true polar wander since 200 Ma, *J. Geophys. Res.*, *96*, 4029-4050, 1991.

Bird, R.T., S.F. Tebbens, M.C. Kleinrock, and D.F. Naar, Episodic triple-junction migration by rift propagation and microplates, *Geology*, *27*, 911-914, 1999.

Carbotte, S., and K. Macdonald, East Pacific Rise 8°-10°30'N: Evolution of ridge segments and discontinuities from SeaMARC II and three-dimensional magnetic studies, *J. Geophys. Res.*, *97*, 6959-6982, 1992.

Cassignol, C., and P.-Y. Gillot, Range and effectiveness of unspiked potassium-argon dating: Experimental groundwork and applications, in *Numerical Dating in Stratigraphy*, edited by G.S. Odin, pp. 159-179, John Wiley, New York, 1982.

Chase, C.G., Plate kinematics: The Americas, East Africa, and the rest of the world, *Earth Planet. Sci. Lett.*, 37, 355-368, 1978.

Chu, D., and R.G. Gordon, Current plate motion across the Red Sea, *Geophys. J. Int.*, 135, 313-328, 1998.

Consiglio Nazionale delle Ricerche (CNR) and Centre National de la Recherche Scientifique (CNRS), Geological map of Afar, scale 1:500,000, 2, Central and southern Afar, Geotechnip, La Celle St. Cloud, France, 1975.

Courtillot, V., Opening of the gulf of Aden and Afar by progressive tearing, *Phys. Earth Planet. Inter.*, *21*, 343-350, 1980.

Courtillot, V., Propagating rifts and continental breakup, *Tectonics*, *1*, 239-250, 1982.

Courtillot, V., A. Galdéano, and J. L. Le Mouel, Propagation of an accreting plate boundary: A discussion of new aeromagnetic data in the Gulf of Tadjurah and Southern Afar, *Earth Planet. Sci. Lett.*, *47*, 144-160, 1980.

Courtillot, V., J. Achache, F. Landre, N. Bonhommet, P. Y. Galibert, R. Montigny, and G. Féraud, Episodic spreading and rift propagation: New paleomagnetic and geochronologic data from the Afar passive margin, *J. Geophys. Res.*, *89*, 3315-3333, 1984.

Courtillot, V. , R. Armijo, and P. Tapponnier, Kinematics of the Sinaï triple junction and a two-phase model of Arabia-Africa rifting, in *Continental Extensional Tectonics*, edited by M.P. Coward, J.F. Dewey, and P.L. Hancock, *Spec. Publ. Geol. Soc. Am.*, *28*, 559-573, 1987.

Courtillot, V., C. Jaupart, I. Manighetti, P. Tapponnier, and J. Besse, On causal links between flood basalts and continental breakup, *Earth Planet. Sci. Lett.*, *166*, 177-195, 1999.

Cyaden Scientific Team, Tectonics of the westernmost gulfs of Aden and Tadjourah from submersible observations, *Nature*, *319*, 396-399, 1986.

De Chabalier, J. B., and J. P. Avouac, Kinematics of the

Asal rift (Djibouti) determined from the deformation of Fieale volcano, *Science*, *265*, 1677-1681, 1994.

Demarest, H. Jr., Error analysis for the determination of tectonic rotation from paleomagnetic data, *J. Geophys. Res.*, *88*, 4321-4328, 1983.

Fox, P.J., N.R. Grindlay, K.C. Macdonald, The mid-atlantic ridge (31°S-34°30'S): Temporal and spatial variations of accretionary processes, *Mar. Geophys. Res.*, *13*, 1-20, 1991.

Gasse, F., Etude de préfaisabilité des ressources géothermiques de la zone du Hanle-Gaggade, 98 pp., Geotermica Ital. SRL, Inst. Supérieur d'Etudes et de Rech. Sci. et Tech., Djibouti, 1983.

Gasse, F., Tectonic and climatic controls on lake distribution and environments in Afar from Miocene to present, in *Lacustrine Basin Exploration: Case Studies and Modern Analogs*, edited by B. Katz, *AAPG Mem.*, *50*, 19-41, 1991.

Gasse, F., and M. Fournier, Plio-Quaternary deposits and *Tectonics* of the margins of the Gulf of Tadjoura (Republic of Djibouti), *Bull. Cent. Rech. Explor. Prod. Elf-Aquitaine*, *7*, 285-300, 1983.

Gouin, P., *Earthquake History of Ethiopia and the Horn of Africa*, 259 pp., Int. Dev. Res. Cent., Ottawa, Ont., 1979.

Gruszow, S., Etude aéromagnétique et paléomagnétique du Territoire de la République de Djibouti, Ph.D. thesis, Univ. of Paris 7, 1992.

Gudmundsson, A., Ocean-ridge discontinuities in Iceland, *J. Geol. Soc. London*, *152*, 1011-1015, 1995.

Hall, S. and R.W. Girdler, Total intensity anomaly chart of the junction of the Red Sea, Gulf of Aden and Ethiopian rifts, report, Dep. of Geophys. and Planet. Phys., Univ. Newcastle upon Tyne, England, 1970.

Hey, R., A new class of "pseudofaults" and their bearing on plate tectonics: A propagating rift model, *Earth Planet. Sci. Lett.*, *37*, 321-325, 1977.

Hey, R.N., F.K. Duennebier, and W.J. Morgan, Propagating rifts on mid-ocean ridges, *J. Geophys. Res.*, *85*, 2647-2658, 1980.

Hey, R.N., J.M. Sinton, and F.K. Duennebier, Propagating rifts and spreading centers, in *The Geology of North America*, vol. N, *The Eastern Pacific Ocean and Hawaii*, edited by E.L. Winterer, D.M. Hussong, and R.W. Decker, pp. 161-176, Geol. Soc. of Am., Boulder, Colo., 1989.

Hey, R.N., P.D. Johnson, F. Martinez, J. Korenaga, M.L. Somers, Q.J. Huggett, T.P. LeBas, R.I. Rusby, and D.F. Naar, Plate boundary reorganization at a large-offset, rapidly propagating rift, *Nature*, *378*, 167-170, 1995.

Irving, E., *Paleomagnetism and Its Application to Geological and Geophysical Problems*, 399 pp., John Wiley, New York, 1964.

Jacques, E., Fonctionnement sismique et couplage élastique des failles en Afar, Ph.D. thesis, Univ. of Paris 7, 1995.

Jacques, E., G.C.P. King, P. Tapponnier, J.C. Ruegg, and I. Manighetti, Seismic triggering by stress changes after the 1978 events in the Asal rift, Djibouti, *Geophys. Res. Lett.*, *23*, 2481-2484, 1996.

Kidane, T., Contribution à l'étude paléomagnétique et géochronologique de l'évolution cinématique de la dépression Afar au cours des trois derniers millions d'années, Ph.D. thesis, Inst. de Phys. du Globe de Paris, 1999.

Klaus, A., W. Icay, D. Naar, and R.N. Hey, SeaMARC II survey of a propagating limb of a large nontransform offset near 29S along the fastest spreading East Pacific Rise segment, *J. Geophys. Res.*, *96*, 9985-9998, 1991.

Kleinrock, M.C., and R.N. Hey, Detailed *Tectonics* near the tip of the Galapagos 95.5°W propagator: How the lithosphere tears and a spreading axis develops, *J. Geophys. Res.*, *94*, 13,801-13,838, 1989a.

Kleinrock, M.C., and R.N. Hey, Migrating transform zone and lithospheric transfer at the Galapagos 95.5°W propagator, *J. Geophys. Res.*, *94*, 13,859-13,878, 1989b.

Lahitte, P., Le volcanisme Plio-Quaternaire lié aux mécanismes d'ouverture de la dépression Afar, Ph.D. thesis, Univ. of Paris XI, 2000.

Lépine, J. C., and J. C. Hirn, Seismotectonics in the Republic of Djibouti, linking the Afar depression and the Gulf of Aden, *Tectonophysics*, *209*, 65-86, 1992.

Lépine, J.C., J.C. Ruegg, and A. Abdallah, Sismicité du rift d'Asal-Ghoubbet pendant la crise sismo-volcanique de novembre 1978, *Bull. Soc. Géol. Fr.*, *12*, 809-816, 1980.

Lonsdale, P., Overlapping rift zones at the 5.5S offset of the East Pacific Rise, *J. Geophys. Res.*, *88*, 9393-9406, 1983.

Lowrie, W., Identification of ferromagnetic minerals in a rock by coercivity and unblocking temperature properties, *Geophys. Res. Lett.*, *17*, 159-162, 1990.

Macdonald, K.C., and P.J. Fox, Overlapping spreading centers: New accretion geometry on the East Pacific Rise, *Nature*, *302*, 55-57, 1983.

Macdonald, K.C., J.C. Sempéré, and P.J. Fox, East Pacific Rise from Siqueiros to Orozco fracture zones: Structure and evolution of overlapping spreading centers, *J. Geophys. Res.*, *89*, 6301-6306, 1984.

Macdonald, K.C., J.C. Sempéré, and P.J. Fox, Reply: The debate concerning overlapping spreading centers and mid-ocean ridge processes, *J. Geophys. Res.*, *91*, 10,501-10,510, 1986.

Macdonald, K.C., J.C. Sempéré, P.J. Fox, and R. Tyce, Tectonic evolution of ridge axis discontinuities by the meeting, linking, or self-decapitation of neighboring ridge segments, *Geology*, *15*, 993-997, 1987.

Macdonald, K.C., R.M. Haymon, S.P. Miller, J.C. Sempéré, and P.J. Fox, Deep-tow and Sea Beam studies of dueling propagating ridges on the East Pacific Rise near 20°40'S, *J. Geophys. Res.*, *93*, 2875-2898, 1988.

Macdonald, K.C., D.S. Scheirer, and S. Carbotte, Mid-ocean ridges: Discontinuities, segments and giant cracks, *Science*, *253*, 986-994, 1991.

Mandl, G., Tectonic deformation by rotating parallel faults: the "bookshelf" mechanism, *Tectonophysics*, *141*, 277-316, 1987.

Manighetti, I., Dynamique des systèmes extensifs en Afar, Ph.D. thesis, Inst. de Phys. du Globe de Paris, 1993.

Manighetti, I., P. Tapponnier, V. Courtillot, S. Gruszow, and P.Y. Gillot, Propagation of rifting along the Arabia-Somalia plate boundary: The Gulfs of Aden and Tadjoura, *J. Geophys. Res.*, *102*, 2681-2710, 1997.

Manighetti, I., P. Tapponnier, P.Y. Gillot, V. Courtillot, E. Jacques, J.C. Ruegg and G. King, Propagation of rifting along the Arabia-Somalia plate boundary: Into Afar, *J. Geophys. Res.*, *103*, 4947-4974, 1998.

Manighetti, I., G.C.P. King, Y. Gaudemer, C. Scholz, and C. Doubre, Slip accumulation and lateral propagation of active normal faults in Afar, *J. Geophys. Res.*, in press, 2001.

Martinez, F., R.N. Hey, and P.D. Johnson, The east ridge system 28.5-32°S East Pacific Rise: Implications for overlapping spreading center development, *Earth Planet. Sci. Lett.*, *151*, 13-31, 1997.

McFadden, P.L., and M.W. McElhinny, the combined analysis of remagnetization circles and direct observations in paleomagnetism, *Earth Planet. Sci. Lett.*, *87*, 152-160, 1988.

McFadden, P.L., and M.W. McElhinny, Classification of the reversal test in paleomagnetism, *Geophys. J. Int.*, *103*, 725-729, 1990.

McFadden, P.L., R.T. Merrill, M W. McElhinny, and S. Lee, Reversals of the Earth's magnetic field and temporal vari-

ations of the dynamo families, *J. Geophys. Res.*, *96*, 3923-3933, 1991.

McKenzie, D.P., and J. Jackson, A block model of distributed deformation by faulting, *J. Geol. Soc. London*, *143*, 349-353, 1986.

McKenzie, D.P., D. Davies, and P. Molnar, Plate *Tectonics* of the Red Sea and East Africa, *Nature*, *224*, 125-133, 1970.

Merrill, R.T., and M.W. McElhinny, *The Earth's Magnetic Field: Its History, Origin, and Planetary Perspective*, pp. 401, Academic, San Diego, Calif., 1983.

Naar, D.F., and R.N. Hey, Speed limit for oceanic transform faults, *Geology*, *17*, 420-422, 1989.

Naar, D.F., and R.N. Hey, Tectonic evolution of the Easter microplate, *J. Geophys. Res.*, *96*, 7961-7993, 1991.

Noir, J., E. Jacques, S. Békri, P.M. Adler, P. Tapponnier, and G.C.P. King, Fluid flow triggered migration of events in the 1989 Dôbi earthquake sequence of central Afar, *Geophys. Res. Lett.*, *24*, 2335-2338, 1997.

Nur A., H. Ron, and O. Scotti, Fault mechanics and the kinematics of block rotation, *Geology*, *14*, 746-749, 1986.

Nur A., H. Ron, and O. Scotti, Kinematics and mechanics of tectonic block rotations, in *Slow Deformation and Transmission of Stress in the Earth*, *Geophys. Monogr. Ser.*, vol. 49, edited by S.C. Cohen and P. Vanicek, pp. 31-46, AGU, Washington, D.C., 1989.

Office de la Recherche Scientifique et Technique d'Outre-Mer (ORSTOM), Tadjoura geological map, scale 1:100,000, Paris, 1985.

Perram, L.J., and K.C. Macdonald, Tectonic and magnetic studies of the dueling propagating spreading centers at 20°40'S on the East Pacific Rise: Evidence for crustal rotations, *J. Geophys. Res.*, *98*, 13835-13850, 1993.

Perram, L.J., and K.C. Macdonald, An overlapping propagating spreading center at 87°30'W on the Galapagos Spreading Center, *Earth Planet. Sci. Lett.*, *121*, 195-211, 1994.

Phipps Morgan, J., and M.C. Kleinrock, Transform zone migration: Implications of bookshelf faulting at oceanic and icelandic propagating ridges, *Tectonics*, *10*, 920-935, 1991.

Phipps Morgan J., and D.T. Sandwell, Systematics of ridge propagation south of 30°S, *Earth Planet. Sci. Lett.*, *121*, 245-258, 1994.

Prévôt, M., and S. Grommé, Intensity of magnetization of subaerial and submarine basalts and its possible change with time, *Geophys. J. R. Astron. Soc.*, *40*, 207-224, 1975.

Rea, D. K., Asymmetric sea-floor spreading and a nontransform axis offset: The East Pacific Rise 20°S survey area, *Geol. Soc. Am. Bull.*, *89*, 836-844, 1978.

Richard, O., Etude de la transition dorsale océanique-rift émergé: Le Golfe de Tadjoura (République de Djibouti), Ph.D. thesis, Univ. of Paris XI, Orsay, 1979.

Rouby D., T. Souriot, J.P. Brun, and P.R. Cobbold, Displacements, strains, and rotations within the Afar depression (Djibouti) from restoration in map view, *Tectonics*, *15*, 952-965, 1996.

Schaefer, H.U., Investigations on crustal spreading in southern and central Afar (Ethiopia), in *Afar Depression of Ethiopia*, vol. 1, edited by E. Pilger and A. Rosler, pp. 289-296, E. Schweizerbart'sche, Stuttgart, Germany, 1975.

Schouten, H., K.D. Klitgord, and D.G. Gallo, Edge-driven microplate kinematics, *J. Geophys. Res.*, *98*, 6689-6701, 1993.

Schult, A., Paleomagnetism of Tertiary volcanic rocks from the ethiopian southern plateau and the Danakil block, *J. Geophys.*, *40*, 203-212, 1974.

Schult, A., Paleomagnetic results from the Ethiopian southeastern plateau and the Danakil block, in *Afar Depression of Ethiopia*, vol. 1, edited by E. Pilger and A. Rosler, pp. 80-85, E. Schweizerbart'sche, Stuttgart, Germany, 1975.

Sempéré, J.C., and K.C. Macdonald, Overlapping spreading centers: Implications from crack growth simulation by the displacement discontinuity method, *Tectonics*, *5*, 151-163, 1986a.

Sempéré, J.C., and K.C. Macdonald, Deep-tow studies of the overlapping spreading centers at 9°03'N on the East Pacific Rise, *Tectonics*, *5*, 881-900, 1986b.

Sichler, B., La biellette danakile: Un modèle pour l'évolution géodynamique de l'Afar, *Bull. Soc. Géol. Fr.*, *6*, 925-933, 1980.

Sigmundsson, F., Tectonic implications of the 1989 Afar earthquake sequence, *Geophys. Res. Lett.*, *19*, 877-880, 1992.

Souriot, T., and J.P. Brun, Faulting and block rotation in the Afar triangle, East Africa: The Danakil "crank-arm" model, *Geology*, *20*, 911-914, 1992.

Stein, R.S., P. Briole, J.C. Ruegg, P. Tapponnier, and F. Gasse, Contemporary, Holocene, and Quaternary deformation of the Asal Rift, Djibouti: Implications for the mechanics of slow spreading ridges, *J. Geophys. Res.*, *96*, *21*,789-21,806, 1991.

Tapponnier, P., and J. Varet, La zone de Mak'arrasou en Afar: un équivalent émergé des "failles transformantes" océaniques, *C. R. Acad. Sci., Ser. D*, *278*, 209-212, 1974.

Tapponnier, P., R. Armijo, I. Manighetti, and V. Courtillot, Bookshelf faulting and horizontal block rotations between overlapping rifts in southern Afar, *Geophys. Res. Lett.*, *17*, 1-4, 1990.

Taylor, B., A. Goodliffe, F. Martinez, and R. Hey, Continental rifting and initial sea-floor spreading in the Woodlark basin, *Nature*, *374*, 534-537, 1995.

Taylor, B., A. Goodliffe, and F. Martinez, How continents break up: Insights from Papua New Guinea, *J. Geophys. Res.*, *104*, 7497-7512, 1999.

Valet, J.P., T. Kidane, V. Soler, J. Brassart, V. Courtillot, and L. Meynadier, Remagnetization in lava flows recording pretransitional directions, *J. Geophys. Res.*, *103*, 9755-9775, 1998.

Vandamme D., V. Courtillot, J. Besse, and R. Montigny, Paleomagnetism and age determinations of Deccan traps: Results of a Nagpur-Bombay traverse and review of earlier work, *Rev. Geophys.*, *29*, 159-190, 1991.

Varet, J., and F. Gasse, Geology of central and southern Afar, report, Cent. Nat. de la Rech. Sci., Paris, 1978.

Wetzel, L.R., D.A. Wiens, and M.C. Kleinrock, Evidence from earthquakes for bookshelf faulting at large nontransform ridge offsets, *Nature*, *362*, 235-237, 1993.

V. Courtillot and Y. Gallet, Laboratoire de Géomagnétisme et Paléomagnétisme, UMR CNRS 7577, Institut de Physique du Globe de Paris, 4 place Jussieu, 75252 Paris cedex 05, France. (courtil@ipgp.jussieu.fr; gallet @ipgp.jussieu.fr)

P.-Y. Gillot, OrsayTerre, UMR CNRS 8616, Bâtiment 504, Université Paris-Sud, 91405 Orsay cedex, France. (gillot@geol.u-psud.fr)

E. Jacques, Institut de Physique du Globe de Strasbourg, UMR CNRS 7516, 67084 Strasbourg cedex, France. (Eric.Jacques@eost.u-strasbg.fr)

I. Manighetti and P. Tapponnier, Laboratoire de Tectonique, Mécanique de la Lithosphère, UMR CNRS 7578, Institut de Physique du Globe de Paris, 4 place Jussieu, 75252 Paris cedex 05, France. (manig@ipgp.jussieu.fr; tappon@ipgp.jussieu.fr)

(Received March 13, 2000; revised September 30, 2000; accepted December 5, 2000.)